REGIONAL GEOHYDROLOGY OF THE GULF COAST AQUIFER IN MATAGORDA AND WHARTON COUNTIES, TEXAS: DEVELOPMENT OF A NUMERICAL MODEL TO ESTIMATE THE IMPACT OF WATER-MANAGEMENT STRATEGIES

Alan R. Dutton
Bernd C. Richter

Prepared for

Lower Colorado River Authority
under Interagency Contract Number IAC (88-89)0910

Bureau of Economic Geology
W. L. Fisher, Director
The University of Texas at Austin
Austin, Texas 78713

April 1990

CONTENTS

Figures

Tables

EXECUTIVE SUMMARY

A ground-water flow model that represents the complex interrelations among aquifer stratigraphy, hydrologic properties, and ground-water availability in the Gulf Coast aquifer system in Matagorda and Wharton Counties and adjacent areas of Texas can be used for evaluating surface- and ground-water management strategies. The hydrological model developed in this study is based on results of detailed mapping of sand-bed distribution, hydraulic head, and hydrochemical facies in horizontal and vertical planes. It differs from previous regional models of the Gulf Coast aquifer by treating the Beaumont Formation in the study area as a hydrostratigraphic unit distinct from the Chicot aquifer unit and by using a smaller grid to represent the study area in greater detail.

The quasi-three-dimensional numerical model is implemented using the U.S. Geological Survey computer code MODFLOW. Transmissivity and storativity are assigned to model blocks as functions of sand percentage mapped for each aquifer unit. The model uses head-dependent source terms, options in the MODFLOW computer code, to simulate interaction between rivers and aquifers as well as regional recharge and discharge. The model includes cross-formational leakage between hydrostratigraphic units. "No-flow" lateral boundaries reflect original ground-water-basin divides. The model excludes interbasin loss of water such as drainage of water to the northeast into the cone of depression underlying much of Harris County. The seaward edges of the model layers representing the Chicot and Evangeline aquifer units also are treated as "no-flow" boundaries where the base of fresh water rises above the top of the aquifer units. Transmissivity, vertical conductance, river leakage rates, and recharge and discharge rates were adjusted to attain a satisfactory match between simulated and estimated prepumping hydraulic heads, which were assumed to represent steady-state hydrologic conditions.

To estimate future water-level changes, the numerical model was calibrated by trial-and-error adjustment of storativities to match simulated hydraulic heads against historic head values. Model

results indicate that future ground-water withdrawals of between 605,000 and 639,000 acre-ft/yr through 2030 locally will result in another 110 to 240 ft of hydraulic-head decline; maximum drawdown is predicted for the Wharton–Jackson–Lavaca–Colorado four-corners area. Calculated average rates of hydraulic-head decline in the Chicot and Evangeline aquifer units were 0.3 to 1.3 ft/yr from 1900 through 1965. Assuming future pumping rates will be controlled by high demand for water, average drawdown rates will reach 1.2 to 2 ft/yr between 1985 and 2000 but will decrease to about 0.5 to 0.6 ft/yr by 2020. The cumulative increase in drawdown of hydraulic head will increase the potential for seawater intrusion and also will increase land-surface subsidence to as much as 2.5 ft by 2030 in western Matagorda and eastern Jackson Counties. The model indicates that clay-bed compaction, which results in subsidence, accounts for 11 and 18 percent of the decreases in stored water by 1985 and 2030, respectively.

The model was used to simulate a well field yielding 22,800 ac-ft/yr from the Chicot aquifer to supplement Colorado River water for irrigation; simulation results indicate that drawdown due to ground-water withdrawal continuing from 1990 to 2030 will be as much as 83 ft, which locally could increase subsidence by approximately 1.5 ft. An artificial recharge project using surface-water spreading basins could recharge more than 1,000 acre-ft/yr per acre of spreading basin, depending partly on the number of recovery wells included in the design.

INTRODUCTION

This study was designed to develop a ground-water flow model and procedures for evaluating surface- and ground-water management strategies affecting the Gulf Coast aquifer system in the area between the Lavaca and Brazos Rivers in the Texas Coastal Plain (fig. 1). The study focused on Matagorda and Wharton Counties, Texas, where most of the surface water diverted from the Colorado River for irrigation is applied. Planning for and management of ground-water development from beneath the lower Colorado and adjacent river basins are needed because of projected growth in demand for water. Artificial recharge and conjunctive use of surface

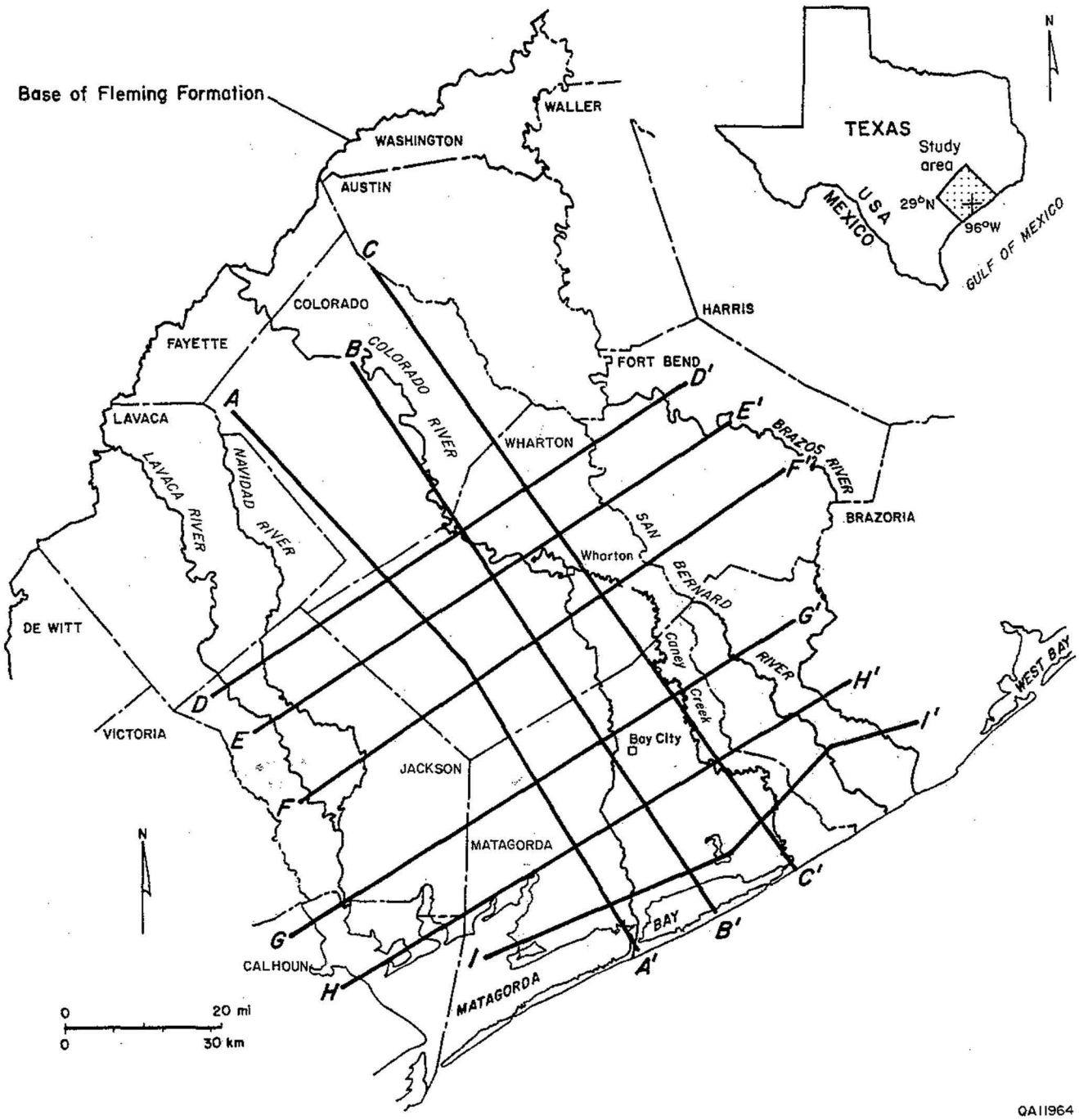

Figure 1. Location of the study area along the Colorado River within the Texas Coastal Plain, showing lines of cross sections.

and ground water, for example, are water-resource-management strategies that have possible application in this part of the coastal plain. A ground-water model that represents the complex interrelation among aquifer stratigraphy, hydrologic properties, and ground-water availability provides a useful tool for evaluating the impacts of management strategies. Ground-water model development, therefore, is part of the overall planning process.

Carr and others (1985) and Ryder (1988) developed regional models of ground-water flow in the Gulf Coast aquifer that include the present study area. Jorgensen (1981) summarized a succession of models used to study flow in the Gulf Coast aquifer near Houston, northeast of the study area. Groschen (1985) simulated flow in the lower part of the Gulf Coast aquifer in the Corpus Christi area to the southwest. A detailed model of flow in the Gulf Coast aquifer beneath the lower Colorado and adjacent river basins, however, has not been developed previously.

The objectives of this study were to develop a predictive model that represents as accurately as possible the historical and expected future patterns of ground-water withdrawal and hydraulic-head change and to demonstrate how such a model can be used to evaluate additional water-resources projects. Study of simulation results contained in this report as well as results to be obtained in future simulations can lead to improved understanding of the hydrodynamics of the Gulf Coast aquifer, including insights into the regional water budget, distribution of hydrologic parameters, and amounts of predicted subsidence. This improved understanding in turn should lead to revision of the conceptual and numerical models as this tool continues to be used for evaluating water-management strategies. In the long term, a future validation study should be conducted, perhaps in the years 2000 and 2010, to compare model predictions to actual experience. This comparison also will result in revision and improvement in the conceptual and numerical models.

Local geology and hydrology of the Gulf Coast aquifer system largely determine the impacts of water-management strategies. To determine these impacts and to provide a tool for evaluating water-resource-management strategies, we developed a quantitative geohydrologic model of the Gulf Coast aquifer in Matagorda and Wharton Counties and adjacent parts of Brazoria, Calhoun,

Colorado, Fort Bend, Jackson, and Lavaca Counties. This report describes the geohydrologic setting of the study area, a conceptual model of the ground-water flow system, a numerical model for calculating hydraulic heads and flow rates, calibration results, and results of steady-state and transient flow simulations. Finally, the model was applied to simulated hypothetical projects to demonstrate its use in evaluating well-field and artificial-recharge projects.

GEOHYDROLOGIC SETTING

The central part of the Texas Coastal Plain is relatively flat, having slight local relief bordering broad river valleys. The climate is subtropical humid, and average annual precipitation is approximately 40 to 44 inches (Hammond, 1969; Larkin and Bomar, 1983). Monthly precipitation is higher than average from June to September, which is also the period of maximum potential evapotranspiration. Northeast of the study area there is a net annual excess of precipitation over evapotranspiration, whereas to the southwest there is a net annual deficit (McGowen and others, 1976).

Geologic units that make up the Gulf Coast aquifer are a coastward-thickening wedge of Pliocene and Pleistocene formations (table 1) that crop out in wide bands parallel to the coastline (fig. 2). Alluvium floors the main river valleys. Pliocene and Pleistocene sands were deposited primarily in fluvial meanderbelt, fluvio-deltaic, and wave-dominated delta systems (Guevara-Sanchez, 1974; Solis, 1981). Sand deposits typically have a dip-elongate orientation and are highly lenticular and discontinuous.

In previous hydrologic reports, the Pliocene and Pleistocene formations have been assigned to various hydrostratigraphic units (table 1). The Chicot and Evangeline aquifers are common names for the main hydrostratigraphic units. Permeable parts of the Willis and Lissie Formations make up the Chicot aquifer unit, whereas permeable parts of the Goliad and upper Fleming Formations make up the Evangeline.

Table 1. Comparison of hydrostratigraphic nomenclature applied to aquifers and confining units.

Stratigraphic Unit			Matagorda County Hammond (1969)		Colorado, Lavaca, and Wharton Counties Loskot and others (1982)	Brazoria County Sandeen and Wesselman (1982)	Houston area Jorgensen (1975)	Regional setting Baker (1979)	Regional setting Carr and others (1985)	Regional setting Ryder (1988)	This report
QUATERNARY	HOLOCENE	Alluvium, coastal deposits	Gulf Coast aquifer		Chicot aquifer	upper Chicot aquifer	upper Chicot aquifer	Chicot aquifer	upper Chicot aquifer	Holocene-upper Pleistocene permeable zone	Alluvium and Beaumont Formation aquifer units
	PLEISTOCENE	Beaumont Formation		"Heavily-pumped zone"							upper Chicot aquifer unit
		Lissie Formation (undifferentiated) / Montgomery Formation				lower Chicot aquifer	lower Chicot aquifer		lower Chicot aquifer	lower Pleistocene-upper Pliocene permeable zone	
		Lissie Formation (undifferentiated) / Bentley Formation									
TERTIARY	PLIOCENE	Willis Formation									lower Chicot and Evangeline aquifer unit
	MIOCENE	Goliad Formation			Evangeline aquifer	Evangeline aquifer	Evangeline aquifer	Evangeline aquifer	Evangeline aquifer	lower Pliocene-upper Miocene permeable zone	
		Fleming Formation		Interval not studied	Burkeville confining layer	Interval not studied	Burkeville confining layer	Burkeville confining layer	Burkeville confining layer	middle Miocene confining unit	Burkeville confining layer

QA12086c

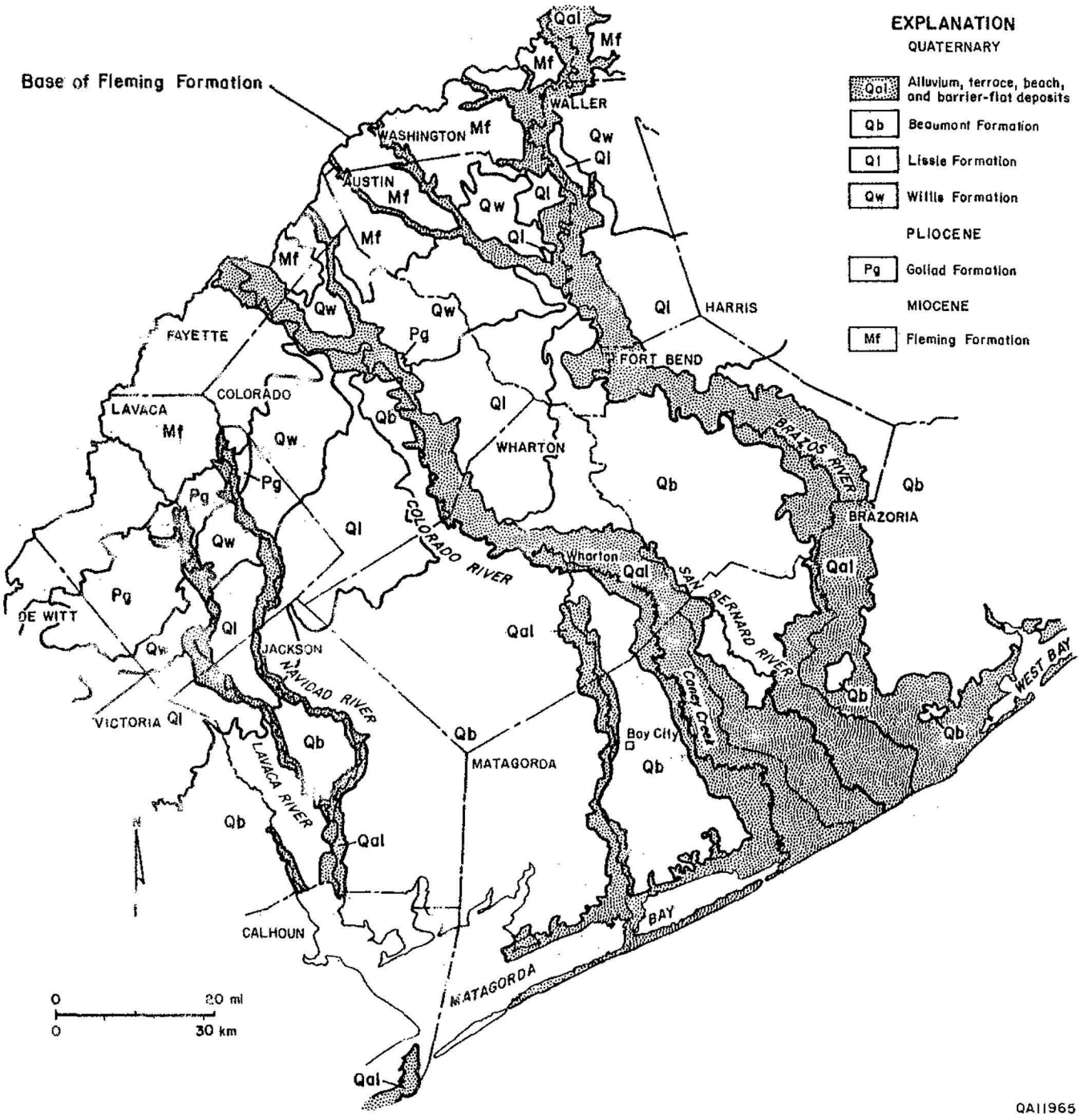

Figure 2. Geologic map of study area. Modified from Proctor and others (1974), Aronow and others (1982), and Brown and others (1987).

The Quaternary Beaumont Formation crops out across most of Matagorda and Wharton Counties (fig. 2) and represents the last major depositional progradation. It is commonly considered to be an aquitard, a unit of low permeability, that overlies and isolates the Gulf Coast aquifer, the main water source throughout much of the Gulf Coast (Carr and others, 1985). The formation locally is a ground-water source, however, and contains considerably more aquifer-type material–sands and silty sands–than generally is recognized. Guevara-Sanchez (1974) and Kreitler and others (1977) identified trends where Beaumont sand is relatively thick in Harris, Fort Bend, and Brazoria Counties. Figure 3 is a fence diagram in which the Beaumont Formation is separated from the Chicot aquifer unit. Geohydrologic justification for this separation is discussed later in this report.

METHODS AND DATA

Geologic Data

Guevara-Sanchez (1974) and Solis (1981) mapped thicknesses of Pliocene and Pleistocene sand deposits in two different areas of the Texas Coastal Plain separated by the Colorado River. They defined different operational mapping units and used different conceptual models of the influence of faults on sand distribution; thus, their results are largely incompatible. Therefore, subsurface geologic information on the area was recompiled and reevaluated as part of this project.

Subsurface geologic information was collected from 587 geophysical and water-well drillers' logs. Geophysical logs were selected that generally start within 500 to 1,000 ft of the land surface. Drillers' logs were used to supplement geophysical logs at shallow depths, although the quality of this information is variable. From the geophysical and drillers' logs, sand beds as thin as 5 ft were identified and tabulated. The mean values of sand percentage in 500-ft-thick intervals estimated from geophysical logs and drillers' logs are not statistically different; therefore, all data were

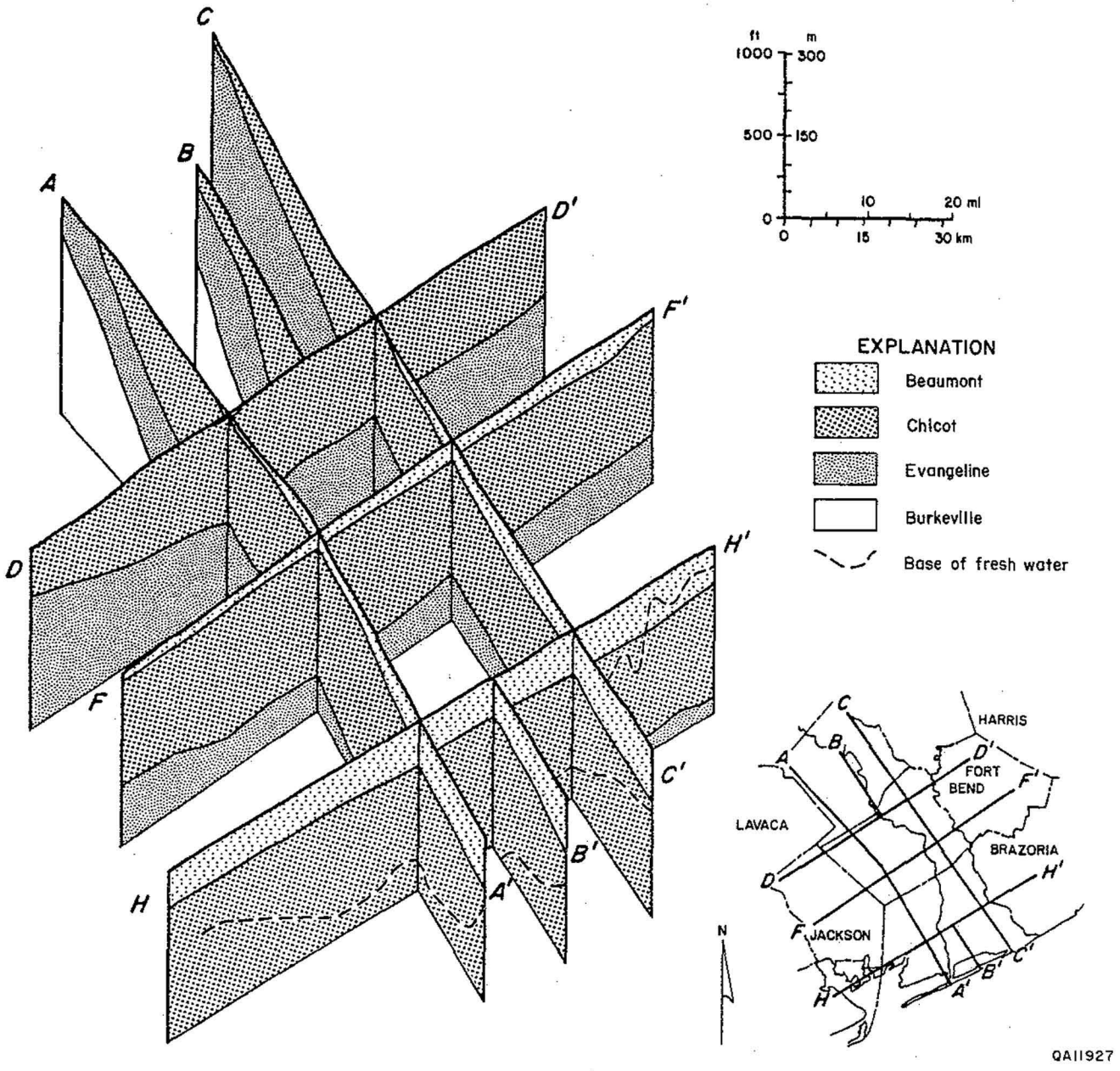

Figure 3. Fence diagram illustrating the stratigraphic relationship between the Chicot and Evangeline aquifers and an aquifer unit in the Beaumont Formation.

pooled to construct maps and cross sections. Data on sand-bed distribution are archived in open-file form at the Bureau of Economic Geology.

Drillers' logs provide information on the distribution of sand and clay beds above the depths where geophysical logs are run in oil and gas wells. The 285 drillers' logs used in this study are less precise than geophysical logs in locating individual sand beds. Also, 112 drillers' logs refer to "sand and clay" beds. We reduced the calculated thickness of discrete sand beds in such intervals to 33 percent of the reported thickness.

Sand-bed intervals identified from geophysical and drillers' logs were tabulated using RS/1 computer software (BBN Software Products Corporation, 1987), which provided a flexible and rapid method for constructing maps of subsurface sand distribution. Our RS/1 program generated a list of sand-percent values for particular slices of the subsurface. Sand-percent maps generated in this study are based on log data covering at least 80 percent of the selected interval and sand beds more than 20 ft thick. To make reliable estimates of sand percent, at least 80 percent of the interval should be covered, but the requirement that more than 90 percent of the interval be covered reduces the amount of usable data. Beds thinner than 10 to 20 ft are not effectively interconnected in a regional flow system (Fogg and others, 1983).

Nine stratigraphic cross section–three dip and six strike sections–were constructed at approximately 10-mi intervals across Matagorda and Wharton Counties (fig. 1). Well locations were orthogonally projected onto the sections, and individual sand beds were displayed using RS/1 algorithms.

Structure-contour maps of the bases of the Chicot and Evangeline aquifers were taken from Carr and others (1985). The structure-contour map of the base of the Beaumont Formation was based on data reported by Guevara-Sanchez (1974) and Solis (1981). The base of fresh water was determined from data contained in various county reports, including Baker (1965), Wilson (1967), Hammond (1969), Wesselman (1972), and Sandeen and Wesselman (1973).

Maps of sand-percentage distribution, aquifer and formation structure, base of fresh water, and land-surface elevation were digitized and converted to computer files. CPS-1, a graphics

computer package (Radian Corporation, 1979), was used extensively to map and interpolate spatial data. Structure values for the 587 well log locations and for nodes of the numerical model were interpolated using CPS-1.

Geohydrologic Data

Historical data on ground-water levels and chemical composition in Matagorda, Wharton, and adjacent counties were compiled from computerized files in the Texas Natural Resources Information System (TNRIS). Some wells have been monitored for as long as 50 yr, providing ample data for history-matching calibration of a ground-water flow model. Latitude and longitude coordinates for approximately half the wells were specified in TNRIS records; locations of the remainder were determined from drillers' log reports. Map locations were then digitized.

Vertical patterns of hydraulic-head variation were projected and mapped on the same cross sections defined for sand bed distributions. The bottom of the wells was posted on the cross sections for contouring hydraulic head. This results in shifting the apparent location of hydraulic-head decline downward relative to the center of ground-water production zone. An alternative plotting approach, locating the contour point at the midpoint of the well screen interval, was not followed because many tops and bottoms of screen intervals were unknown.

Hydraulic-head data were sorted into time periods for constructing plan-view maps of potentiometric surfaces. All 1930's and 1940's data were pooled because relatively little ground-water production had occurred that would have affected hydraulic-head values, and the greater number of wells allows a composite potentiometric-surface map to be defined. Maps of hydraulic head based on consecutive yearly records, 1965/66 and 1985/86, also were prepared. Regional estimates of original or prepumping hydraulic heads were taken from Ryder (1988) for calibrating the steady-state flow model.

Information on transmissivity and storativity was compiled from reports on ground-water resources of the counties in the study area (appendix). A map of reported values of transmissivity

was superposed on maps of sand percentage in the upper and lower units of the Chicot aquifer and the Evangeline aquifer, and sand percentage was interpolated at wells with aquifer test results. Transmissivity varies significantly with sand percentage, regardless of whether sand percentage was based on all sand beds or only on beds of thickness greater than 20 ft (fig. 4a and b). The linear regression depicted in figure 4b was used to estimate transmissivity for the numerical model. No correlation between hydraulic conductivity and sand percentage was found. Transmissivities assigned to finite-difference blocks of the numerical model were calculated from the regression equation:

$$\text{Log}\,(T) = 3.67 + 4.57 \times 10^{-3}\,SP + \varepsilon\, s_e, \qquad (1)$$

where

T is transmissivity in ft^2/day,

SP is sand percentage,

ε is a random variable with a standard normal distribution (mean of 0 and standard deviation of 1),

and s_e is the standard error of estimate from the regression (0.37).

The third term on the right-hand side of equation 1 was used to reproduce the scatter of transmissivity values depicted in figure 4.

Chemical analyses were used along with hydraulic-head data to formulate an understanding of the ground-water flow system in the Gulf Coast aquifer. Data were obtained for counties in the study area from TNRIS computer listings. Reported chemical analyses of ground water vary in completeness and in conditions of sample treatment. For example, temperature, pH, and alkalinity are not always measured on site and therefore are unreliable measurements of in situ values, and pH commonly is not reported. The charge balance of anions and cations is almost always exact, indicating that sodium and potassium were determined together by difference. Chemical analyses were culled to retain the most complete and most valid data, including 975 records.

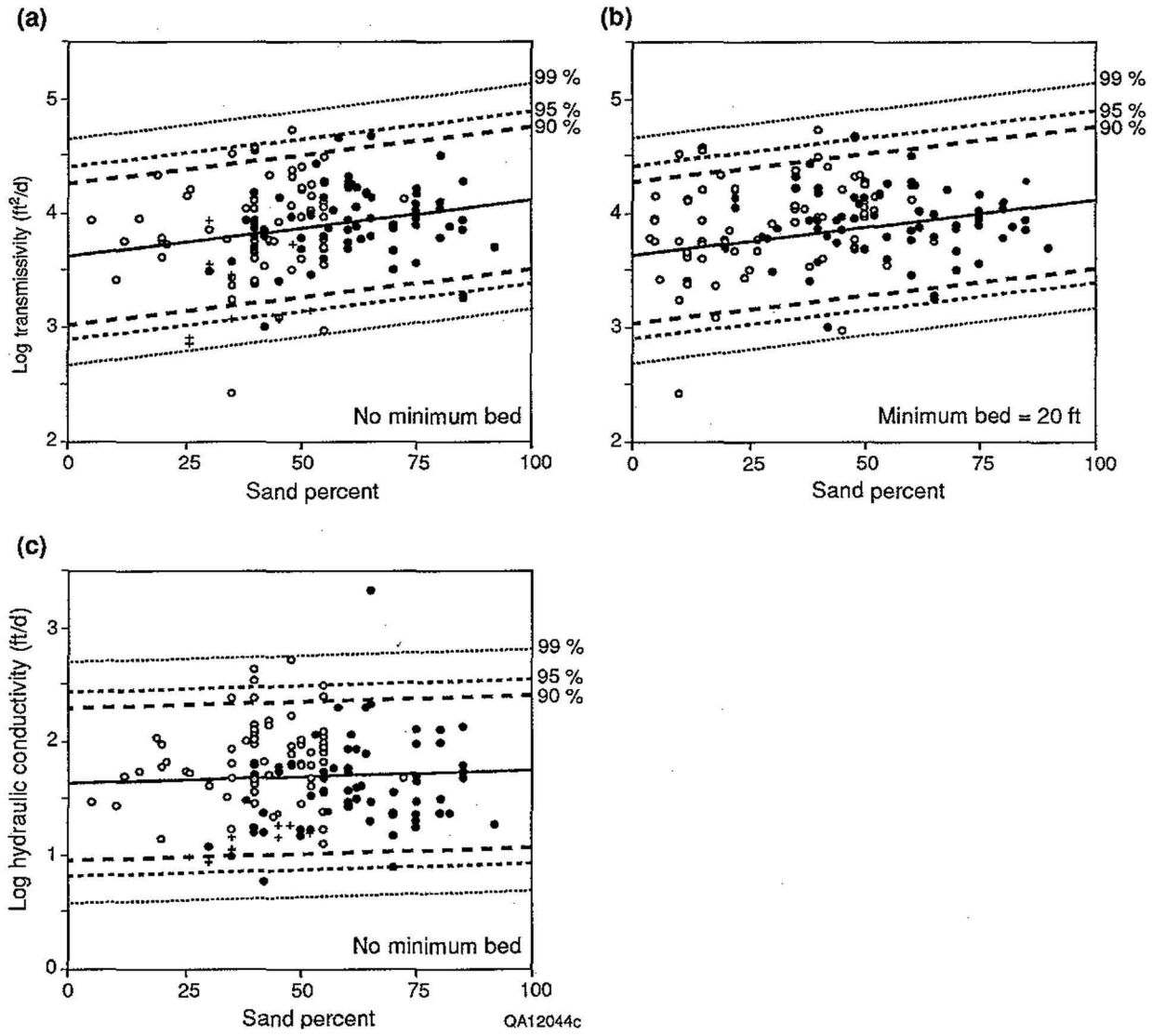

Figure 4. Relationships between sand percent and logarithm of transmissivity (a, b) and logarithm of hydraulic conductivity (c). Lines include linear least-squares regression line (solid), and confidence limits of 90, 95, and 99 percent calculated for a single prediction from a normally distributed population.

DEFINITION OF THE CONCEPTUAL MODEL

Stratigraphic Framework

For this study, maps and cross sections of sand distribution throughout the study area were constructed, building on previous work by Guevara-Sanchez (1974) and Solis (1981). Cross sections A-A′, B-B′, and C-C′ (figs. 5 through 7, respectively) are so-called dip sections that are approximately parallel to the modern and ancient river systems crossing the coastal plain. Sections D-D′ through I-I′ (figs. 8 through 13, respectively) are so-called strike sections, approximately parallel to the strike of the formations.

Several features are common to these sections. First, sands in the Willis and Lissie Formations that make up the Chicot aquifer appear generally thicker than sands of the Fleming and Goliad Formations that comprise the Evangeline aquifer. The boundary between the Evangeline and Chicot aquifer units is close to the transition from thin Evangeline sands to thick Chicot sands. To an extent, this is exaggerated by the dominance of drillers' log data in the top 400 ft of the section; drillers' logs do not resolve thin beds as well as geophysical logs. Note that the lack of sand beds between the upper Chicot and Evangeline in some parts of the nine sections is an artifact of the gap between the general base of drillers' log data and the top of most geophysical logs. Second, sand thickness decreases toward the coast. The vertical and lateral variations in sand-bed thickness reflect the sedimentary record of progradation and retreat of fluvial and deltaic systems discussed by Guevara-Sanchez (1974) and Solis (1981). The third common feature is that the base of fresh water rises irregularly in the stratigraphic section toward the coast, as expected from a general model of seawater intrusion (fig. 14).

Sand-percentage maps initially were made for four layers: (1) the Beaumont; (2) all of the Chicot aquifer unit (table 1) as defined by Jorgensen (1975), Baker (1979), and Carr and others (1985); (3) the Chicot aquifer unit minus the Beaumont Formation; and (4) the Evangeline aquifer

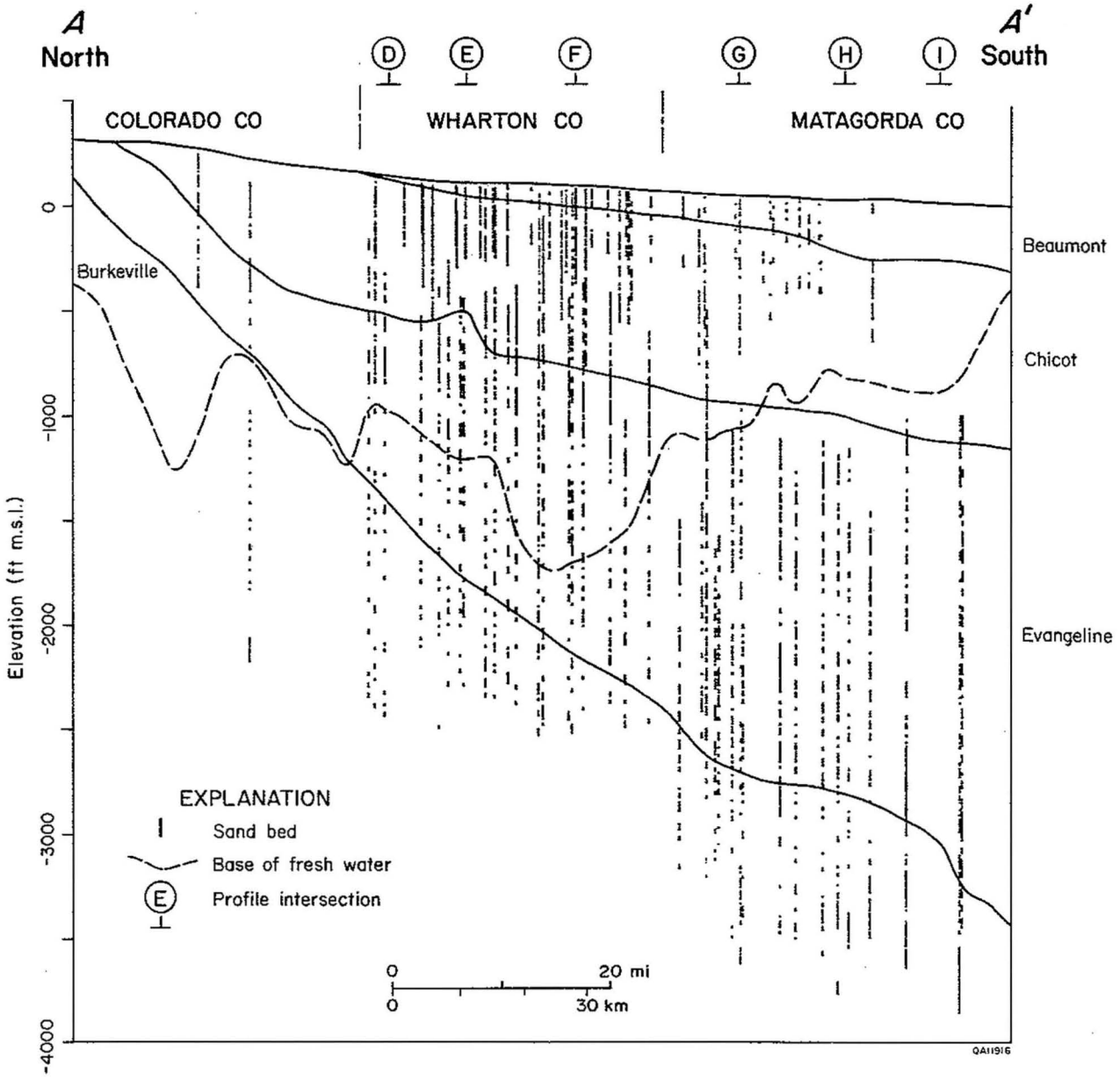

Figure 5. North-south dip cross section A-A′. See figure 1 for location.

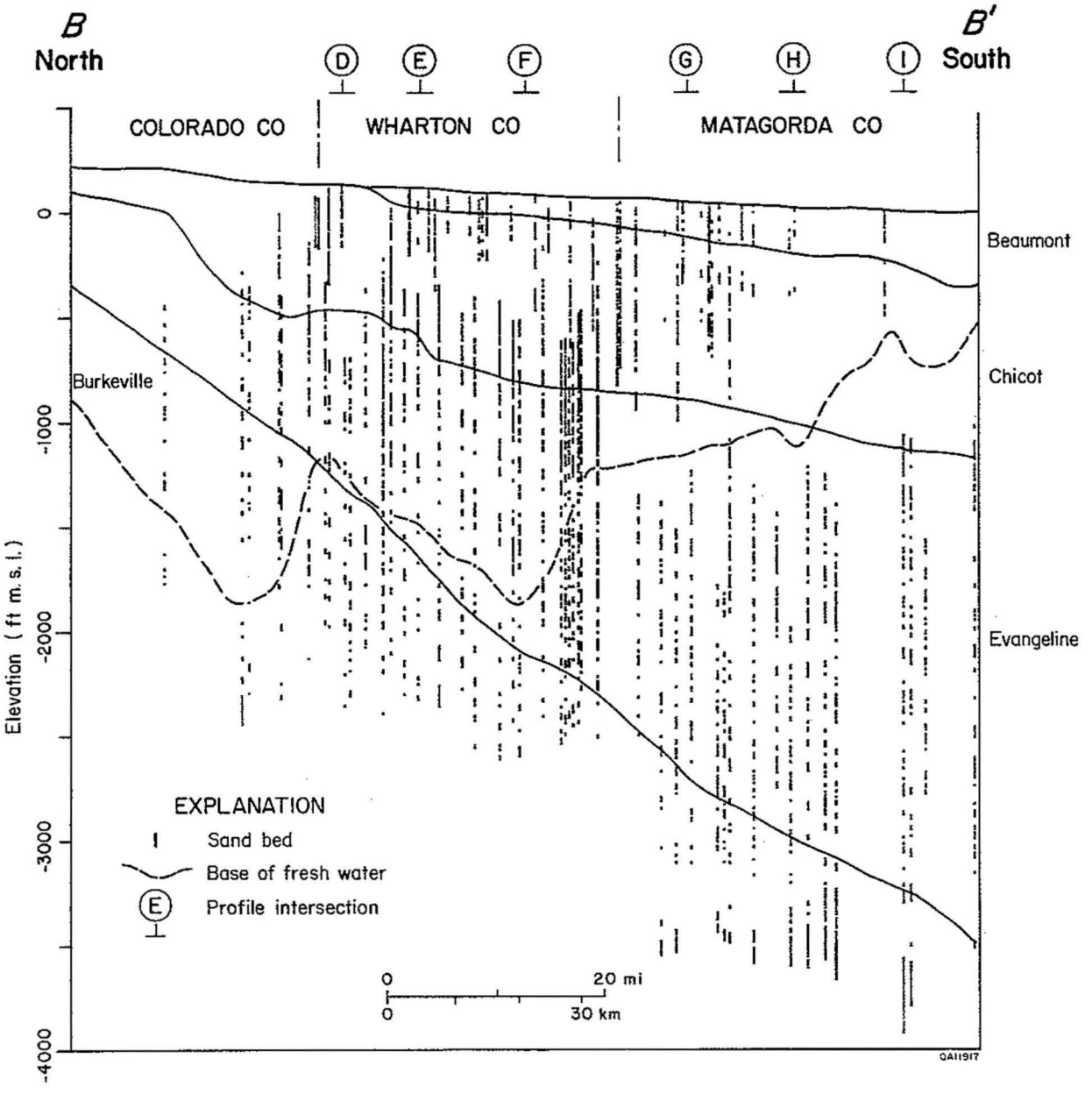

Figure 6. North-south dip cross section B-B′. See figure 1 for location.

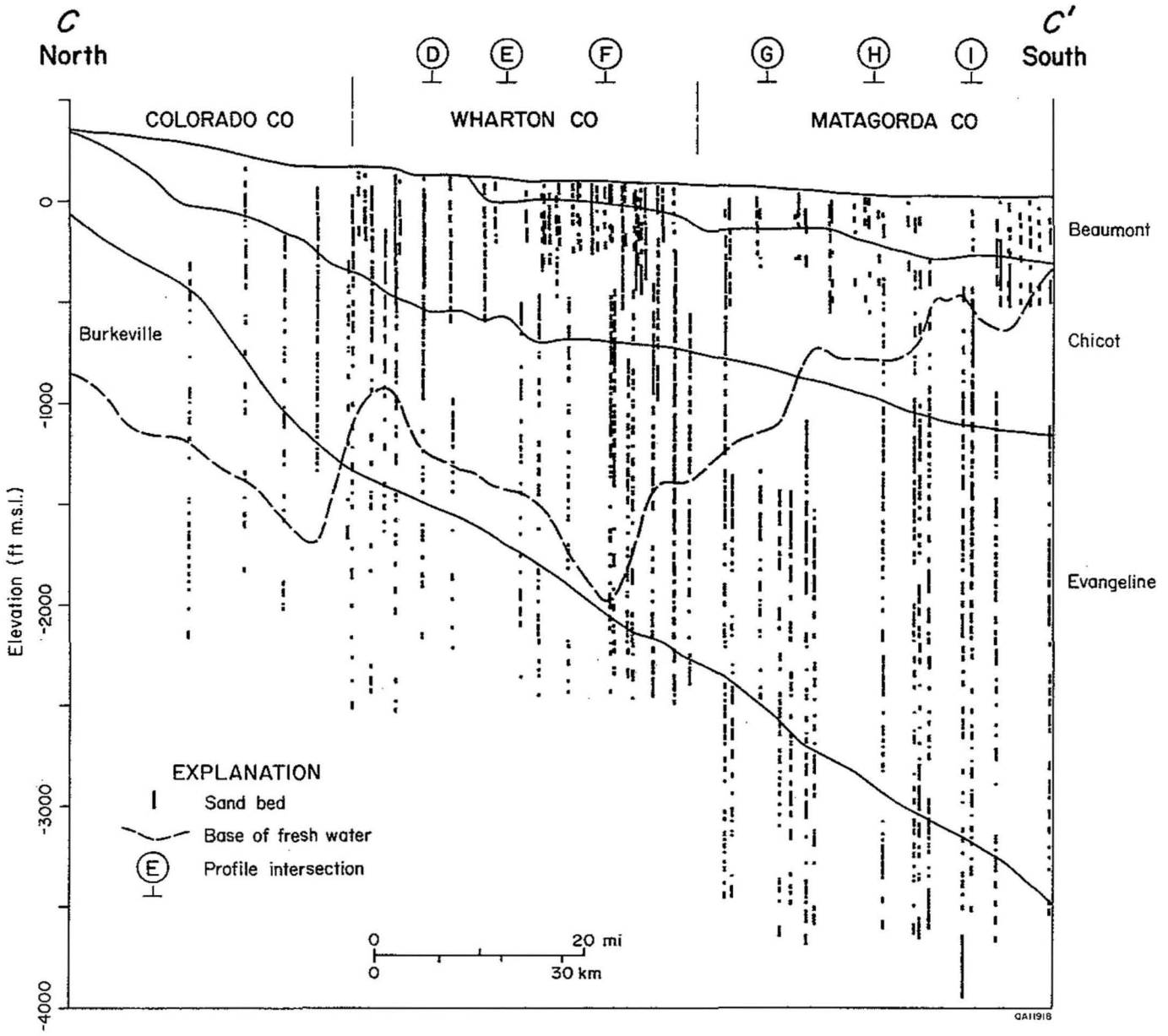

Figure 7. North-south dip cross section C-C′. See figure 1 for location.

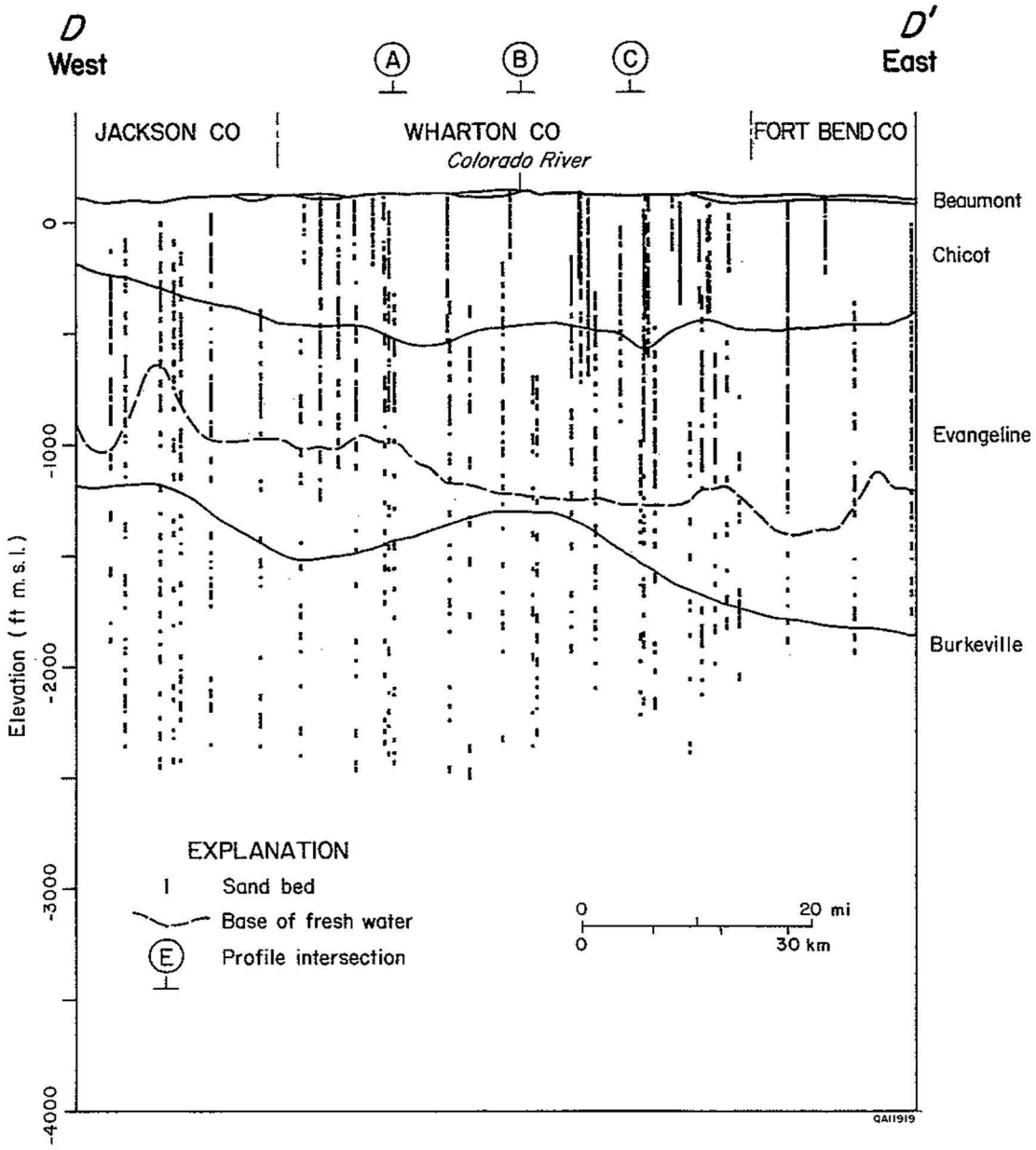

Figure 8. West-east strike cross section D-D′. See figure 1 for location.

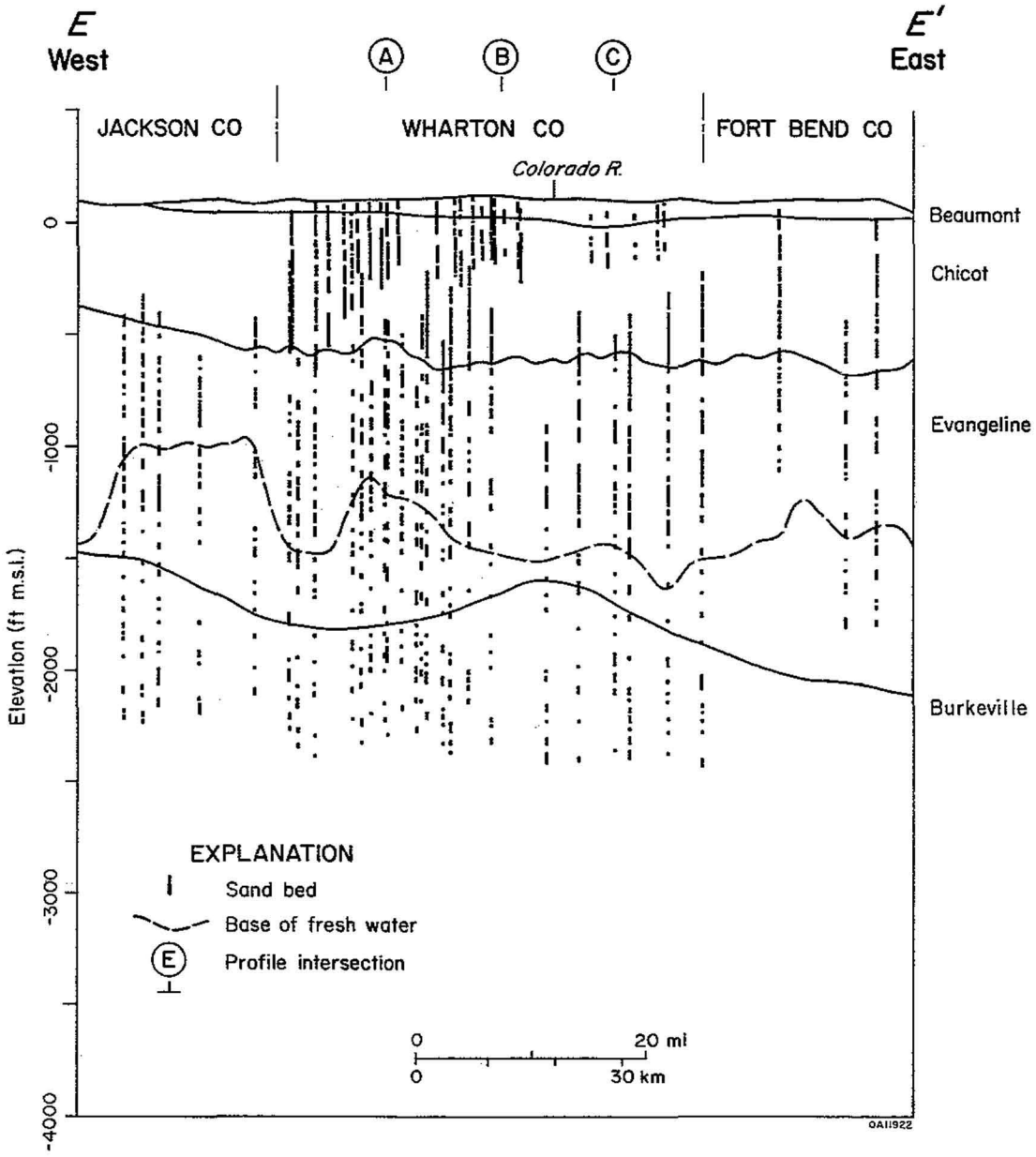

Figure 9. West-east strike cross section E-E′. See figure 1 for location.

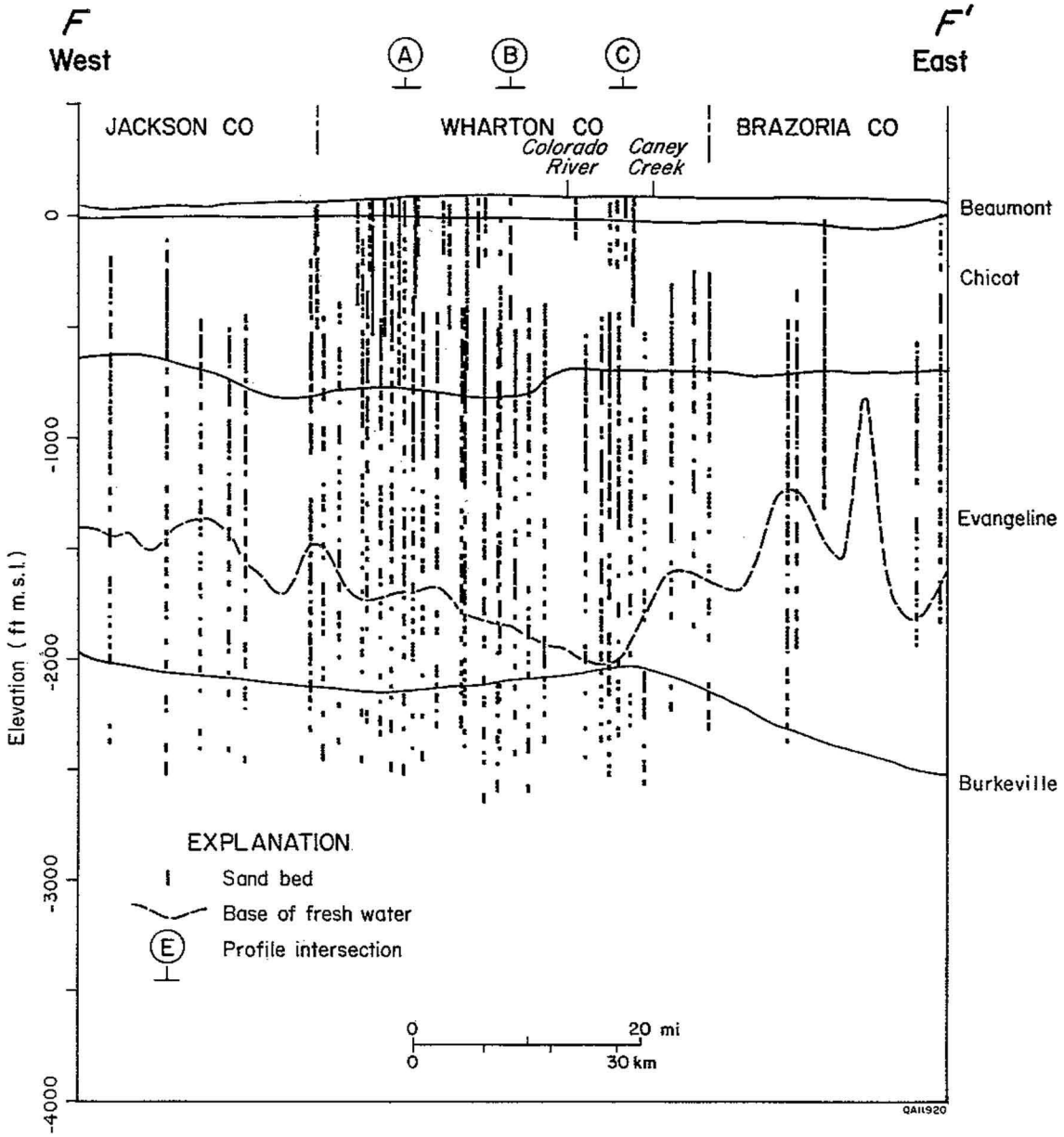

Figure 10. West-east strike cross section F-F'. See figure 1 for location.

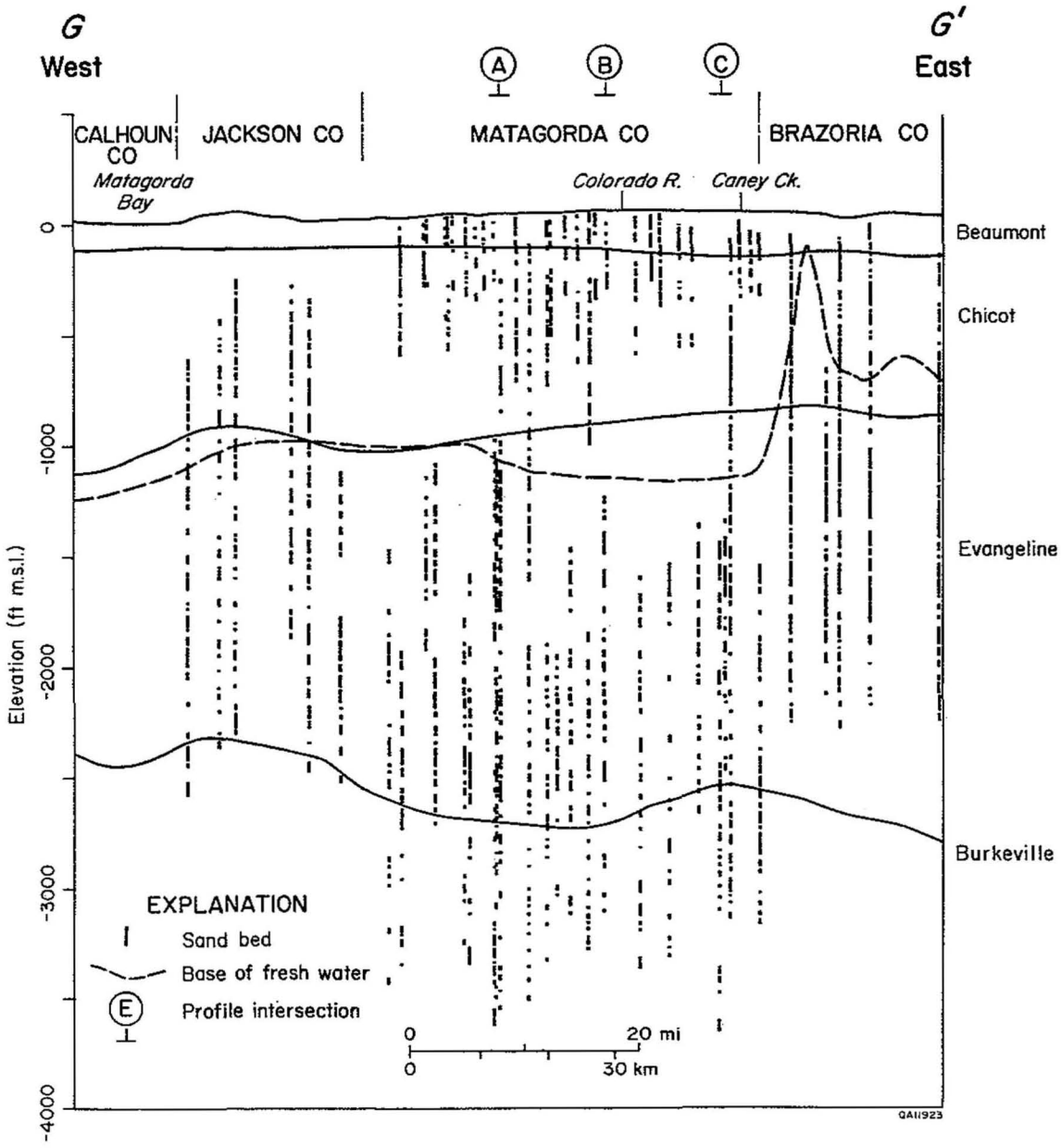

Figure 11. West-east strike cross section G-G'. See figure 1 for location.

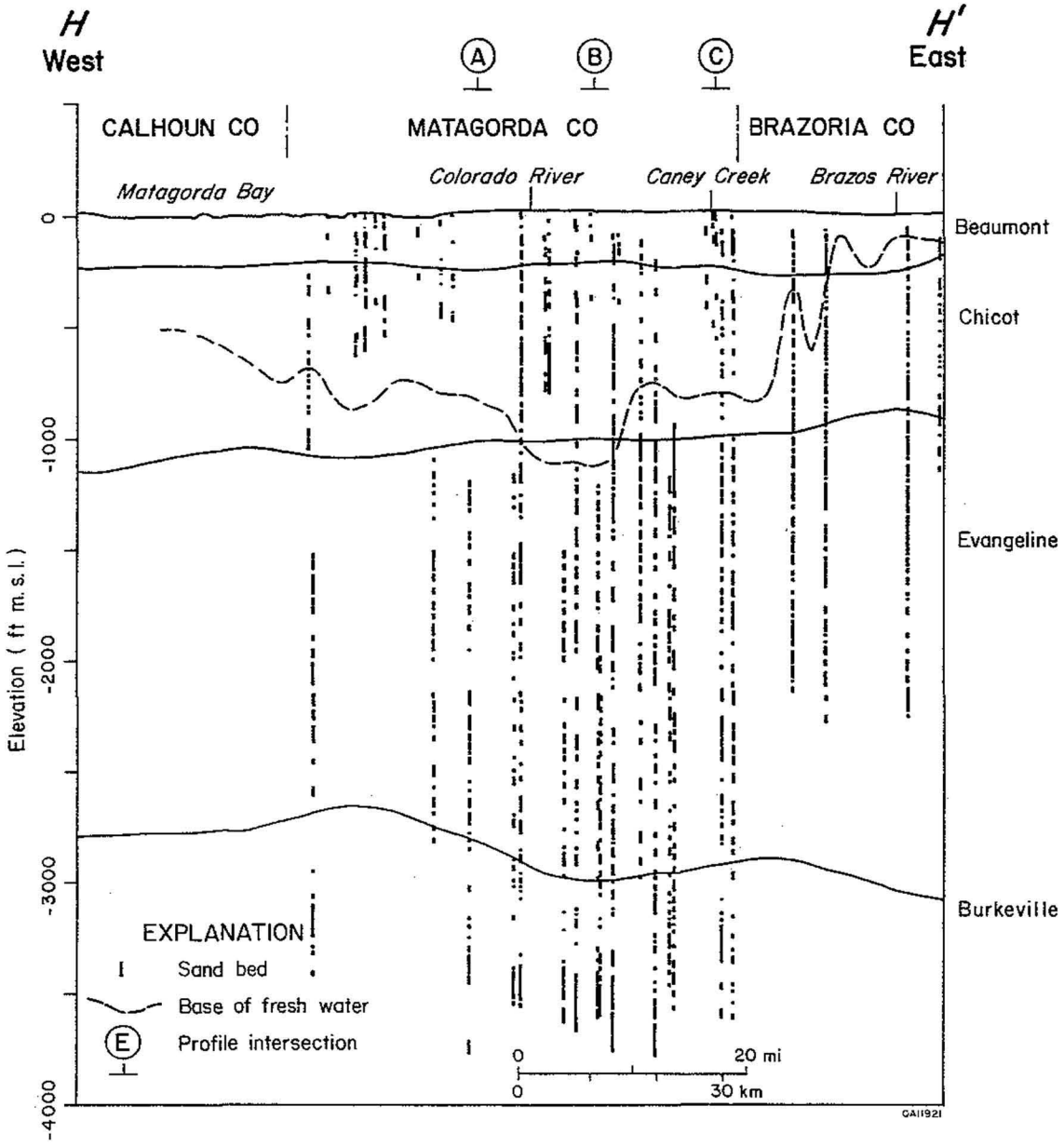

Figure 12. West-east strike cross section H-H′. See figure 1 for location.

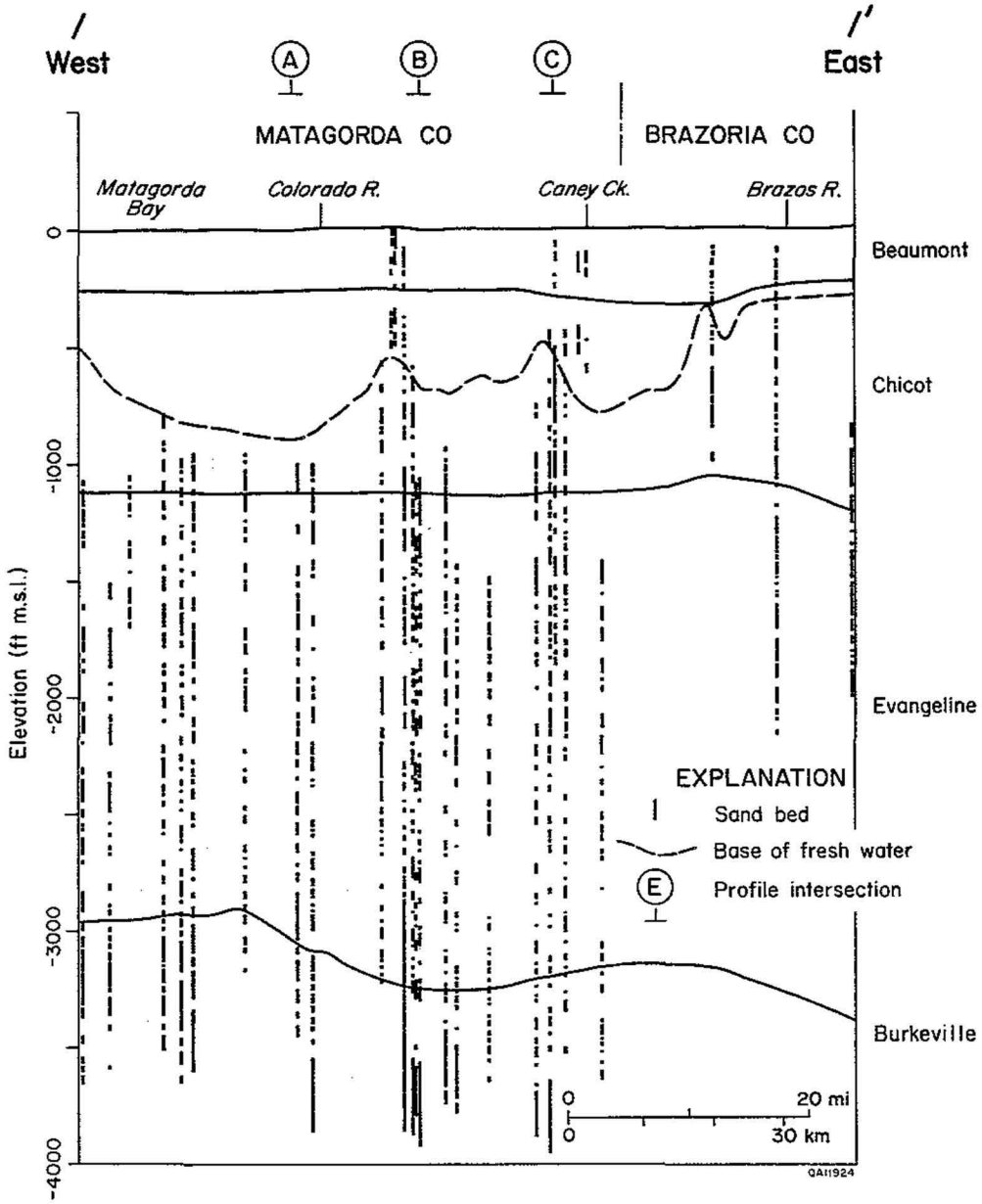

Figure 13. West-east strike cross section I-I'. See figure 1 for location.

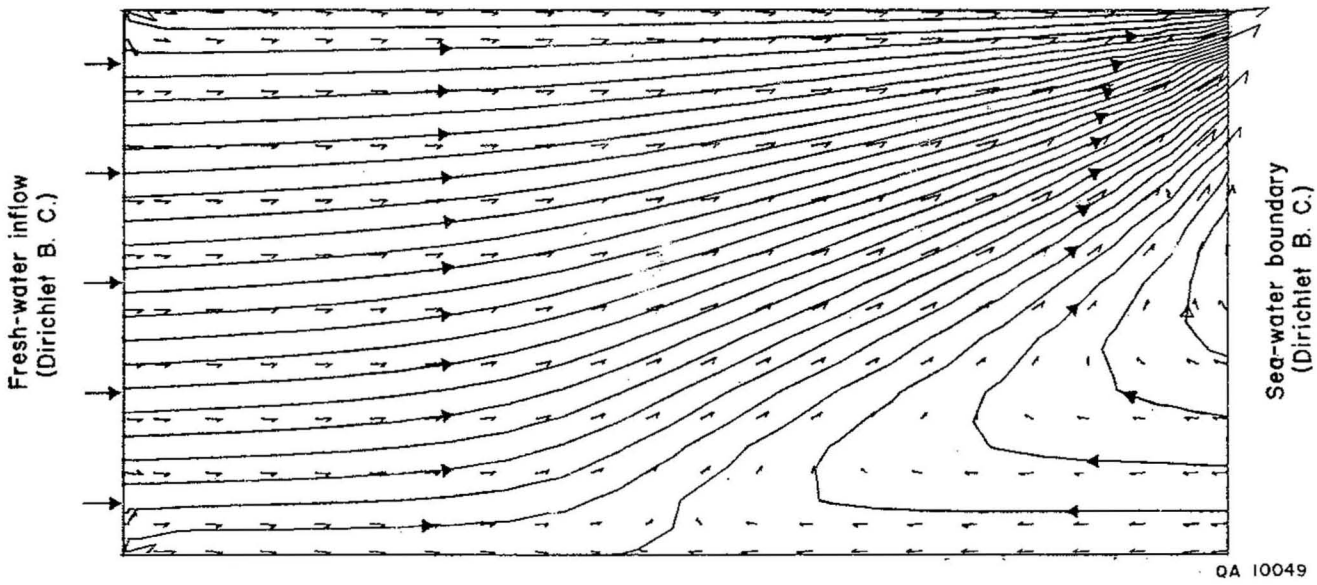

Figure 14. Distribution of flow paths at the interface between seawater beneath the coastal zone and fresh water in a continental ground-water flow system, predicted from a numerical model incorporating variable density of fluids. Dirichlet (prescribed head) boundary conditions are set at both ends of the model. Contour interval is approximately 8.829 ft^3/day (0.25 m^3/day). From Senger (1989).

unit. The stratigraphic interval represented by the third map, the Chicot minus the Beaumont, was split into halves, and sand percentage was mapped in the upper and lower units. Sand distribution had a more well-defined dip orientation in both units, each with overall higher sand percentage values, compared with the original unsplit version. This suggested that the sand distribution pattern of the Willis Formation, which makes up the lower part of the Chicot, is different from the sand distribution of the Lissie Formation, which makes up the upper part of the Chicot aquifer. Cross sections of the depositional systems made by Solis (1981) suggest that a change in depositional patterns coincided with the formation contacts and further justifies the separation of mapping units used in this report. Grouping both units results in an interference in averaged sand percentage values. In the final map version (fig. 15), the lower Chicot was grouped with the Evangeline because geohydrologic data on the Evangeline in the subsurface in Matagorda and Wharton Counties are so sparse that simulation results cannot be well constrained. Data are lacking because there is little ground-water production from the greater depths where salinities are higher.

Sand-distribution patterns of the composite lower Chicot and Evangeline (fig. 15), upper Chicot (fig. 16), and Beaumont Formation (fig. 17) each show dip-elongate trends of high sand percentage differing somewhat in magnitude. Areas with greater than 40 percent sand are shaded in the composite map of the lower Chicot–Evangeline (fig. 15), whereas areas with more than 60 percent sand are shaded in the maps of the upper Chicot and Beaumont (figs. 16 and 17). Sand percentage is generally greater inland, decreasing toward the coast. Toward the southwest boundary of the study area, where there was little data control, the sand-distribution pattern for the Beaumont was extrapolated for use in the numerical model.

Geohydrologic Framework

Hydraulic head measured during the 1930's and 1940's decreases from more than 300 ft in the northern parts of Austin and Colorado Counties, in the outcrop of the Evangeline aquifer unit, to approximately 0 ft at the coast line (fig. 18). Regional maps of the potentiometric surface shown

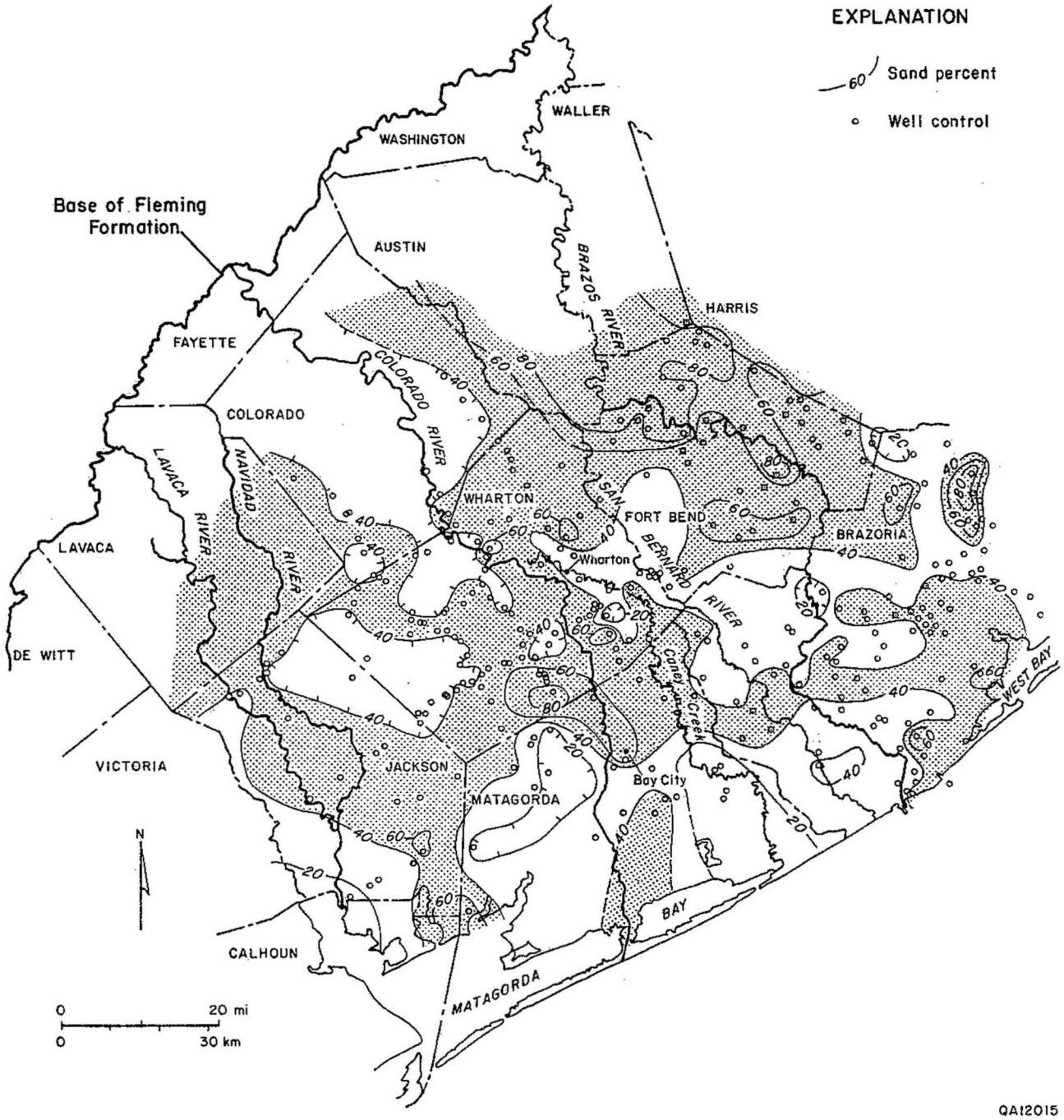

Figure 15. Sand-percent map of the lower Chicot and Evangeline hydrologic units, as defined in table 1. Contour interval is 20 percent. Only sand beds greater than 20 ft thick are included.

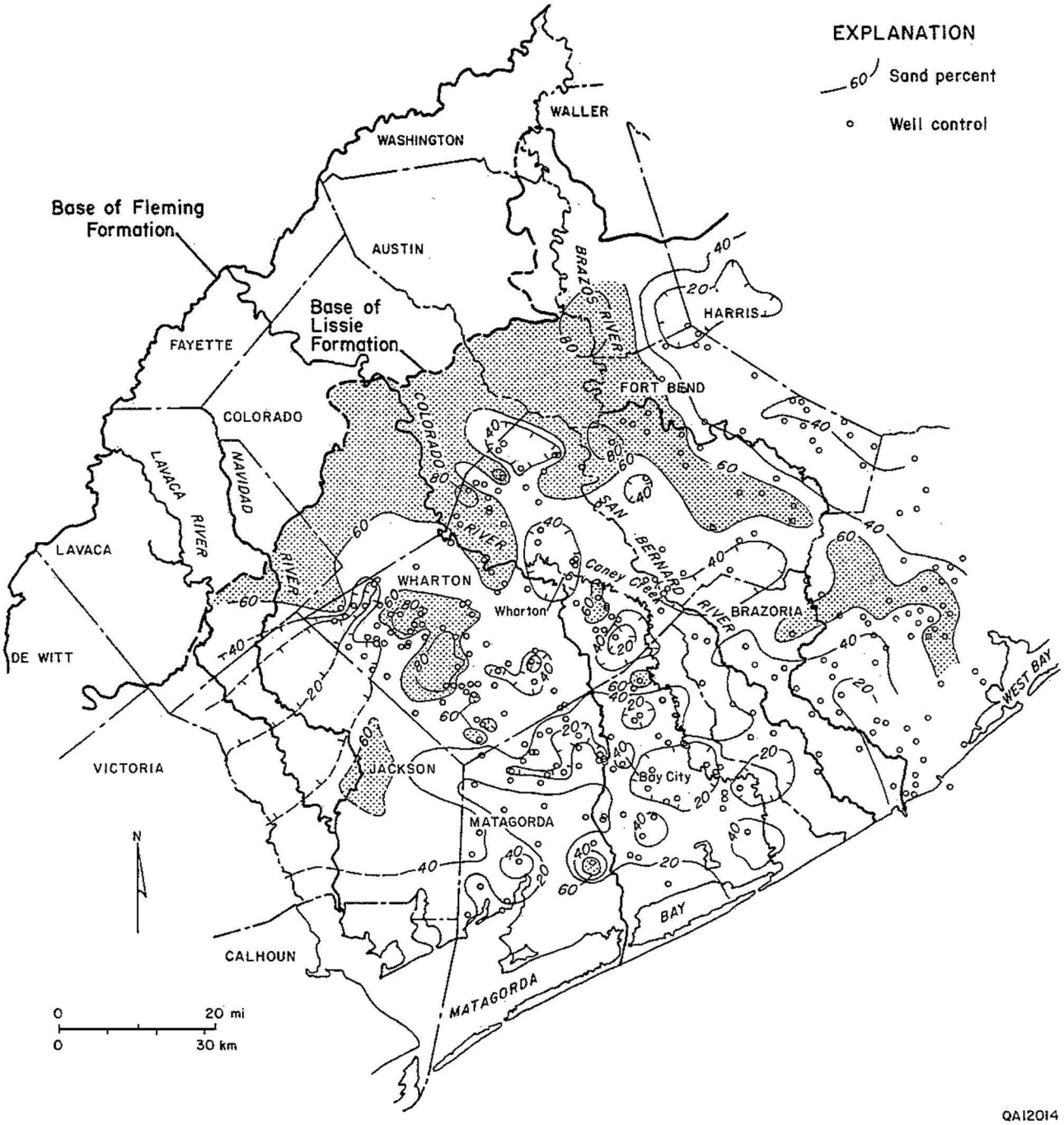

Figure 16. Sand-percent map of the upper Chicot hydrologic unit, as defined in table 1. Contour interval is 20 percent. Only sand beds greater than 20 ft thick are included.

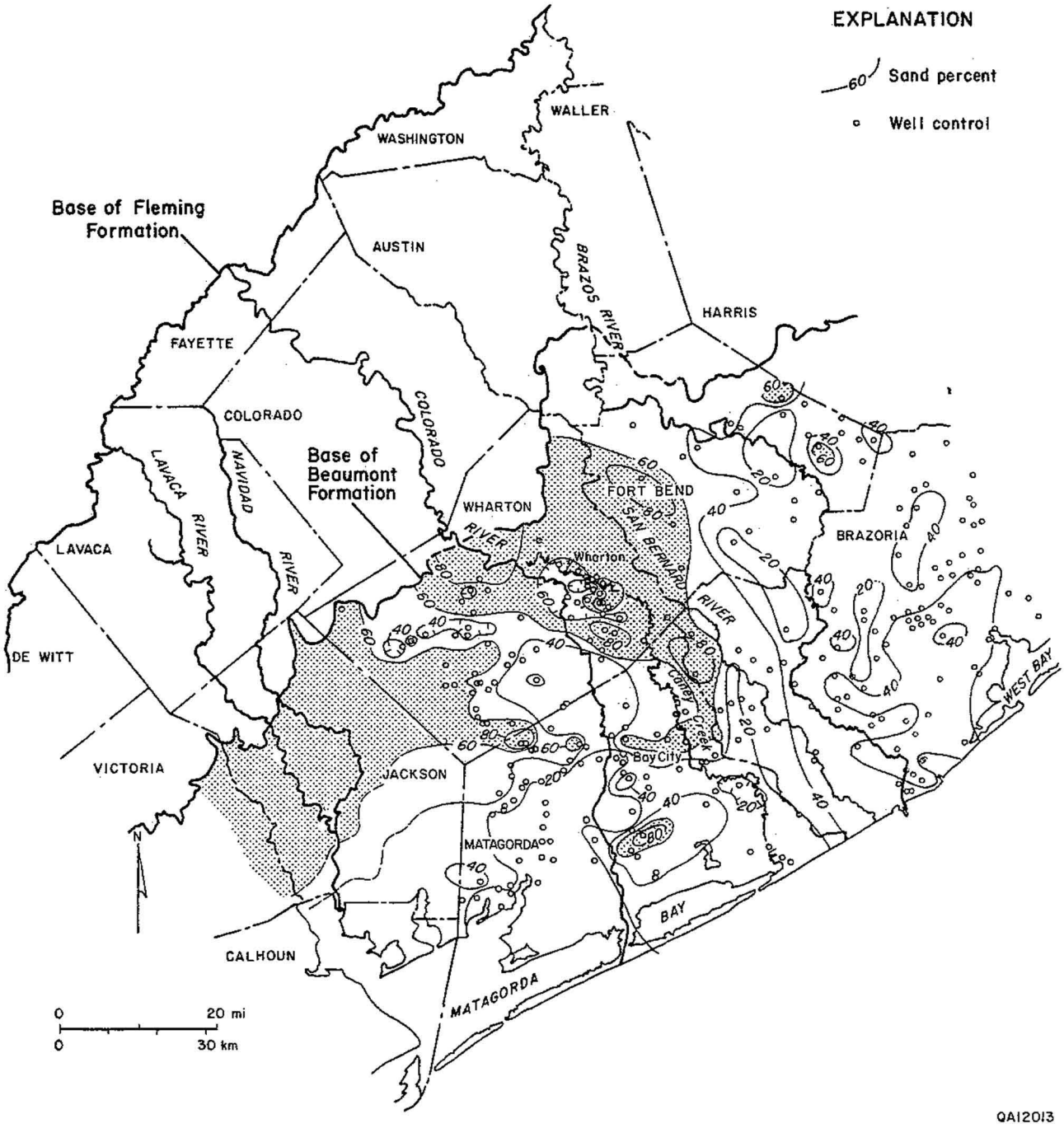

Figure 17. Sand-percent map of the Beaumont Formation. Contour interval is 20 percent. Only sand beds greater than 20 ft thick are included.

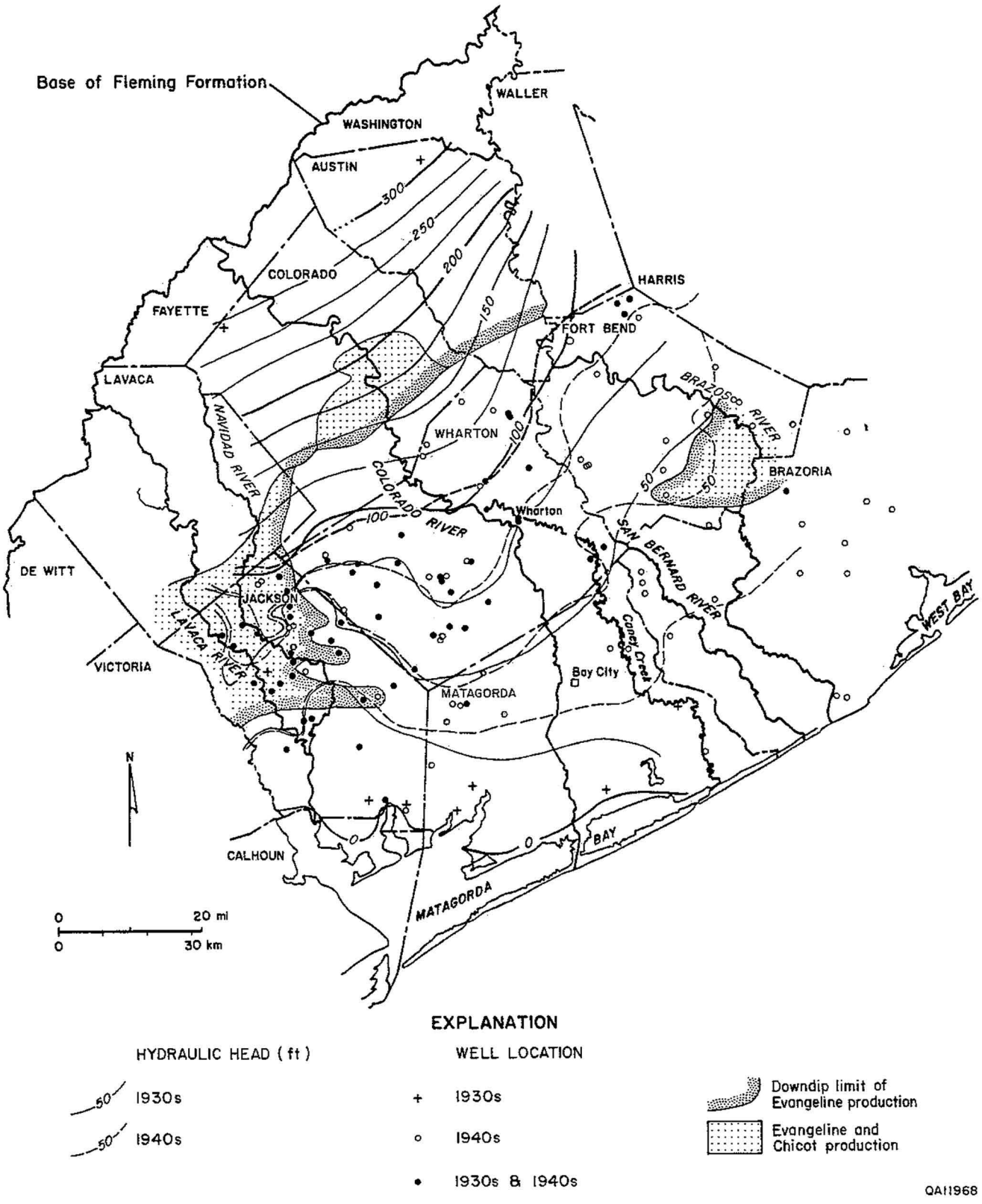

Figure 18. Composite hydraulic-head surface for the Gulf Coast aquifer from measurements made during the 1930's and 1940's. Data from the 1940's are not contoured in Colorado or Austin Counties. Contour interval is 25 ft.

by Ryder (1988) indicate the existence of broad valleys in the potentiometric surface underlying the topographic valleys of the Lavaca and Navidad Rivers to the southwest and the Brazos River to the northeast. Comparison of potentiometric-surface maps for the 1930's and 1940's (fig. 18), 1965/66 (fig. 19), and 1985/86 (fig. 20) indicates how water levels responded to increases in pumping in the region. The position of the 150-, 100-, and 50-ft contours are relatively constant over the 20-yr period. With increasing use of ground water for agricultural, domestic, municipal, and industrial uses since the 1940's, hydraulic head has decreased throughout the study area. The most significant decline in the area occurred in Brazoria and Matagorda Counties. The position of the 0-ft elevation contour in Matagorda and Jackson Counties moved inland between the 1930's and 1940's (fig. 18) and 1960's (fig. 19). The inland retreat of the 0-ft hydraulic-head contour indicates that the landward-directed gradient for advective flow of seawater has increased, which will eventually and increasingly influence ground-water salinity in the coastal part of the aquifer. Carr and others (1985) estimated that water-level declines of as much as 80 to 100 ft have accrued from 1900 through 1975 in western Wharton and eastern Jackson Counties. The drop of hydraulic head in Matagorda and Wharton Counties, however, has not been nearly as great as the 300- to 420-ft decline experienced in the Harris County area to the northeast.

Vertical sections show how hydraulic head varies with depth in the different aquifer units (figs. 21–23). Lines of section are the same as those depicting sand-bed distribution. Contours are based not only on well locations given on each section but also on intersections where the dip and strike sections cross. Hydraulic head values included in the cross sections were not culled on the basis of year of measurement; therefore, the sections include original (steady-state) as well as declining (transient) hydraulic heads. Figure 24 is a fence diagram illustrating the hydraulic-head variation in three dimensions. The gradients in hydraulic head indicate the presence of vertical components of ground-water flow within the coastal aquifer setting.

Hydrologic properties vary within each aquifer unit (table 2). Measured transmissivity values calculated from pumping tests in the Chicot and Evangeline aquifers (appendix) nearly follow a logarithmic-normal distribution (solid-line histogram, fig. 25); therefore, mean and standard

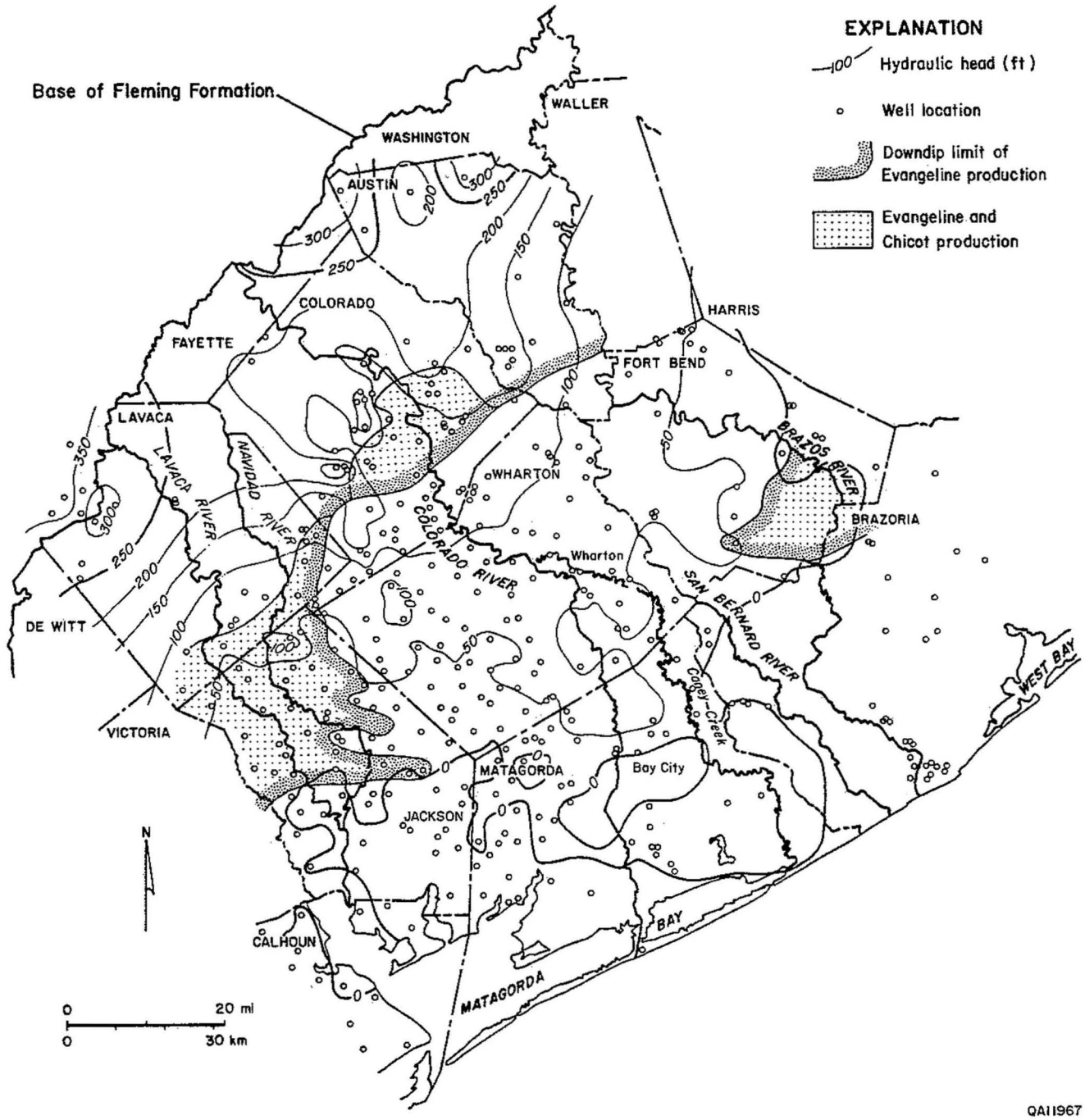

Figure 19. Composite hydraulic-head surface for the Gulf Coast aquifer in study area for the 2-yr period 1965/66. The map does not differentiate aquifer units at various depths. Contour interval is 25 ft.

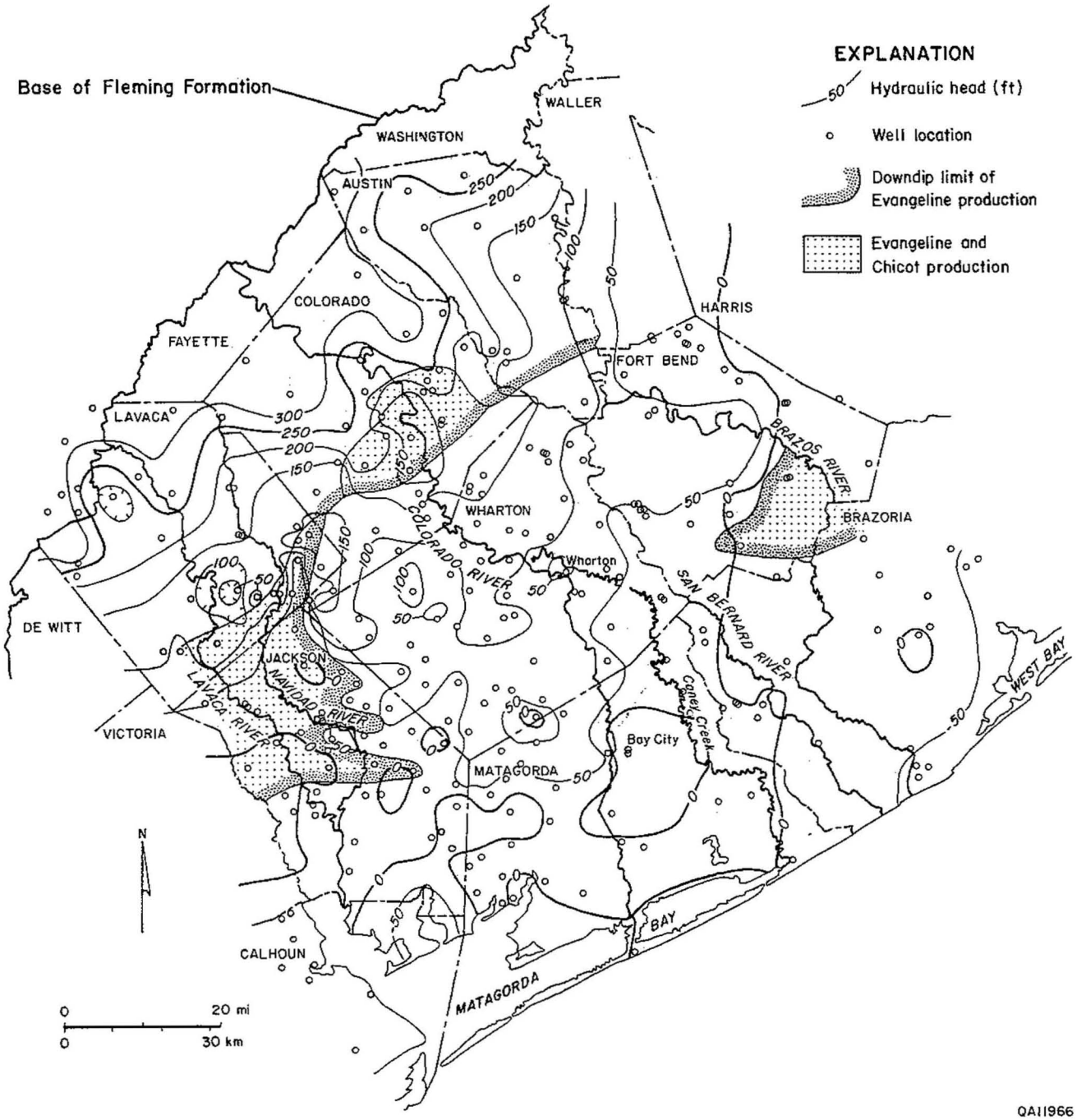

Figure 20. Composite hydraulic-head surface for the Gulf Coast aquifer in study area for the 2-yr period 1985/86. The map does not differentiate aquifer units at various depths. Contour interval is 25 ft.

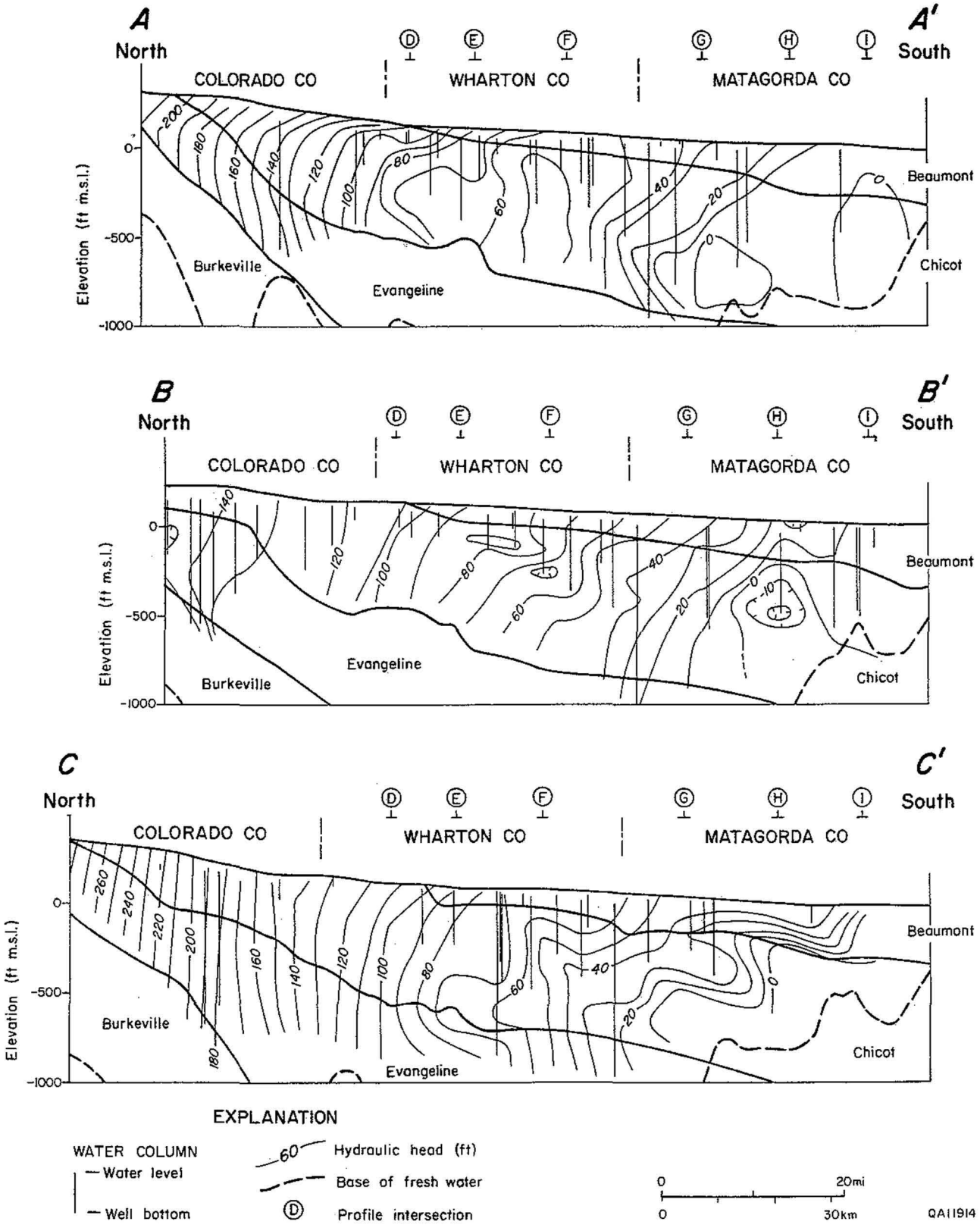

Figure 21. Cross section of hydraulic head along dip lines A-A′, B-B′, and C-C′. See figure 1 for location. Contour interval is 10 ft.

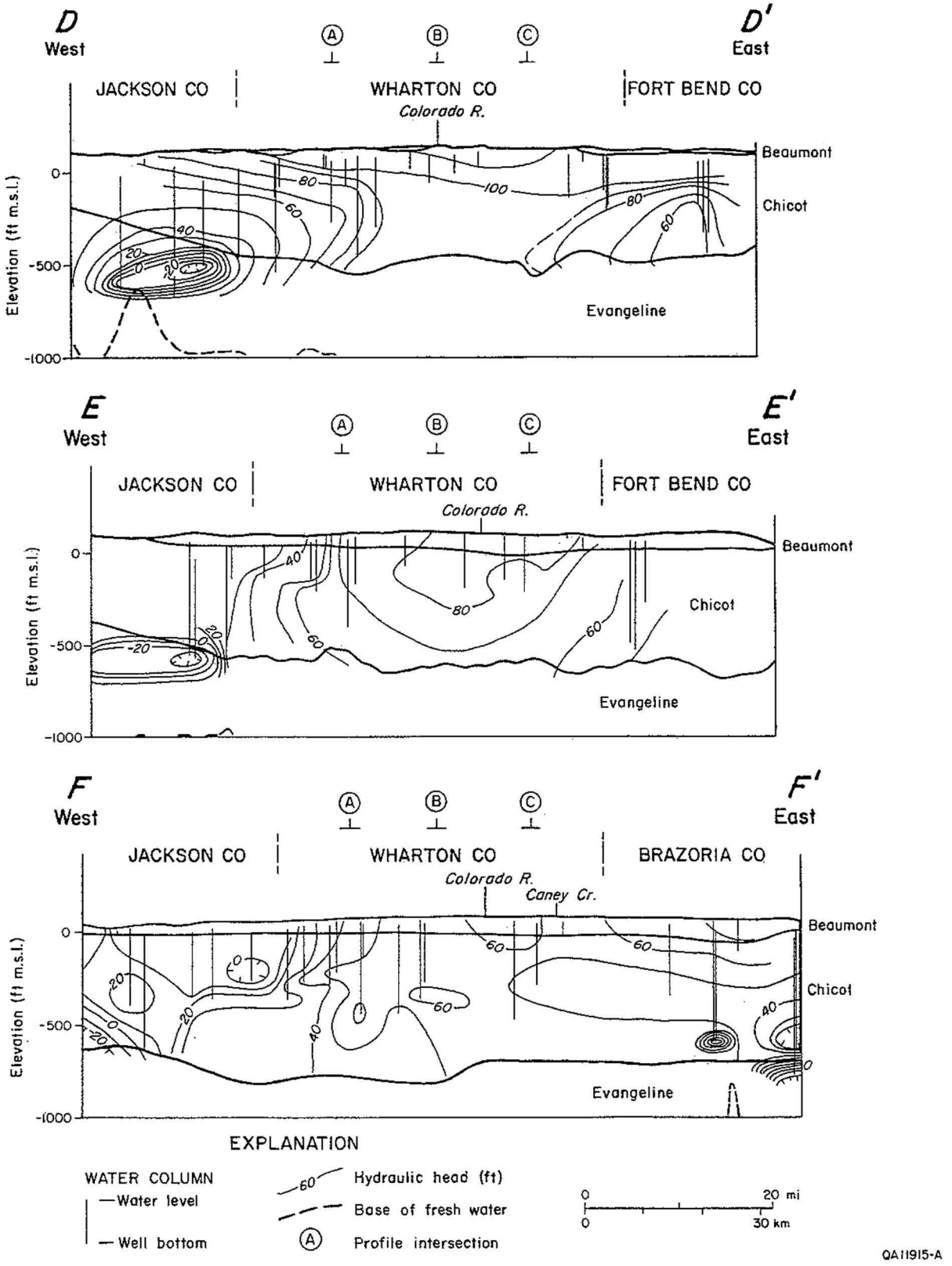

Figure 22. Cross section of hydraulic head along strike lines D-D′, E-E′, and F-F′. See figure 1 for location. Contour interval is 10 ft.

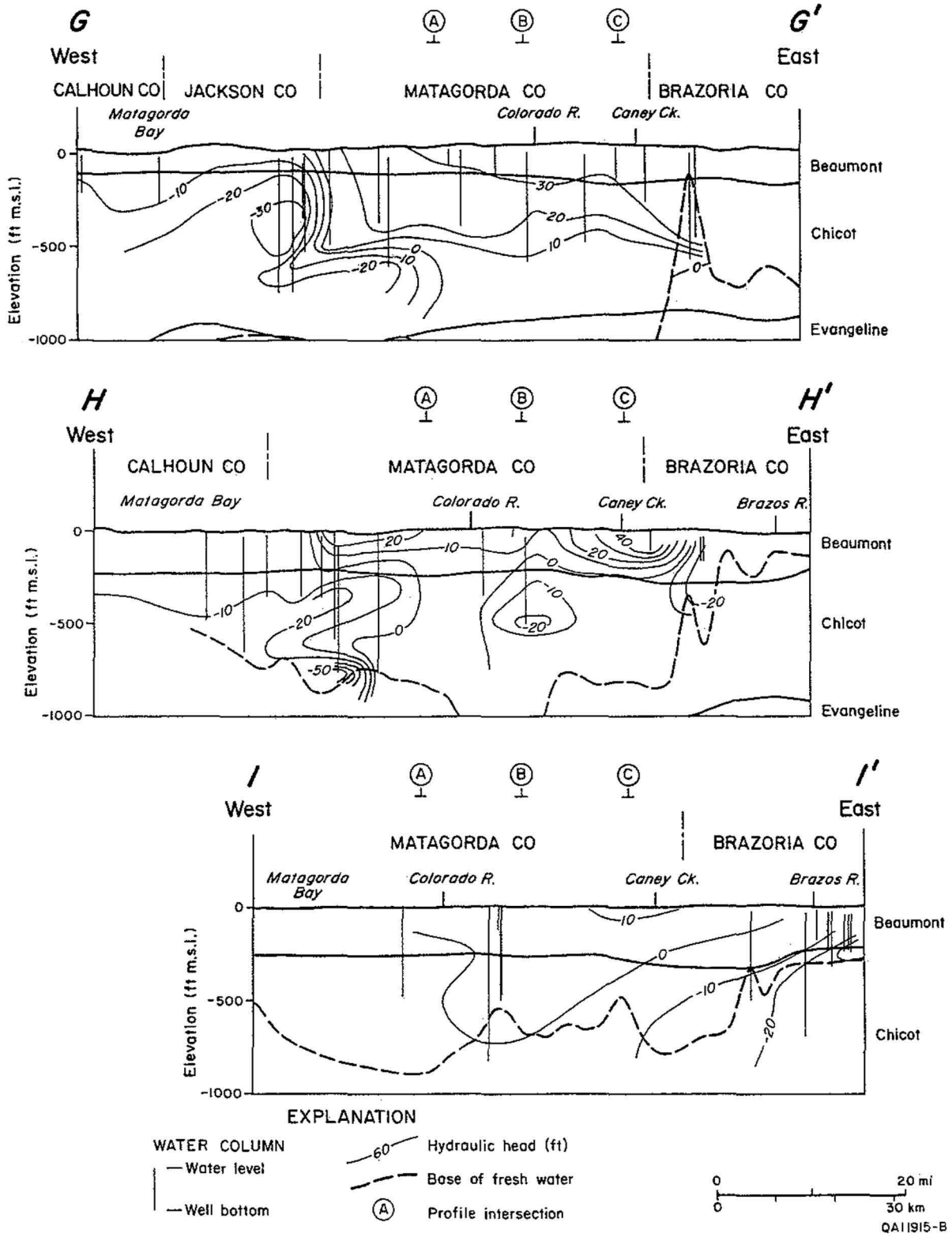

Figure 23. Cross section of hydraulic head along strike lines G-G′, H-H′, and I-I′. See figure 1 for location. Contour interval is 10 ft.

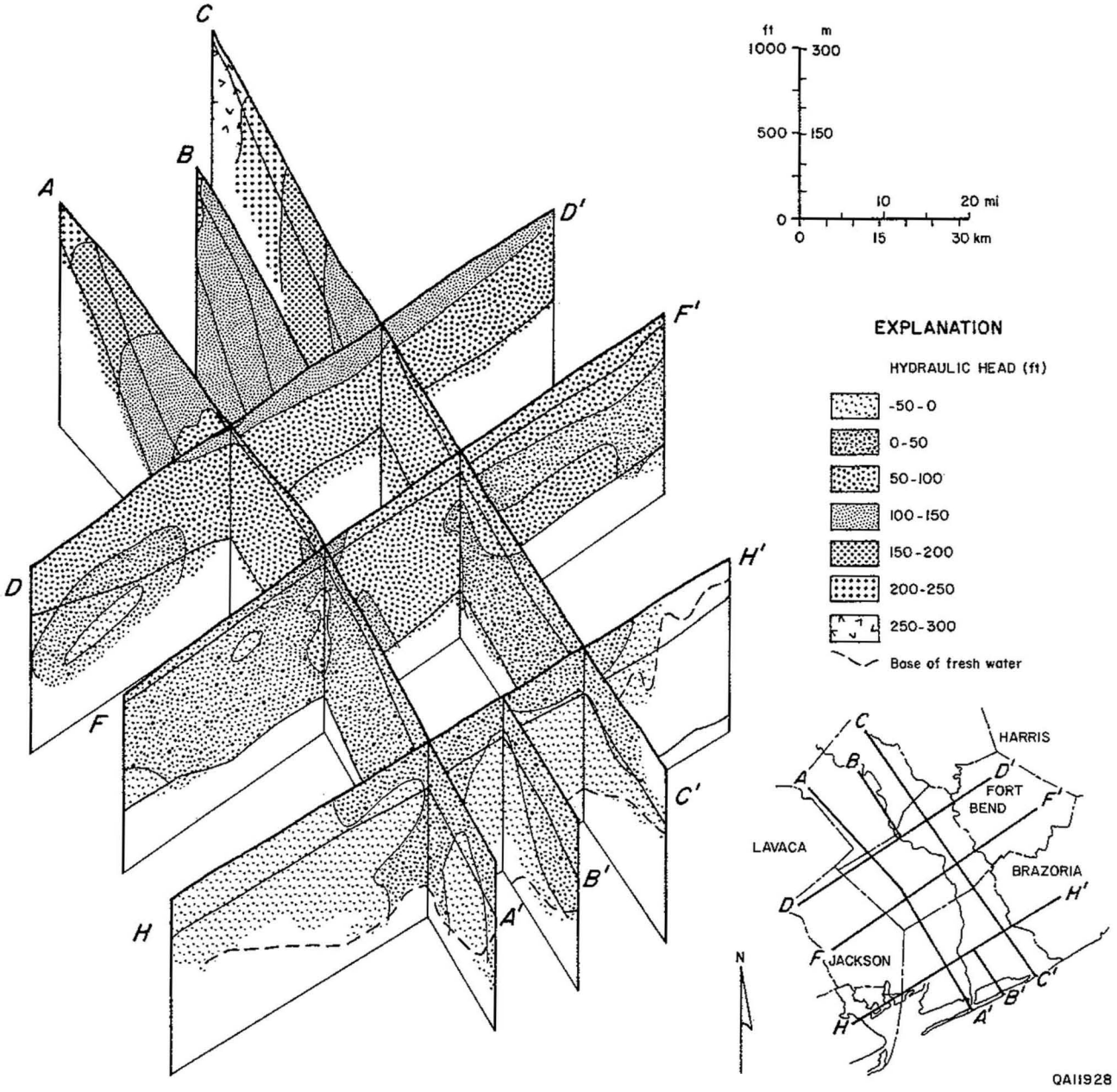

Figure 24. Fence diagram showing the distribution of hydraulic head in the Beaumont, Chicot, and Evangeline hydrologic units.

Table 2. Hydrologic parameters used in the numerical model.

Parameter	Observed		Initial			Calibrated		
	Beaumont Formation	Chicot and Evangeline*	Layer 1	Layer 2	Layer 3	Layer 1	Layer 2	Layer 3
Mean transmissivity (ft^2/day)	-	7,400	141	1,698	832	933	7,413	4,074
Maximum transmissivity (ft^2/day)	-	53,345	3,315	37,120	23,306	28,835	75,766	48,526
Minimum transmissivity (ft^2/day)	-	267	7	52	0.3	9	358	0.4
Mean hydraulic conductivity (ft/d)	13	50	1	5	1	7	23	5
Maximum hydraulic conductivity (ft/d)	22	2,125	40	337	28	22	440	358
Minimum hydraulic conductivity (ft/d)	5.70	6	0.04	0.25	0.04	0.13	0.79	0.15
Mean storativity	-	4.00E-4	1.32E-1	5.98E-3	1.28E-3	1.30E-1	5.90E-3	1.50E-3
Maximum storativity	-	-	2.39E-1	3.95E-1	2.96E-1	2.39E-1	8.89E-1	6.66E-1
Minimum storativity	-	1.80E-5	3.11E-2	2.51E-4	1.06E-4	3.11E-2	6.28E-6	7.20E-6
Mean vertical hydraulic conductivity (ft/d)	-	-	1.50E-5	1.06E-4	3.60E-6	4.75E-3	2.38E-3	5.58E-4
Maximum vertical hydraulic conductivity (ft/d)	-	-	7.99E-4	6.07E-3	1.07E-4	6.76E-1	2.30E-1	2.63E-1
Minimum vertical hydraulic conductivity (ft/d)	-	-	6.05E-8	5.54E-6	6.91E-8	1.05E-4	7.94E-5	2.27E-5

* see Appendix

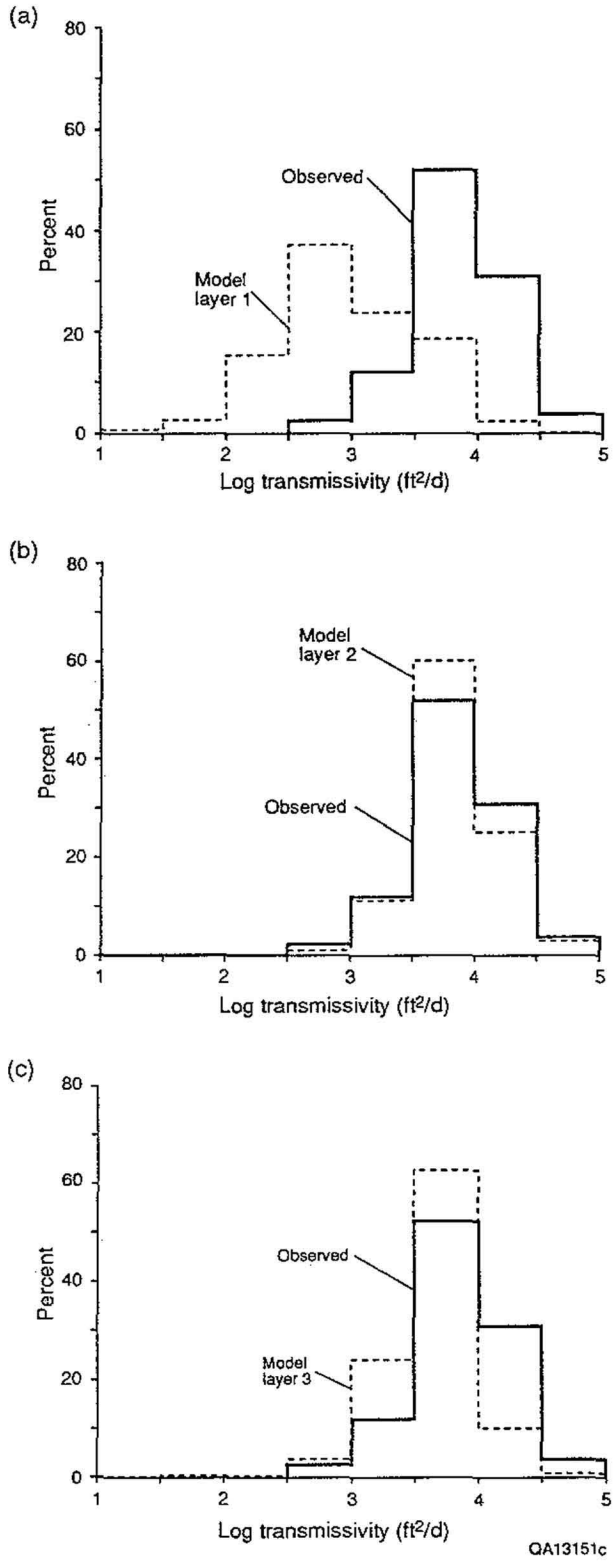

Figure 25. Distribution of estimated transmissivity in the Chicot and Evangeline aquifers (solid line) and calibrated transmissivity values (dashed lines) in layers 1 (a), 2 (b), and 3 (c) of the numerical model.

deviations were calculated using the logarithms of values. The mean observed transmissivity is approximately 7,400 ft^2/day (log(T) = 3.87); the standard deviation of the logarithm of transmissivities is 0.39. The mean value of hydraulic conductivity is approximately 50 ft/day (log(K) = 1.69); the standard deviation of the logarithm of hydraulic conductivity is 0.40. Fewer data are available for the Beaumont Formation. Bentley (1980) tested hydraulic conductivity of Beaumont sand deposits in Brazoria County. Hydraulic conductivity ranged from 5.7 to 22 ft/day, and the average value of 7 measurements was 13 ft/day. Carr and others (1985) estimated that transmissivity in the Gulf Coast aquifer in the study area ranges from 12,000 to 18,000 ft^2/day in the Chicot and from 6,000 to 9,000 ft^2/day in the Evangeline. Carr and others (1985) estimated storativity to range from 0.05 to 0.1 in the outcrops of the Chicot and Evangeline aquifers, respectively, and to decrease gradually with increasing confinement in the subsurface to values of 0.0004 to 0.0005. Ryder (1988) used constant values of hydraulic conductivity in each of his model layers, assigning a value of 170 ft/day to the layer representing the Holocene–upper Pleistocene permeable, 20 ft/day to the lower Pleistocene–upper Pliocene permeable zone, and 60 ft/day to the lower Pliocene-upper Miocene permeable zone. Ryder (1988) estimated vertical conductivities of the three layers to be 10^{-2}, 10^{-3}, and 10^{-4} ft/day.

Ca-HCO_3, Na-HCO_3, and mixed-cation-HCO_3 hydrochemical facies are most common in this part of the Gulf Coast aquifer (figs. 26–28). Hydrochemical facies are named for the ions that account for at least 50 percent of total equivalent concentration as depicted in Piper diagrams (Piper, 1944; Back, 1966); mixed-cation and mixed-anion hydrochemical facies are waters in which no one cation or anion is dominant. As indicated by Kreitler and others (1977) for the Houston–Galveston area, a Ca-HCO_3 facies occurs mainly inland near the recharge area, whereas a Na-HCO_3 facies occurs downdip in the aquifer system; a mixed-cation-HCO_3 facies generally lies intermediate between the other two facies. Foster (1950) and Kreitler and others (1977) interpreted the hydrochemical gradation to be due to ionic exchange of dissolved calcium for sodium adsorbed on clays as ground water flows downdip in the Gulf Coast aquifer. The position of the boundary between the hydrochemical facies is a function of flow rate, supply of calcium (mainly from calcite

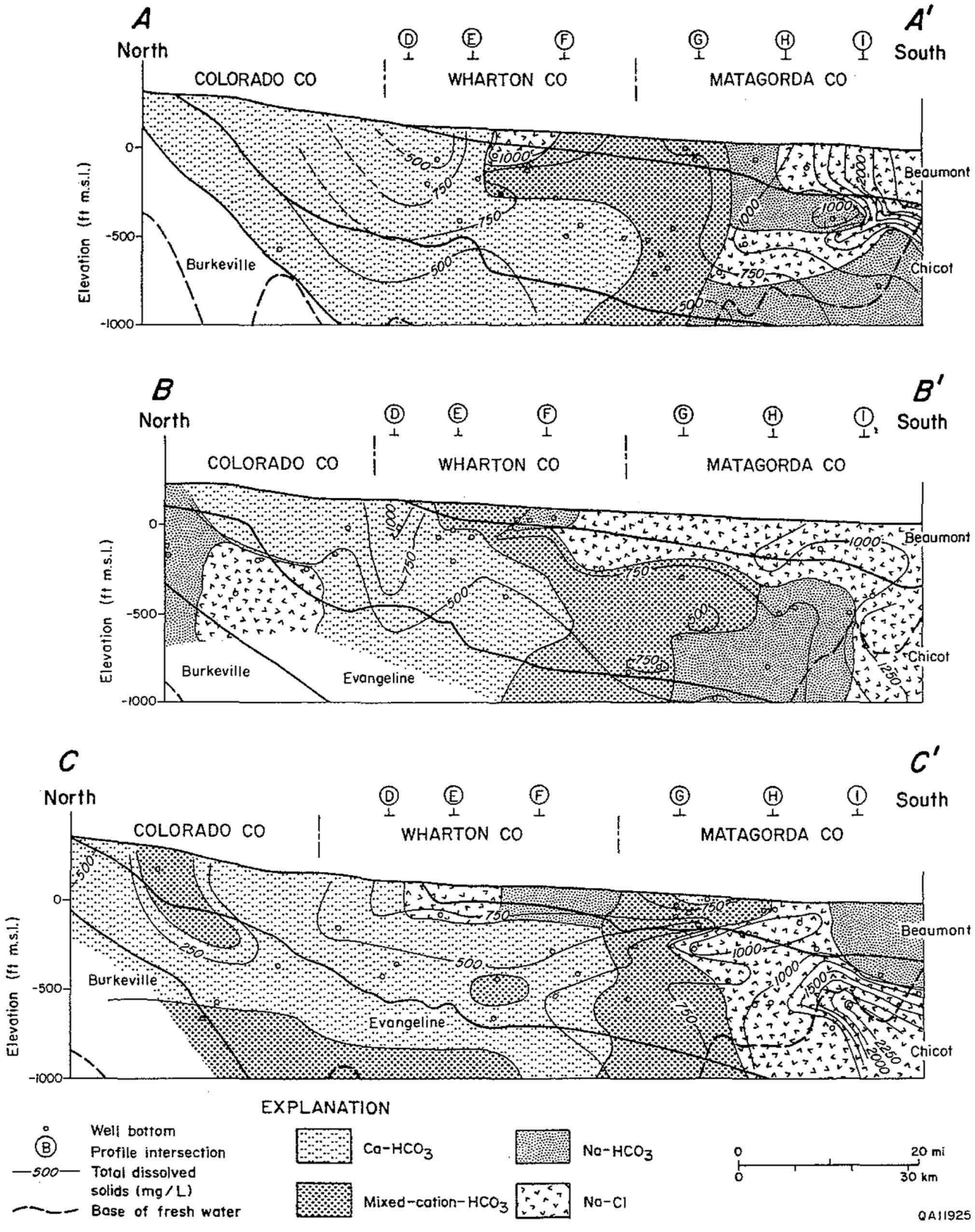

Figure 26. Cross section of hydrochemical facies and TDS along dip lines A-A′, B-B′, and C-C′. See figure 1 for location. Salinity contour interval is 250 mg/L.

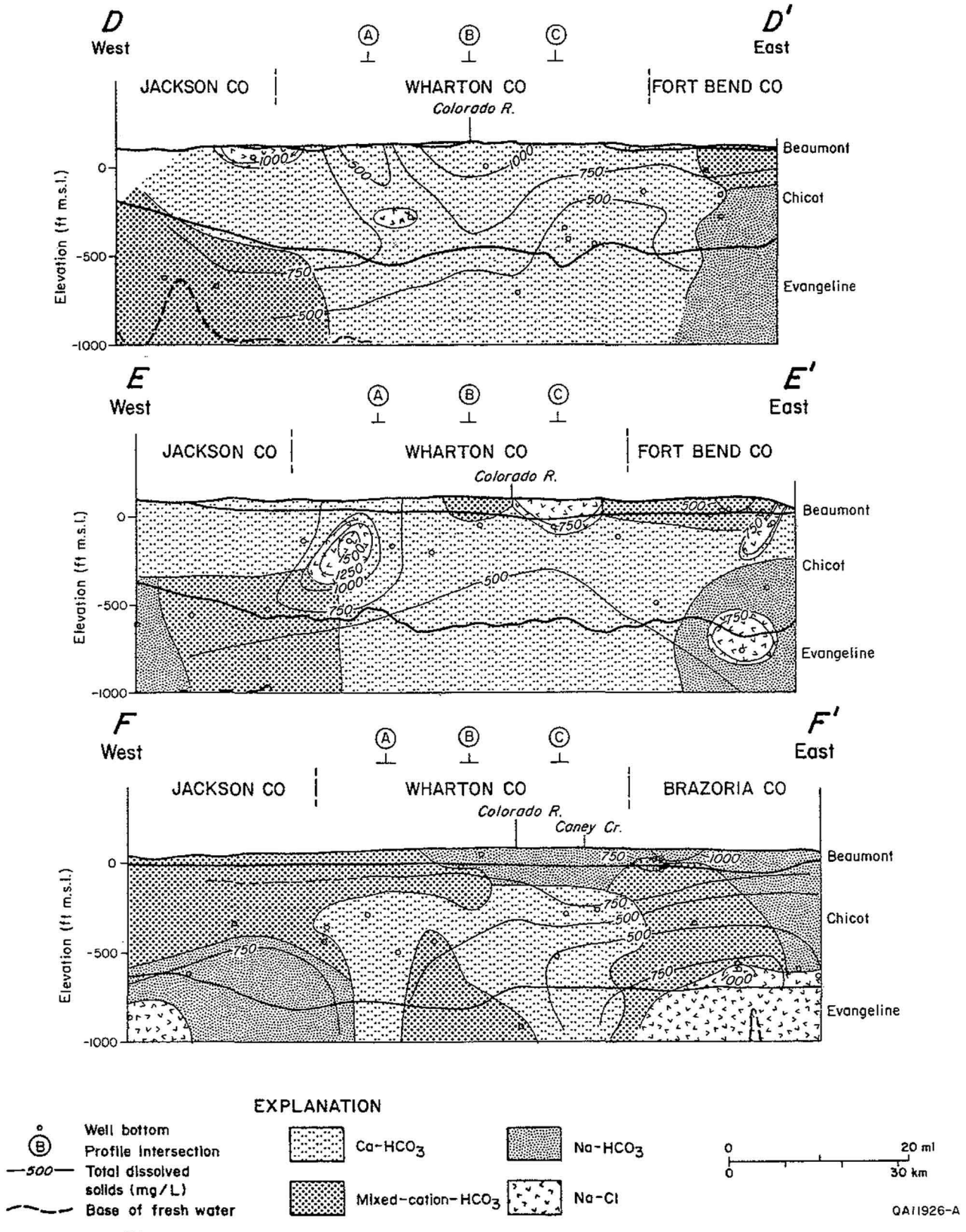

Figure 27. Cross section of hydrochemical facies and TDS along strike lines D-D′, E-E′, and F-F′. See figure 1 for location. Salinity contour interval is 250 mg/L.

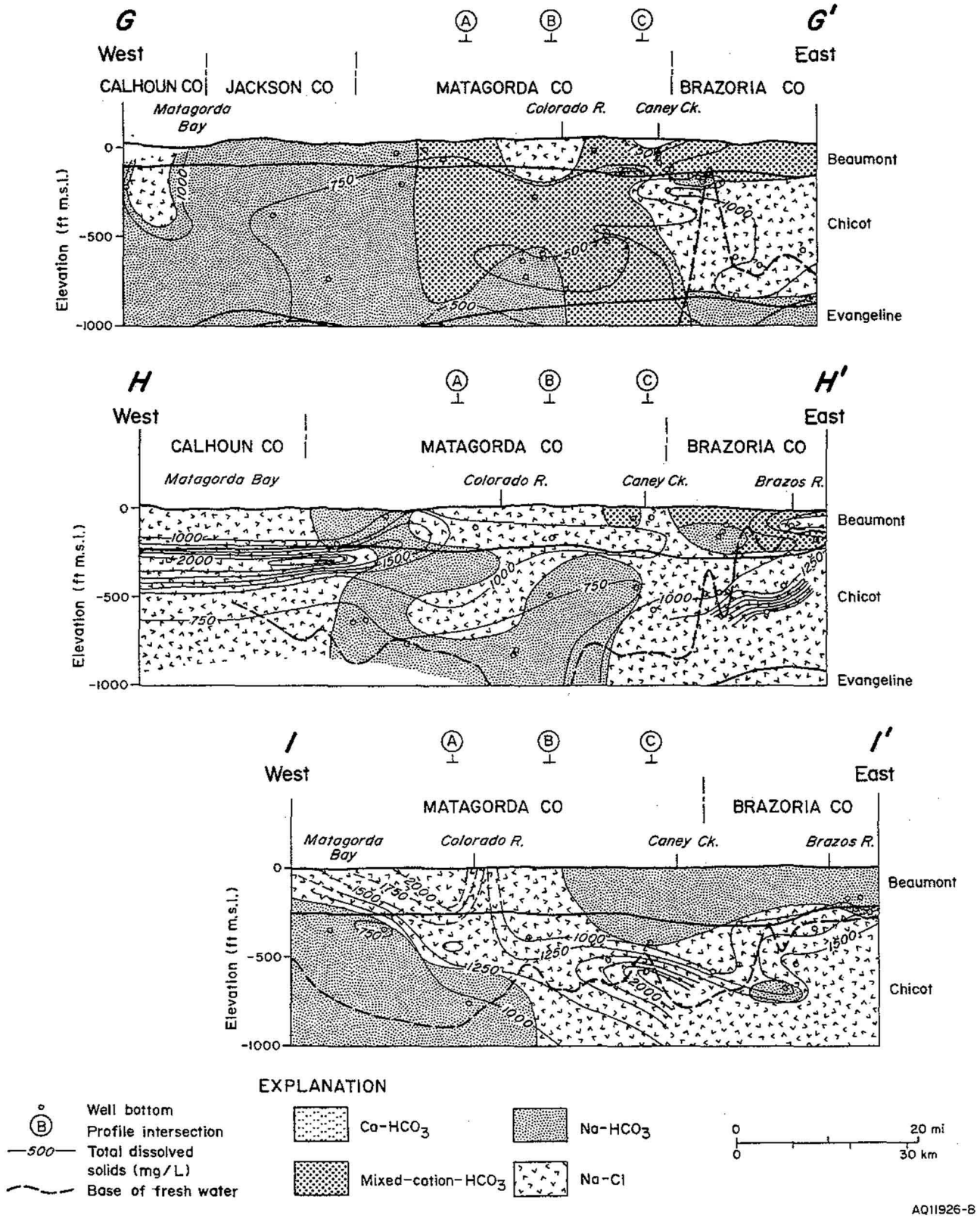

Figure 28. Cross section of hydrochemical facies and TDS along strike lines G-G′, H-H′, and I-I′. See figure 1 for location. Salinity contour interval is 250 mg/L.

and calcium-rich silicates in the outcrop), and amount of exchangeable sodium. In addition, Na-Cl and Ca-Cl facies are also significant in the study area. Na-Cl hydrochemical facies most likely reflect the influence of seawater on ground-water quality, whether as a result of presence of connate seawater in the upper Cenozoic sediments, recharge of sodium and chloride ions borne inland as aerosols, or subsurface intrusion of seawater owing to density gradients in ground water. The origin of Ca-Cl facies with salinity less than 3,000 mg/L, mapped with Na-Cl facies, is less well understood. Mixed-anion facies probably reflect mixing of continental ground water and seawater. Figures 29 and 30 are fence diagrams illustrating the variations of salinity and hydrochemical facies in three dimensions.

NUMERICAL MODEL

Model Design

The computer code MODFLOW (McDonald and Harbaugh, 1984) was used to simulate hydraulic heads and calculate water flow rates. MODFLOW uses a block-centered, finite-difference approximation to solve the ground-water flow equation

$$\partial/\partial x(K_{xx}\,\partial h/\partial x) + \partial/\partial y(K_{yy}\,\partial h/\partial y) + \partial/\partial z(K_{zz}\,\partial h/\partial z) = S_s\,\partial h/\partial t + W \qquad (2)$$

where

x, y, and z are cartesian coordinates aligned with major axes of the flow system,

K_{xx}, K_{yy}, and K_{zz} are hydraulic conductivities in the x, y, and z directions, respectively,

h is hydraulic head,

S_s is specific storage, and

W is volumetric flux per unit volume, a general term used to represent sources or sinks of water.

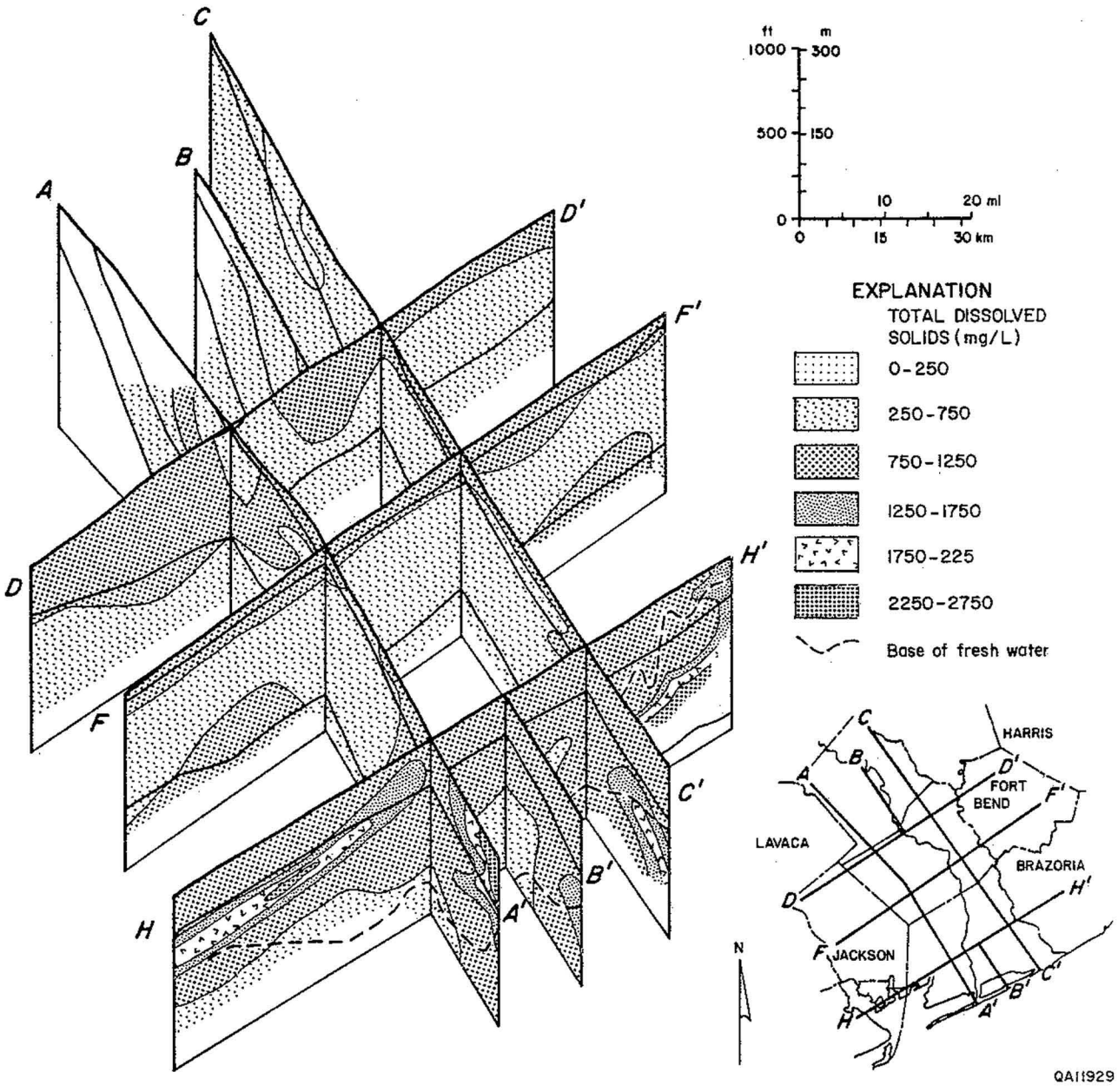

Figure 29. Fence diagram showing TDS distribution in the Beaumont, Chicot, and Evangeline hydrologic units.

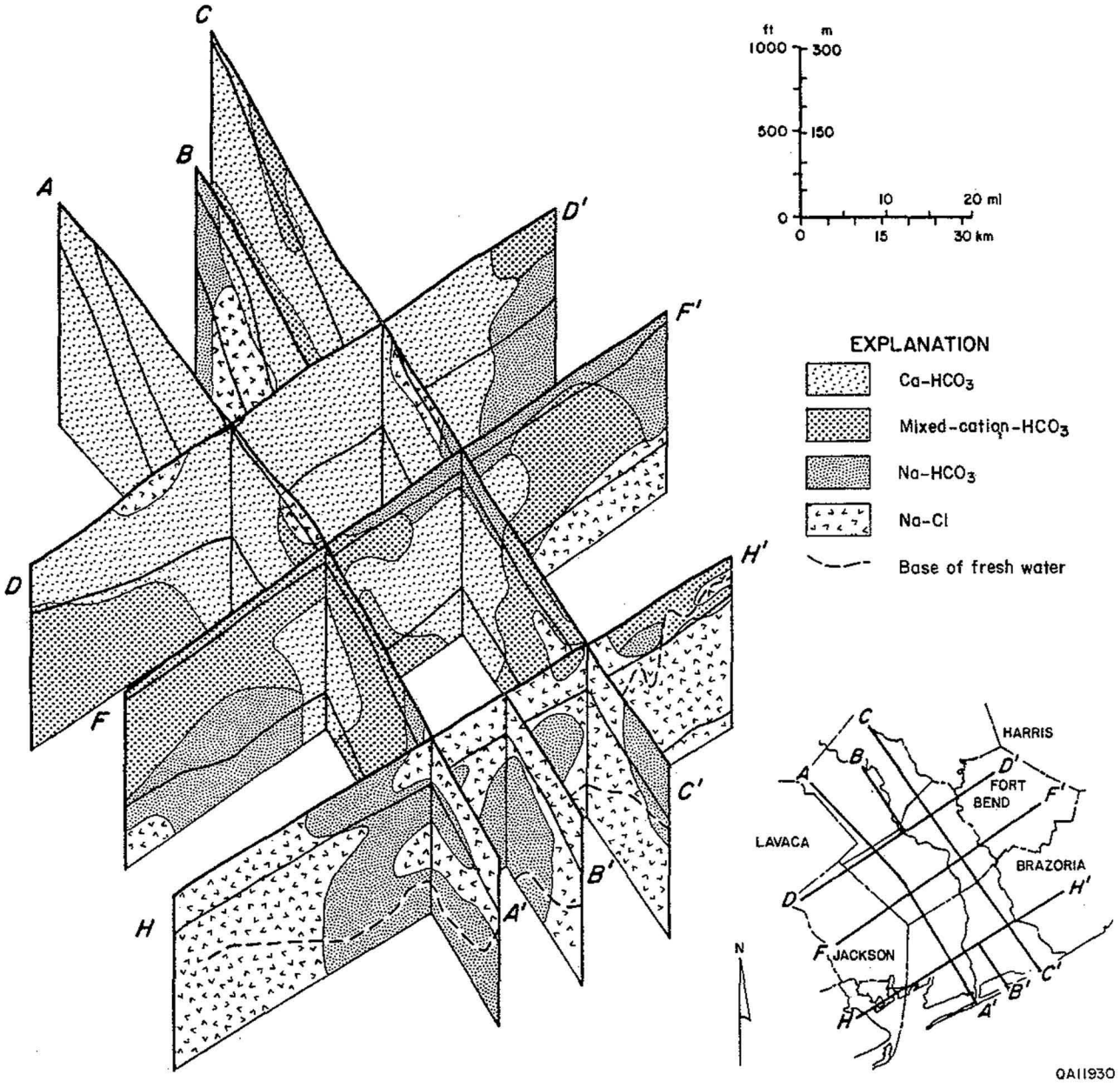

Figure 30. Fence diagram showing distribution of hydrochemical facies in the Beaumont, Chicot, and Evangeline hydrologic units.

In the simulations, the volumetric flux term represented recharge and discharge at the upper surface of the model as well as interaction between surface and ground waters owing to river leakage.

Defining the numerical model included specifying (1) the effective hydrologic units to be modeled, (2) the finite-difference grid of blocks, (3) the properties of the units, and (4) the location and type of model boundaries, including source terms such as rivers, recharge and discharge, and wells. Boundary conditions, structural elevations of layers, vertical and horizontal hydraulic conductivities, and storativities were assigned to each block. Latitude and longitude of block centers were specified in universal transverse mercator (UTM) projection coordinates. Geohydrologic and structural data were digitally interpolated from regional maps for each block center position using algorithms included in the CPS-1 graphics package.

Three model layers were used to simulate flow in the Gulf Coast aquifer system. Layer 1 represents flow in the Beaumont Formation, layer 2 represents flow in the upper Chicot aquifer unit, and layer 3 represents flow in the combined lower Chicot–Evangeline aquifer unit (table 1). Figure 31 summarizes the components of the conceptual hydrologic model upon which the numerical model is based.

Boundary configurations constrain flow paths in the aquifer units to be downdip from the northwesternmost outcrop limits and directed toward the coast. Vertical flow of ground water between formations is controlled by the vertical gradient in hydraulic head and vertical hydraulic conductivity (expressed as vertical conductance in the numerical model). Figures 5 through 13 indicate that there is no distinct or continuous confining layer separating aquifer units. The layers are differentiated more by trends in the thicknesses of sand beds and by net distribution of sand. The model developed in this study, therefore, does not specify separate confining layers. In comparison, Carr and others (1985) defined confining layers between the Chicot and Evangeline and above the Chicot. Thicknesses of their confining layers represented the net thickness of clay beds between the center planes of each formation. Carr and others (1985) assigned different values of storativity and compressibility to the aquifer and confining layers. In this study, storativity

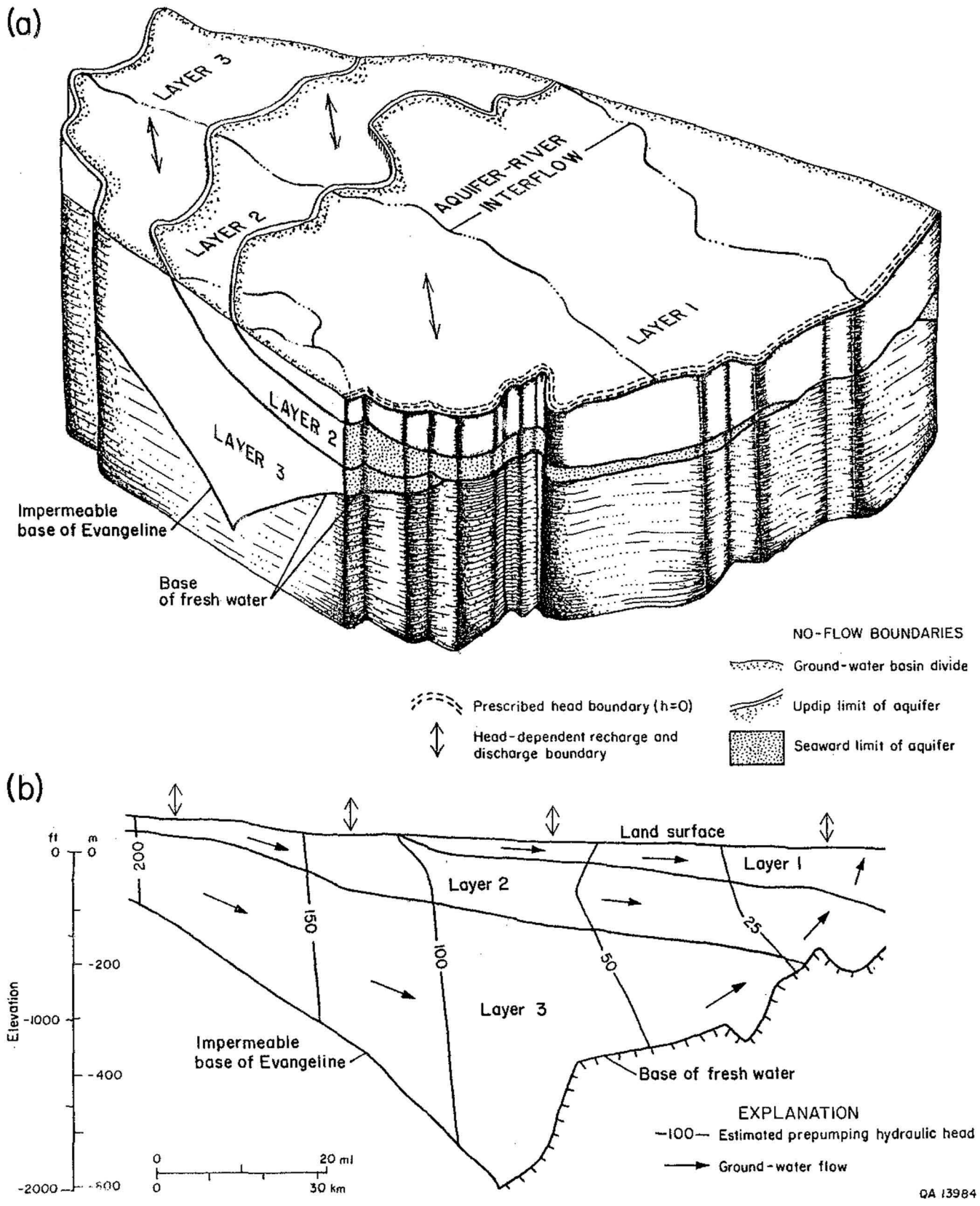

Figure 31. Schematic block diagram (a) and cross section along line A-A′ (b) illustrating layers and boundary conditions included in the conceptual model of the ground-water flow system.

values were assigned to aquifer units in the model as a weighted average of storage in sands and clays at each block.

The finite-difference numerical model was constructed with a 56-row by 50-column by 3-layer grid of blocks. Figures 32 through 34 show the active nodes used in the model. Rows are aligned parallel to the coast line (x direction) and extend approximately from the valleys of the Lavaca and Navidad Rivers in the southwest to the Brazos River valley in the northeast. Columns extend inland, perpendicular to the coast (y direction), to the updip limit of the Evangeline aquifer outcrop in the Fleming Formation. Block size is a compromise between amount of computer memory required to run the model, amount of geohydrologic data available for assigning properties to each block, and interest in accurately predicting responses of ground water to stresses in areas as small as possible. Block faces range from 1.5 mi wide in Matagorda and Wharton Counties to 2.5 mi wide in adjacent counties; block areas range from 2.25 to 6.25 mi^2. In comparison, Carr and others (1985) used block widths that ranged from 2.5 to 24 mi, and Ryder (1988) used a 5-mi-wide block size.

Not all of the 2,800 blocks in each layer are active in the grid, as shown in figures 32 through 34. The area included in the model was selected to place lateral boundaries along naturally occurring hydrologic features where effects of boundaries on simulation results for Matagorda and Wharton Counties would be minimal. Lateral hydrologic boundaries were selected where potentiometric contours are approximately perpendicular to natural boundaries, such as river basins. A "no-flow" boundary or hydrologic divide is suggested where hydraulic-head contours cross the Lavaca and Navidad Rivers at right angles along the west side of the study area and across the Brazos River valley along the east side (fig. 18, see Ryder, 1988). Interbasin flow of water, that is, discharge of water from the vicinity of the Colorado River into the area of influence of the ground-water cone of depression beneath the Houston area in Harris County, is not allowed in this model. Most blocks east of the Brazos River in Fort Bend, Waller, and Harris Counties are inactive. The "no-flow" lateral boundaries were kept fixed in both steady-state and transient

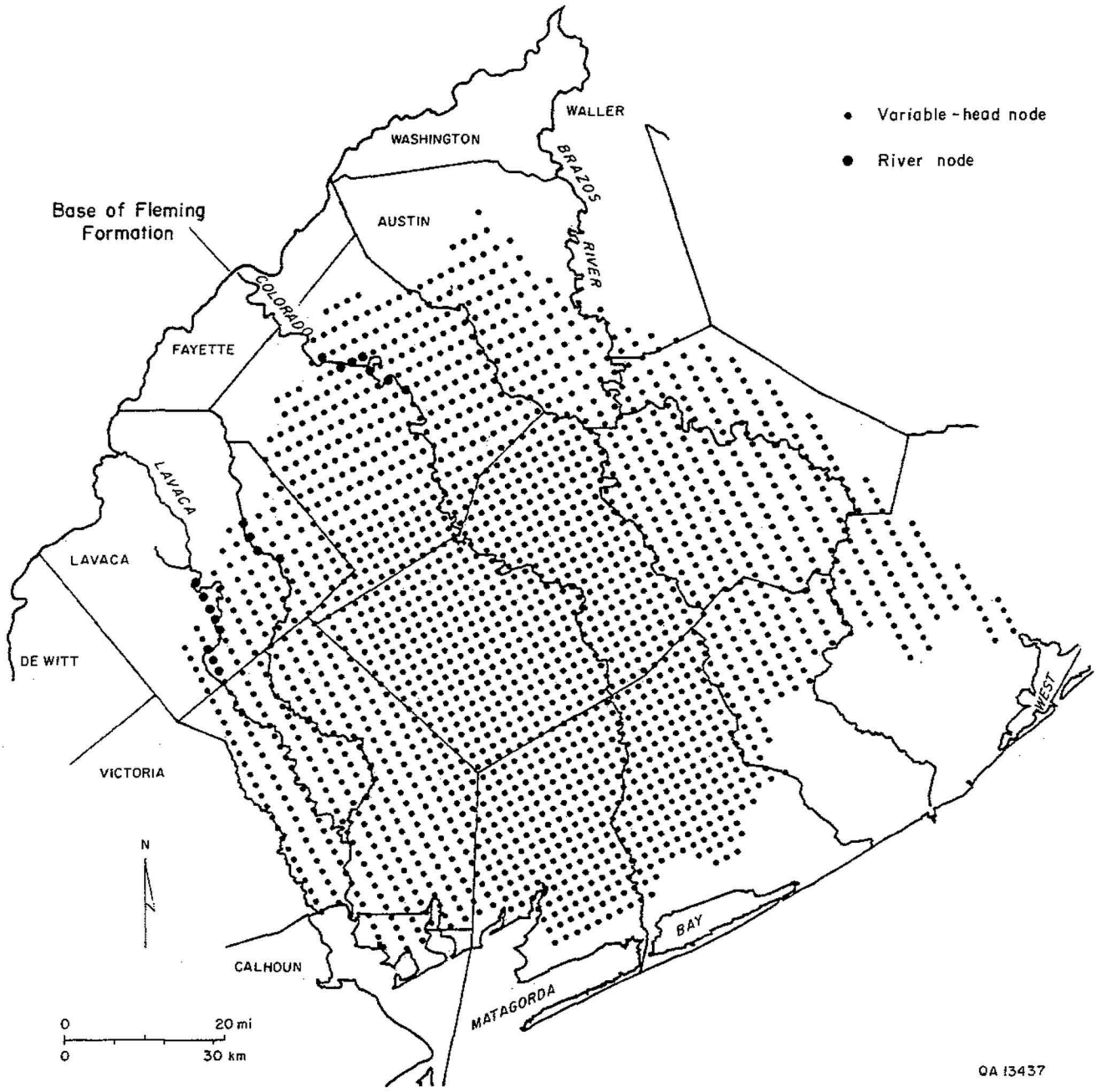

Figure 32. Plan-view location of the 1974 nodes of active blocks in layer 3 of the finite-difference grid.

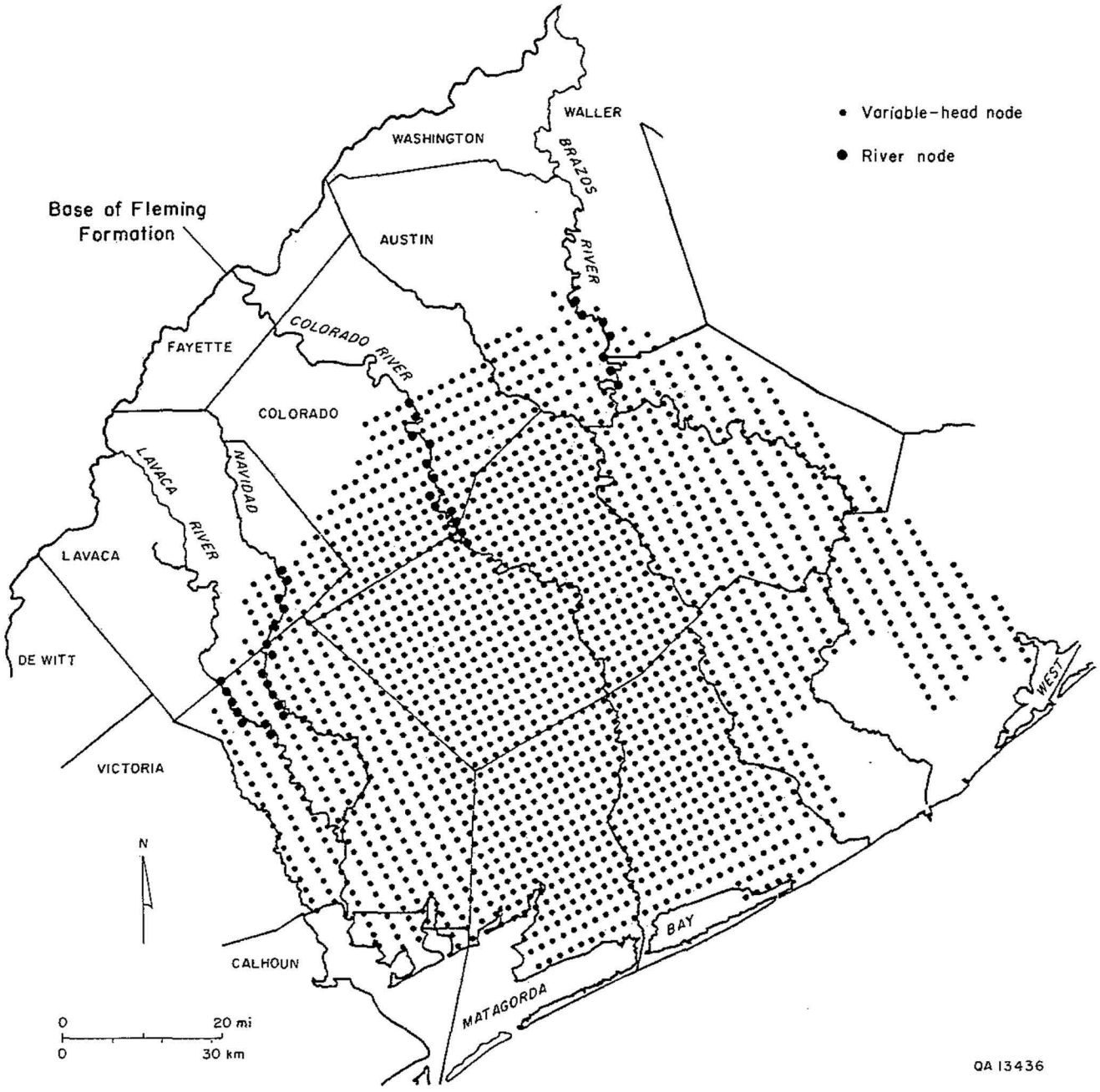

Figure 33. Plan-view location of the 1892 nodes of active blocks in layer 2 of the finite-difference grid.

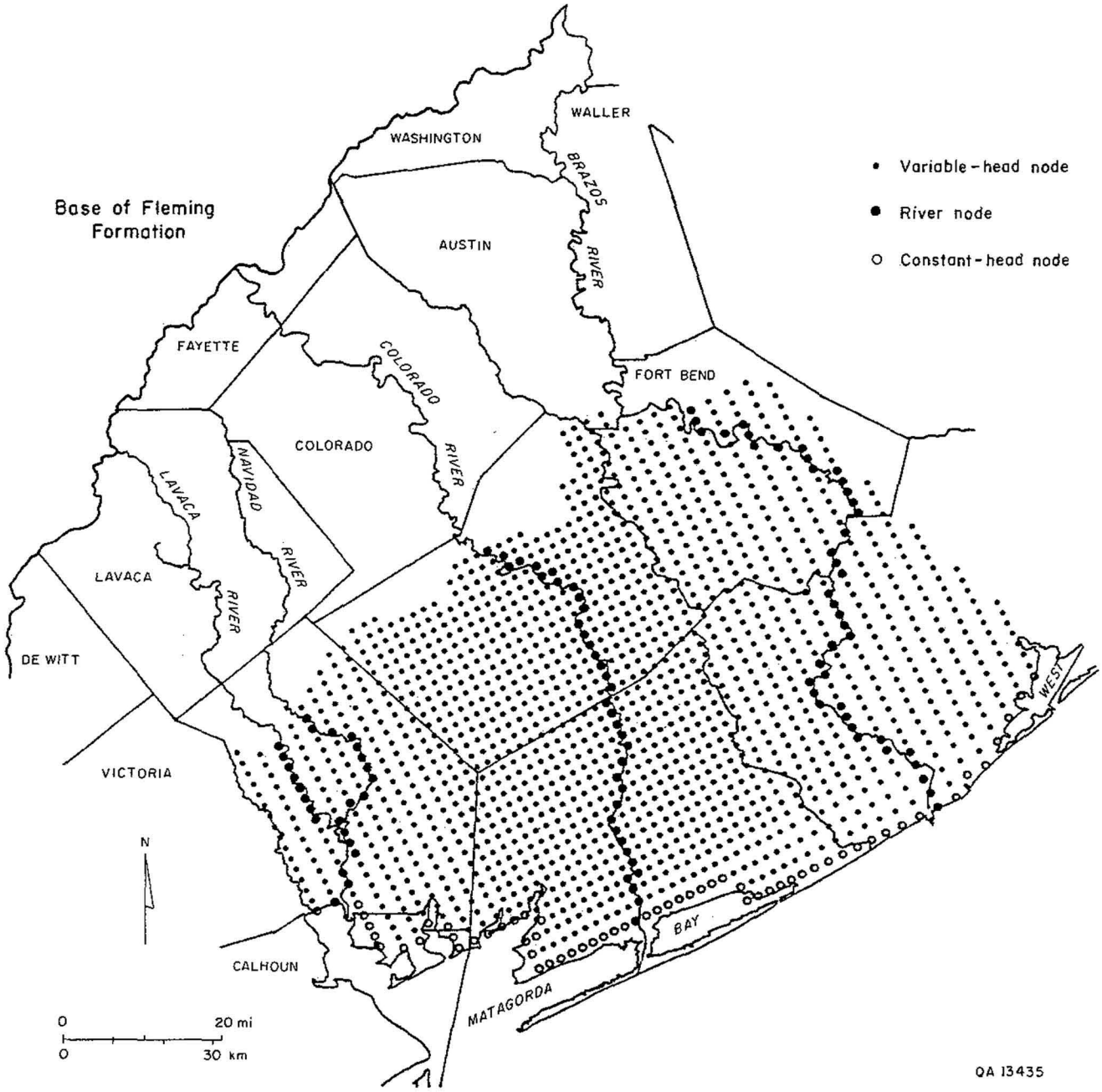

Figure 34. Plan-view location of the 1588 nodes of active blocks in layer 1 of the finite-difference grid.

simulations. Effects of this boundary condition on calculated hydraulic-head drawdown is discussed later in this report.

The northwestern limits of the aquifer outcrops are treated as "no-flow" (Newmann-type) boundaries (fig. 31a). The lower boundary of the model also is a "no-flow" boundary. Assuming that flow paths of fresh continental water and of seawater are fixed and the interface between fresh and saline waters is constant (fig. 14), the base of fresh water can be treated as an impermeable hydrologic boundary. The seaward edges of layers 2 and 3 (see figs. 32 and 33) have "no-flow" boundaries where the base of fresh water is higher than the top of the layer (fig. 31b). The seaward limit of layer 1 has a prescribed head of zero (figs. 31a and 34), which represents base level of the Gulf of Mexico.

To simulate recharge and discharge, a head-dependent flux boundary is assigned to the uppermost active blocks in the model, representing the outcrop of each aquifer layer. Direction of flow (recharge is downward and has a positive value in the water budget) is determined by the gradient between the calculated hydraulic head in the aquifer block and the hydraulic head in an imaginary bounding block that represents a near-surface water table. The rate of recharge or discharge is controlled by the value of boundary conductance or leakance assigned to the block. For this report, hydraulic heads of the imaginary blocks were taken from Ryder (1988) who calculated them as a function of land-surface elevation using the method of Williams and Williamson (1989). The constant hydraulic heads at the nodes of imaginary bounding blocks in this model were set equal to the heads at the nearest nodes in Ryder's (1988) grid.

Interaction between ground water and surface water in the Colorado, Brazos, Lavaca, and Navidad Rivers is represented in the model by specifying "river nodes" where the direction of flow is determined by the gradient in hydraulic head between the calculated hydraulic head in the aquifer block and the hydraulic head in the river reach. The rate of leakage between the river and the aquifer is controlled by the value of conductance assigned to river-bed sediments. Hydraulic heads of the river reaches were estimated from topographic maps.

Table 2 summarizes initial estimates and final "calibrated" values of hydrologic properties used in the model. Distribution of transmissivities calculated from sand-percentage values using equation 1 are shown in figure 25. Variance in transmissivity and storativity is influenced by the sand-percent distribution in each layer. Initial estimates of storativity were based on regional patterns given in Carr and others (1985) and were multiplied by the complement of sand percent. Some values in the outcrop zone were automatically assigned values of specific storage that are too high (0.5 to 0.8); these block values were not corrected in the simulations contained in this report. Storativities were further adjusted to develop a good match between simulation results and historical water-level hydrographs from selected wells in Matagorda and Wharton Counties. MODFLOW incorporates an option to adjust values of parameters in rectangular groups of blocks. This option was used to further adjust storativity values in the vicinity of wells with known hydrographs used for calibration. Vertical hydraulic conductivity, used to calculate vertical conductance between layers in the McDonald-Harbaugh computer code, also was weighted on a block-by-block basis by sand-percent values. Within each model block, horizontal transmissivities are assumed to be isotropic, that is, equal in both strike and dip (x and y) directions.

Calibration

Because only a composite, multi-aquifer, hydraulic-head surface could be supported by data collected during this study, hydraulic-head surfaces estimated by Ryder (1988) for permeable zones in Holocene and upper Pleistocene rocks, lower Pleistocene and upper Pliocene rocks, and lower Pliocene and upper Miocene rocks (table 1) were used in the so-called state-state calibration. Transmissivity, river-bed conductance, and recharge conductance were iteratively adjusted by comparing simulated hydraulic heads to the mapped contours of "prepumping" hydraulic head defined by Ryder (1988).

Hydraulic heads calculated by the calibrated, steady-state model were used as initial conditions for simulation of transient-flow conditions in the aquifer. Pumping rates estimated by

Carr and others (1985) for their central subregion model were used to simulate historic ground-water declines. Carr and others (1985) included four pumping or stress periods during which average pumping rates were constant: 1900–1945, 1946–1960, 1961–1970, and 1971–1975. Carr and others (1985) based their estimates on the proportion of well screens in each aquifer and on total production estimated by county. Ground-water production rates for each of the 2,132 blocks of the Carr and others (1985) central-subregion model (subsequently referred to as the Carr model) were divided by block area to yield an average pumping rate per unit area. Block centers in the Carr model were given a UTM longitude and latitude coordinate. Then, block centers of each of the 2,800 active and inactive blocks in layers 2 and 3 of the model developed in this study (referred to as the LCRA model) were assigned the unit pumping rate of the closest corresponding block center in the Carr model. Block centers in the LCRA model to which pumping rates greater than 0.001 ft^3/s were assigned for the period 1900–1945 are shown in figure 35, 1946–1960 in figure 36, 1961–1970 in figure 37, and 1971–1975 in figure 38. Unit rates were multiplied by the area of the LCRA-model blocks. Pumping rates for the period from 1976 through 1985 were based on county estimates made by the Texas Water Development Board. Pumping rates for the period from 1986 through 2030 were based on predictions of total water demand in each county made by the Lower Colorado River Authority (Q. Martin, written communication, 1988) and by the Texas Water Development Board (B. Molz, written communication, 1987). Pumping rates for stress periods later than 1975 were based on the same proportional distribution of pumping in blocks in layers 2 and 3 as was specified for the period of 1971 through 1975 (fig. 38). Pumping rates are listed in table 3. All production that was allocated to the lower Chicot in the Carr model was assigned to the upper Chicot in this model (that is, the hydrologically equivalent layer 2 [table 1]). No active pumping wells in layer 3 were assigned to Calhoun County (figs. 35–38).

Simulations were run with a time-step acceleration parameter of 1.2. Stress periods were divided into 12 time steps. Water levels in 1965, for example, were represented by the hydraulic heads calculated at the ninth time step of the third stress period (1961–1970), and water levels in 1985 were represented by the twelfth time step of the fifth stress period (1976–1985). Calculated

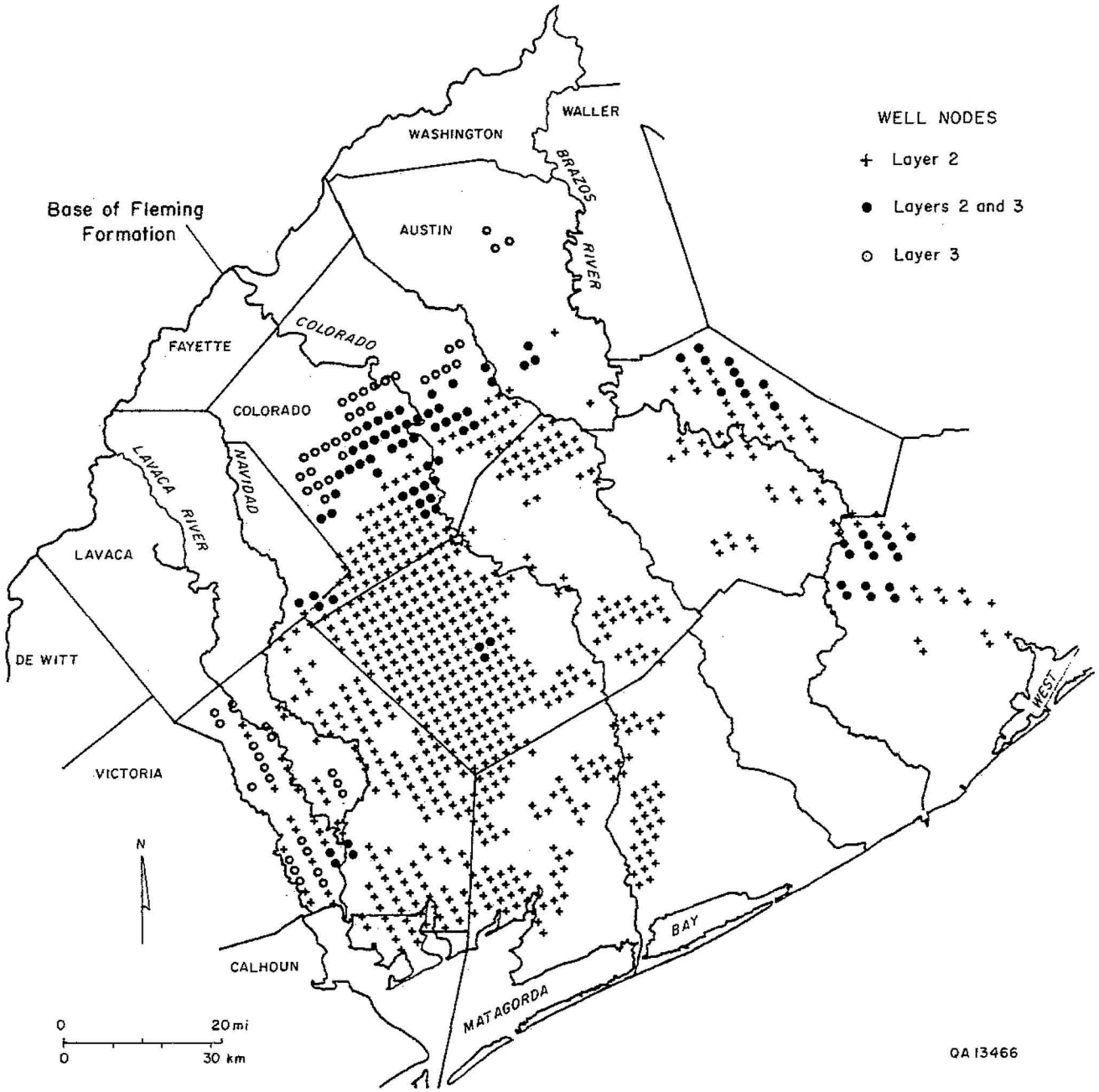

Figure 35. Active blocks in layers 2 and 3 of the finite-difference grid with ground-water production during 1900 through 1945.

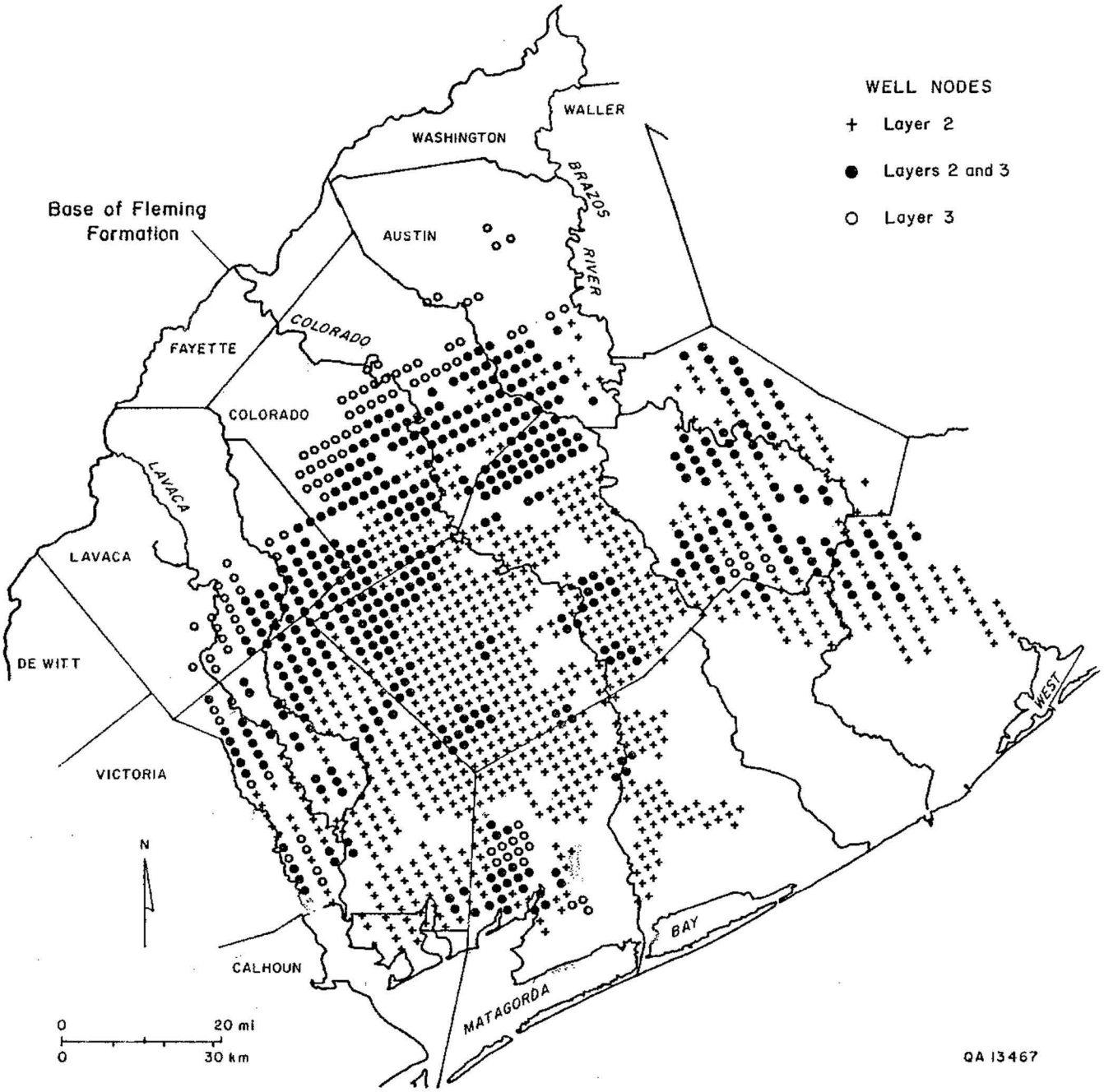

Figure 36. Active blocks in layers 2 and 3 of the finite-difference grid with ground-water production during 1946 through 1960.

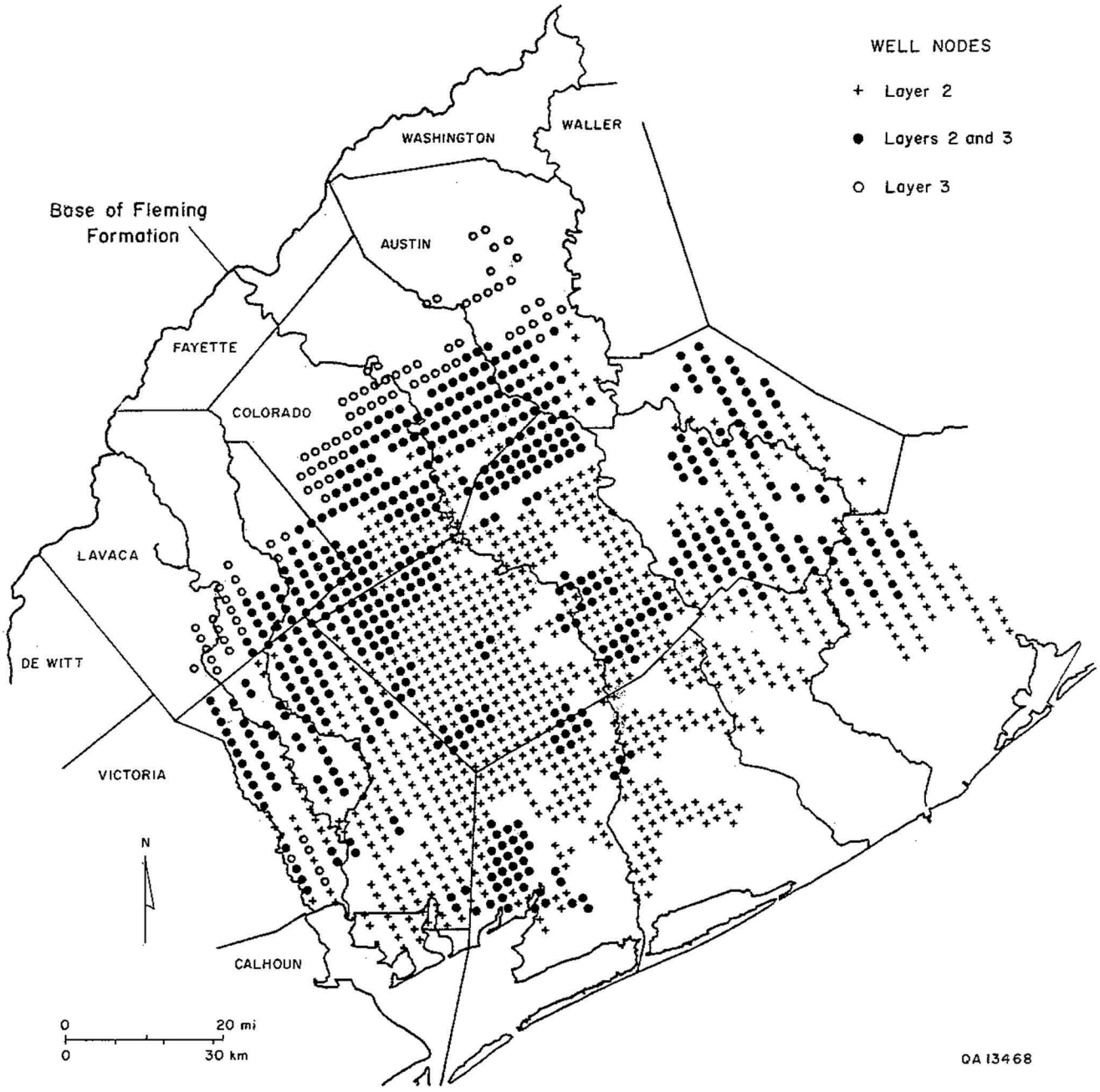

Figure 37. Active blocks in layers 2 and 3 of the finite-difference grid with ground-water production during 1961 through 1969.

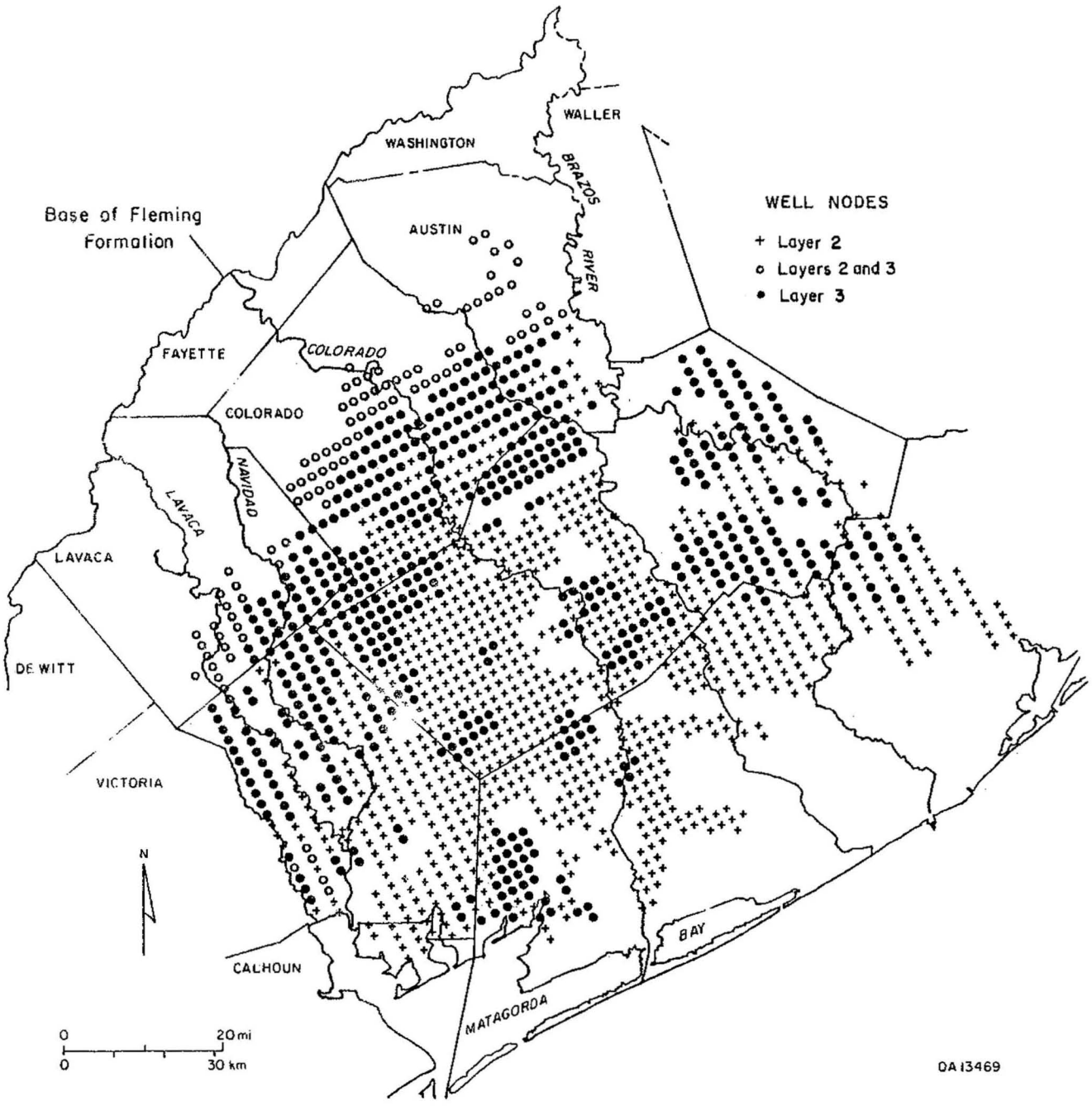

Figure 38. Active blocks in layers 2 and 3 of the finite-difference grid with ground-water production during 1970 through 1975.

Table 3a. Average total pumping rates (acre-ft/yr) in modeled area of each county.

Years	Matagorda	Wharton	Colorado	Calhoun	Jackson	Lavaca	Brazoria	Fort Bend	Austin	Total
					Historic					
1900–1945	4,059	26,701	8,970	287	7,532	713	1,155	1,678	293	51,387
1946–1960	16,367	93,915	28,569	524	70,389	13,622	7,865	20,331	6,654	258,237
1961–1970	22,656	147,166	45,880	476	95,797	29,228	15,509	42,425	11,156	410,292
1971–1975	32,048	186,299	68,329	532	127,319	30,370	17,466	44,405	14,005	520,774
1976–1985	33,125	121,330	32,875	5,223	66,560	15,096	20,179	29,736	6,400	330,524
					Projected High					
1986–1990	42,003	199,973	48,659	5,223	96,753	26,179	90,017	96,098	16,889	621,796
1991–2000	42,003	199,973	48,659	5,223	83,333	23,815	85,142	101,007	16,730	605,885
2001–2010	42,003	199,973	48,659	5,223	81,490	23,950	85,684	111,356	17,594	615,933
2011–2020	42,003	199,973	48,659	5,223	79,713	29,276	86,261	120,837	18,485	630,431
2021–2030	42,003	199,973	48,659	5,223	77,901	29,276	86,567	130,841	19,190	639,634
					Projected Low					
1986–1990	42,003	199,973	48,659	5,223	77,813	23,306	80,836	81,985	13,831	573,629
1991–2000	42,003	199,973	48,659	5,223	65,925	20,783	76,074	82,233	13,403	554,278
2001–2010	42,003	199,973	48,659	5,223	62,615	20,210	75,219	86,133	13,445	553,480
2011–2020	42,003	199,973	48,659	5,223	59,345	19,536	74,413	89,545	13,514	552,212
2021–2030	42,003	199,973	48,659	5,223	56,142	24,727	73,754	93,298	13,509	557,289

Table 3b. Average pumping rates (acre-ft/yr) in each county for layer 2 of the model.

Years	Matagorda	Wharton	Colorado	Calhoun	Jackson	Lavaca	Brazoria	Fort Bend	Austin	Total
					Historic					
1900–1945	4,059	26,690	7,915	287	6,798	417	1,122	1,542	193	49,024
1946–1960	13,645	91,242	18,456	524	61,345	6,229	7,777	18,007	2,536	219,761
1961–1970	19,455	142,579	25,468	476	81,027	12,162	15,420	36,578	4,388	337,553
1971–1975	28,586	181,162	37,516	532	105,396	13,797	17,300	32,864	5,833	422,987
1976–1985	29,548	117,987	18,048	5,223	55,100	6,858	19,989	22,014	2,666	277,433
					Projected High					
1986–1990	37,464	194,449	26,715	5,223	80,097	11,896	89,166	71,135	7,035	523,181
1991–2000	37,464	194,449	26,715	5,223	68,983	10,818	84,334	74,776	6,966	509,728
2001–2010	37,464	194,449	26,715	5,223	67,458	10,880	84,867	82,429	7,327	516,813
2011–2020	37,464	194,449	26,715	5,223	65,988	13,300	85,441	89,448	7,699	525,727
2021–2030	37,464	194,449	26,715	5,223	64,484	13,300	85,745	96,857	7,994	532,232
					Projected Low					
1986–1990	37,464	194,449	26,715	5,223	64,418	10,587	80,068	60,685	5,760	485,369
1991–2000	37,464	194,449	26,715	5,223	54,572	9,443	75,348	60,872	5,583	469,669
2001–2010	37,464	194,449	26,715	5,223	51,828	9,181	74,510	63,764	5,601	468,735
2011–2020	37,464	194,449	26,715	5,223	49,126	8,876	73,708	66,285	5,629	467,476
2021–2030	37,464	194,449	26,715	5,223	46,469	11,233	73,053	69,057	5,625	469,288

Table 3c. Average pumping rates (acre–ft/yr) in each county for layer 3 of the model.

Years	Matagorda	Wharton	Colorado	Calhoun	Jackson	Lavaca	Brazoria	Fort Bend	Austin	Total
					Historic					
1900–1945	0	11	1,055	0	733	296	33	135	101	2,363
1946–1960	2,722	2,673	10,113	0	9,044	7,393	88	2,325	4,119	38,476
1961–1970	3,201	4,587	20,412	0	14,770	17,067	88	5,846	6,768	72,739
1971–1975	3,462	5,137	30,814	0	21,922	16,573	166	11,541	8,172	97,787
1976–1985	3,577	3,343	14,827	0	11,460	8,238	191	7,722	3,734	53,091
					Projected High					
1986–1990	4,539	5,525	21,944	0	16,657	14,283	851	24,963	9,854	98,615
1991–2000	4,539	5,525	21,944	0	14,350	12,997	808	26,231	9,764	96,156
2001–2010	4,539	5,525	21,944	0	14,031	13,070	817	28,928	10,266	99,120
2011–2020	4,539	5,525	21,944	0	13,725	15,976	820	31,390	10,787	104,704
2021–2030	4,539	5,525	21,944	0	13,417	15,976	822	33,984	11,196	107,402
					Projected Low					
1986–1990	4,539	5,525	21,944	0	13,395	12,719	768	21,299	8,071	88,260
1991–2000	4,539	5,525	21,944	0	11,353	11,340	727	21,362	7,820	84,609
2001–2010	4,539	5,525	21,944	0	10,787	11,028	709	22,369	7,844	84,745
2011–2020	4,539	5,525	21,944	0	10,219	10,660	705	23,260	7,885	84,736
2021–2030	4,539	5,525	21,944	0	9,672	13,495	701	24,242	7,884	88,001

hydraulic-head distribution representing 1985 conditions was used as the initial condition for simulating water-level changes for the "future" period from 1986 through 2030. Simulations of future conditions were run using 5- and 10-yr stress periods. Water levels in 2030, for example, were represented by the twelfth time step of the fifth stress period (2021–2030). Simulations of artificial recharge were run with stress periods varying in length from 1 to 10 yr to provide additional resolution of changes in flux and hydraulic head during the early part of the project.

RESULTS

Steady-State Flow System

Figures 39 through 41 show simulated and observed hydraulic-head surfaces representing the prepumping or steady-state condition in the Beaumont (layer 1), upper Chicot (layer 2), and lower Chicot and Evangeline (layer 3), respectively. Table 2 lists the values of adjusted parameters after completion of model calibration. The adjusted horizontal and vertical hydraulic conductivities generally gave an excellent match between simulated and observed values. The final distributions of transmissivities in layers 2 and 3 are similar to the estimated transmissivity distribution in the Chicot and Evangeline aquifers (figs. 25b and 25c). The mean transmissivity of the Beaumont Formation is lower than the mean transmissivity of the deeper formation (fig. 25a).

Interaction of ground water in layer 1 and surface water in the several coastal rivers proved to be a crucial part of the model. Without the river interaction, the simulated hydraulic-head contours strike across the study area in a relatively straight line and do not match the observed inland bend of the contours across the Lavaca, Navidad, and Brazos River valleys.

Figure 42 shows the distribution of simulated recharge and discharge for the prepumping or "steady-state" condition across the study area, calculated using the general-head boundary option of MODFLOW (McDonald and Harbaugh, 1984). Discharge areas occur where the calculated heads in the uppermost aquifer unit are at higher elevations than the heads at the imaginary

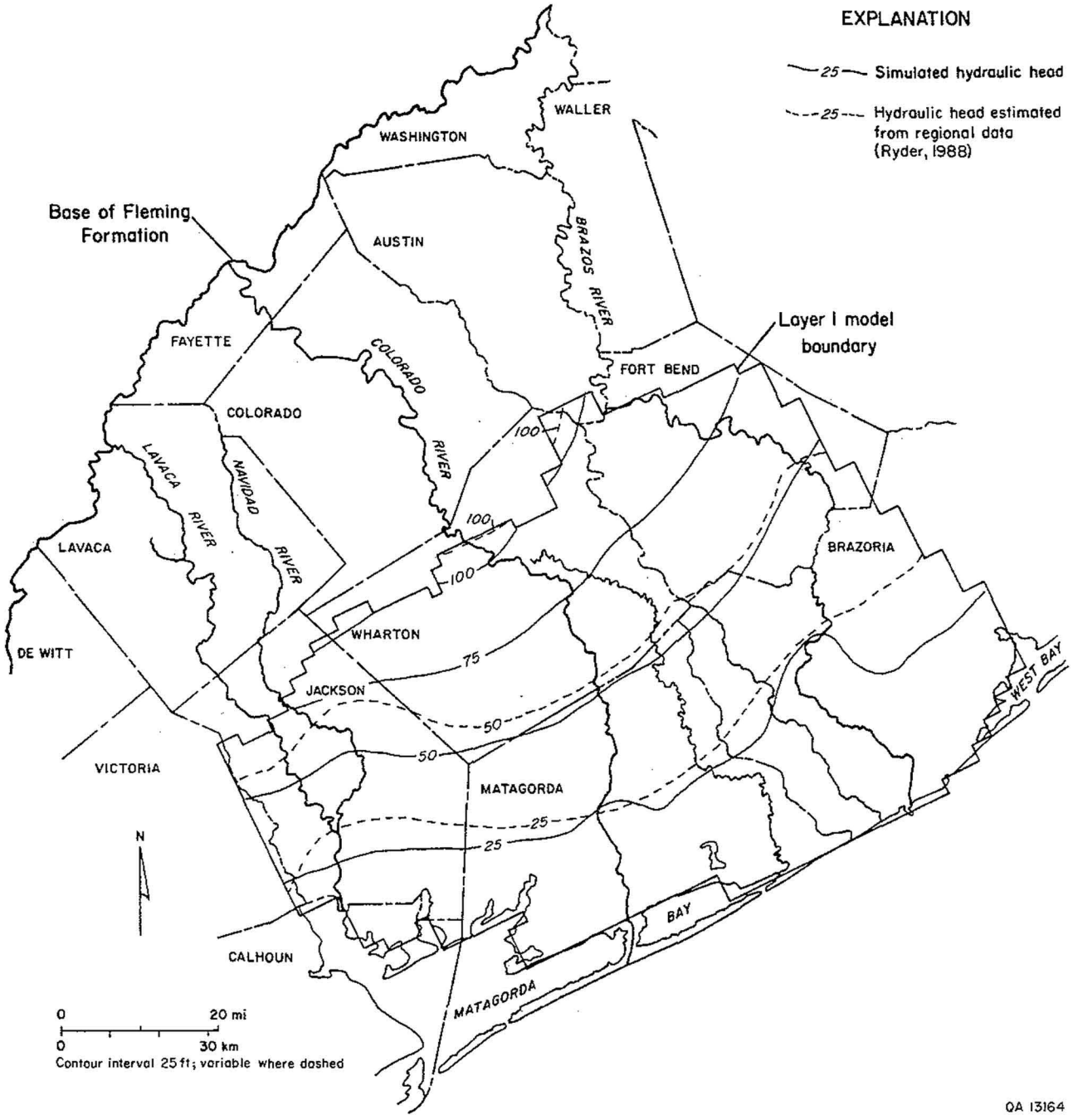

Figure 39. Comparison of simulated (solid line) and observed (dashed line) values of hydraulic head in the Beaumont Formation (layer 1) at the initial prepumping or steady-state condition.

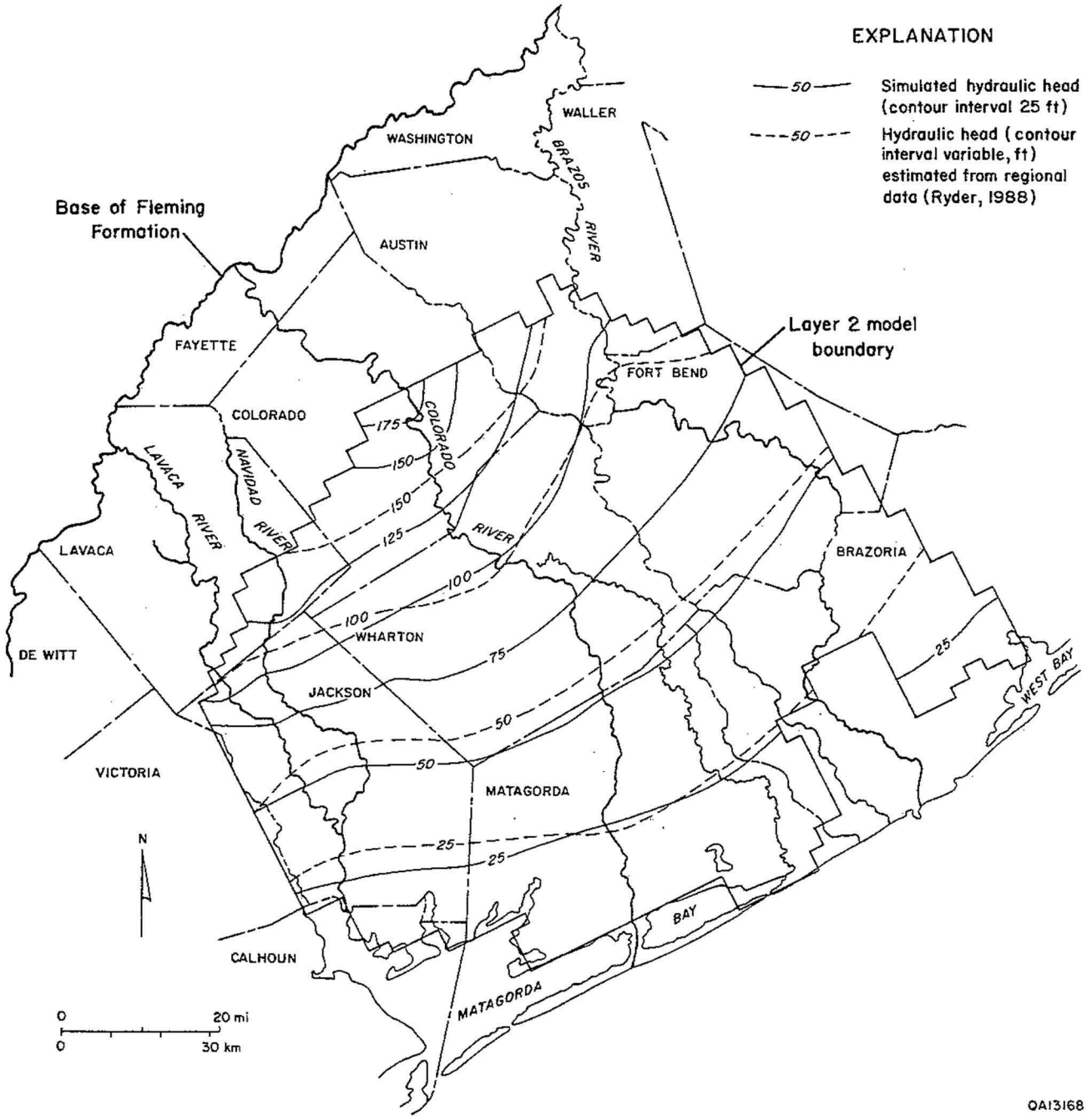

Figure 40. Comparison of simulated (solid line) and observed (dashed line) values of hydraulic head in the upper Chicot aquifer unit (layer 2) at the initial prepumping or steady-state condition.

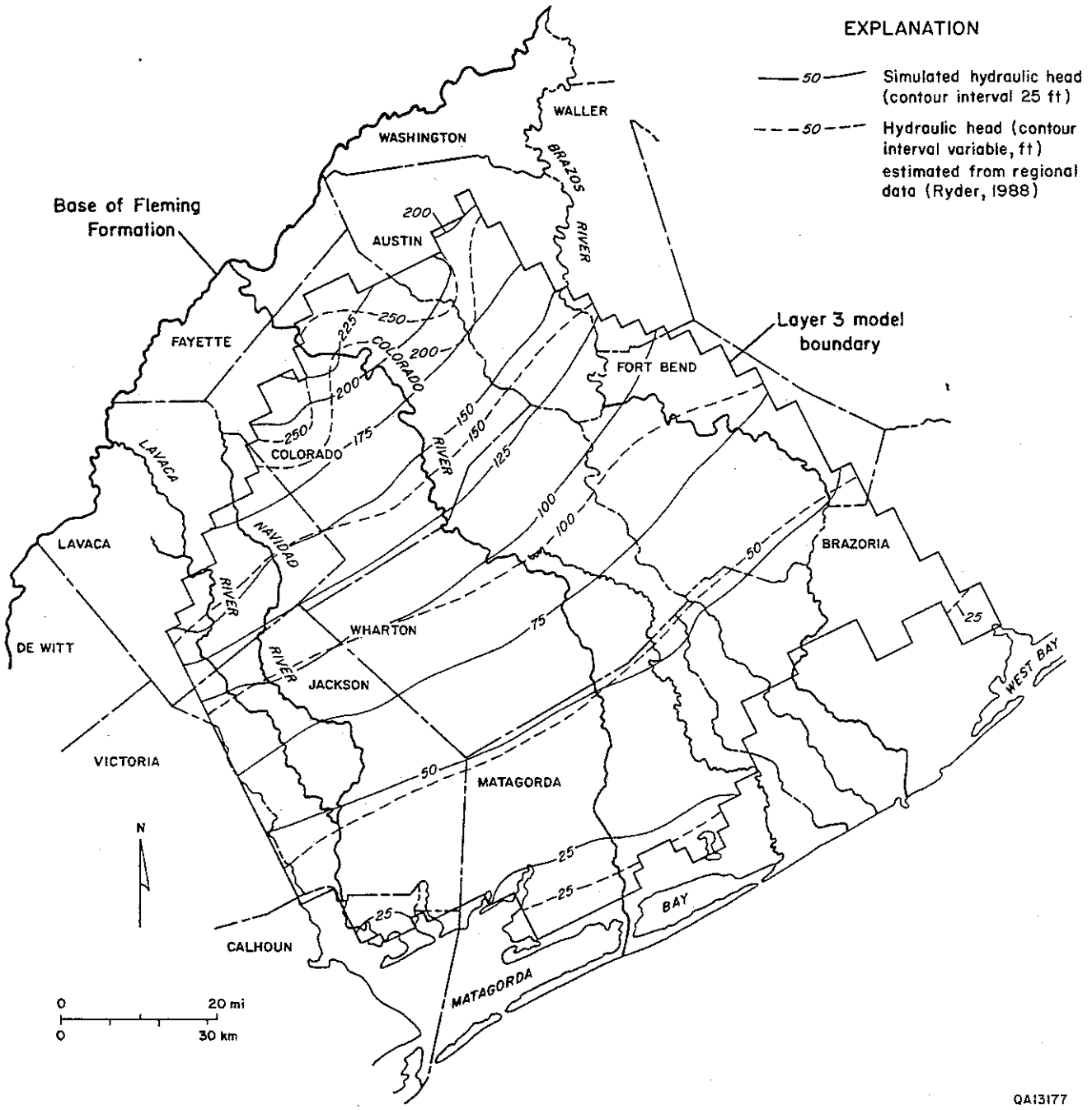

Figure 41. Comparison of simulated (solid line) and observed (dashed line) values of hydraulic head in the lower Chicot and Evangeline aquifer units (layer 3) at the initial prepumping or steady-state condition.

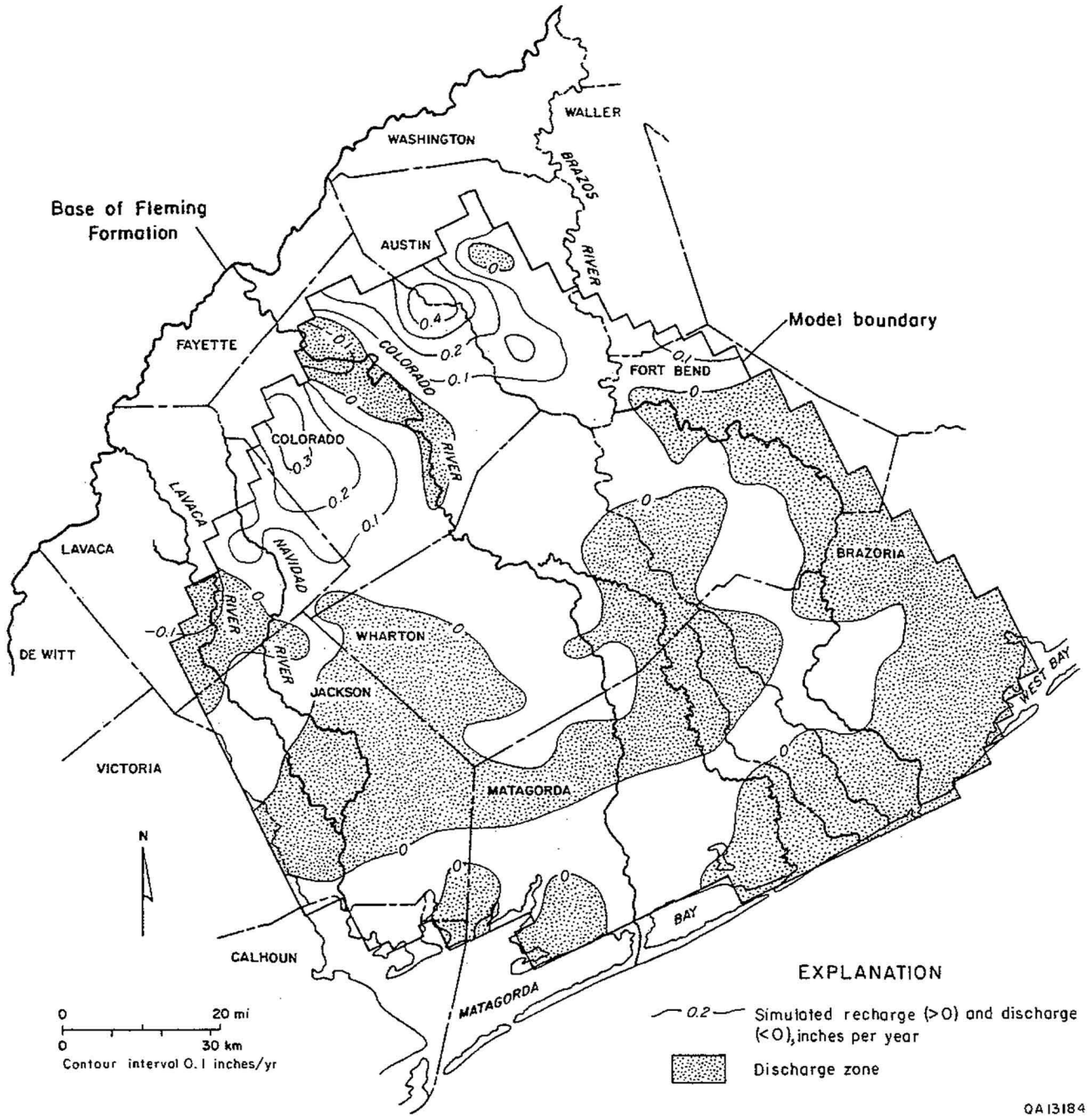

Figure 42. Distribution of recharge and discharge calculated for the prepumping or steady-state conditions.

bounding node. Note that the calculated recharge is as much as 0.4 inch/yr across the upland areas east and west of the Colorado River. Ryder (1988) estimated that recharge rates in these areas were less than 2 inches/yr. The prediction that the center of the study area is a discharge area is based on the hydraulic head in the aquifer node being higher than the water-table elevation in the imaginary bounding node. Leakage of water between the Colorado River and layer 1 also influences the value of head in layer 1.

Historical Flow System

Ground-water production from layers 2 and 3 of the model is summarized in figure 43 and table 3; simulations reported here focus on the high-demand estimates for the 1986–2030 period. Most ground water comes from the Chicot aquifer unit; production is negligible from the Evangeline aquifer unit in Matagorda County (figs. 35–38; see also figs. 19–21) and from the Beaumont Formation throughout the study area.

Figure 44 shows the locations of wells with hydrographs that were used in trial-and-error adjustment of storativity values to obtain a good match between simulated and historic rates of water-level decline in the Gulf Coast aquifer. An acceptable match between simulated drawdowns and hydrographs from some wells with substantial water-level decline was obtained after storativity distributions were slightly adjusted (fig. 45a–f, j, k, and l). Hydrographs for other wells with appreciable declines were not matched as closely but remain acceptable (fig. 45, i, m, and p). Hydrographs that did not exhibit any long-term decline were poorly replicated by simulation results (fig. 45g, h, n, and o). Possible explanations of the discrepancies are that (1) production rates were overestimated in some blocks of the model, (2) estimates of storativity are grossly in error for local sets of blocks, and (3) some observation wells are completed in layers that are poorly connected to the regional ground-water flow system.

Simulated hydraulic-head surfaces representing 1965 conditions for layers 2 and 3 in the model are shown in figures 46 and 47, respectively. The simulated results can be compared to

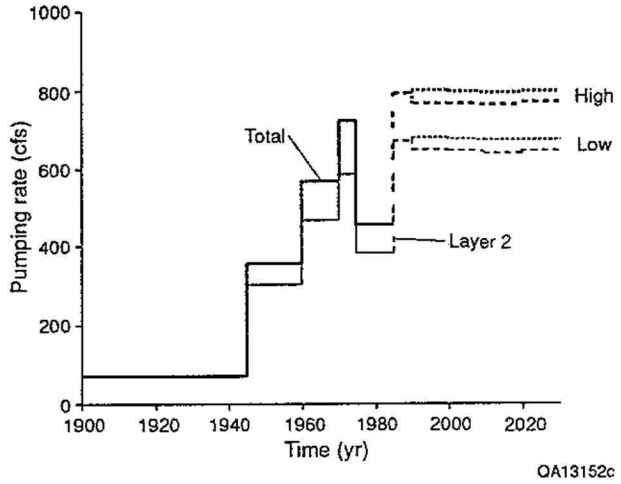

Figure 43. Pumping rates used in transient simulations. The difference between total and layer 2 pumping rates gives the pumping rate for layer 3 used in the model. Solid lines represent historical data; dashed lines represent predicted rates.

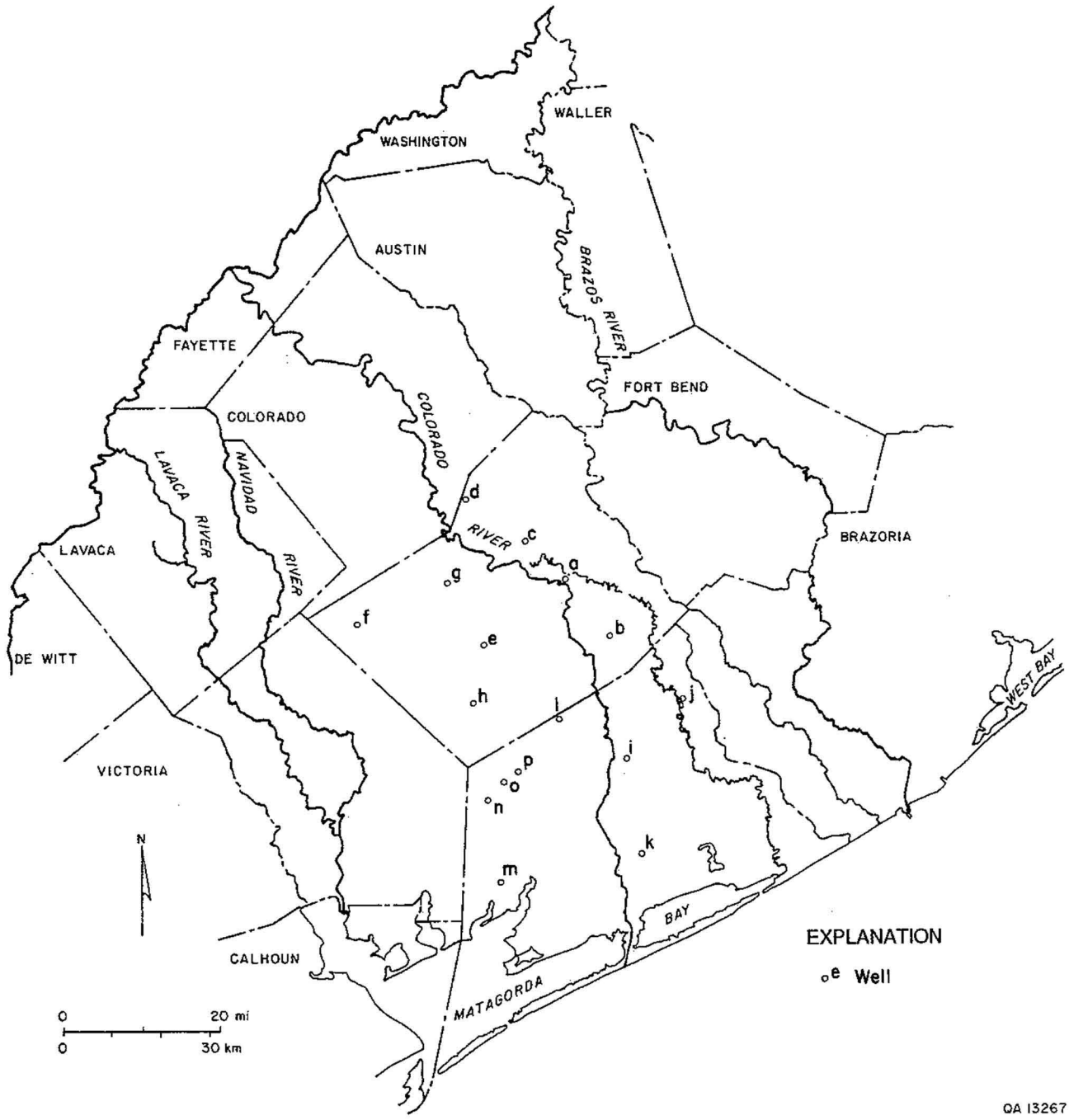

Figure 44. Location of selected wells with historical hydrographs used to calibrate values of storativity used in the model simulations.

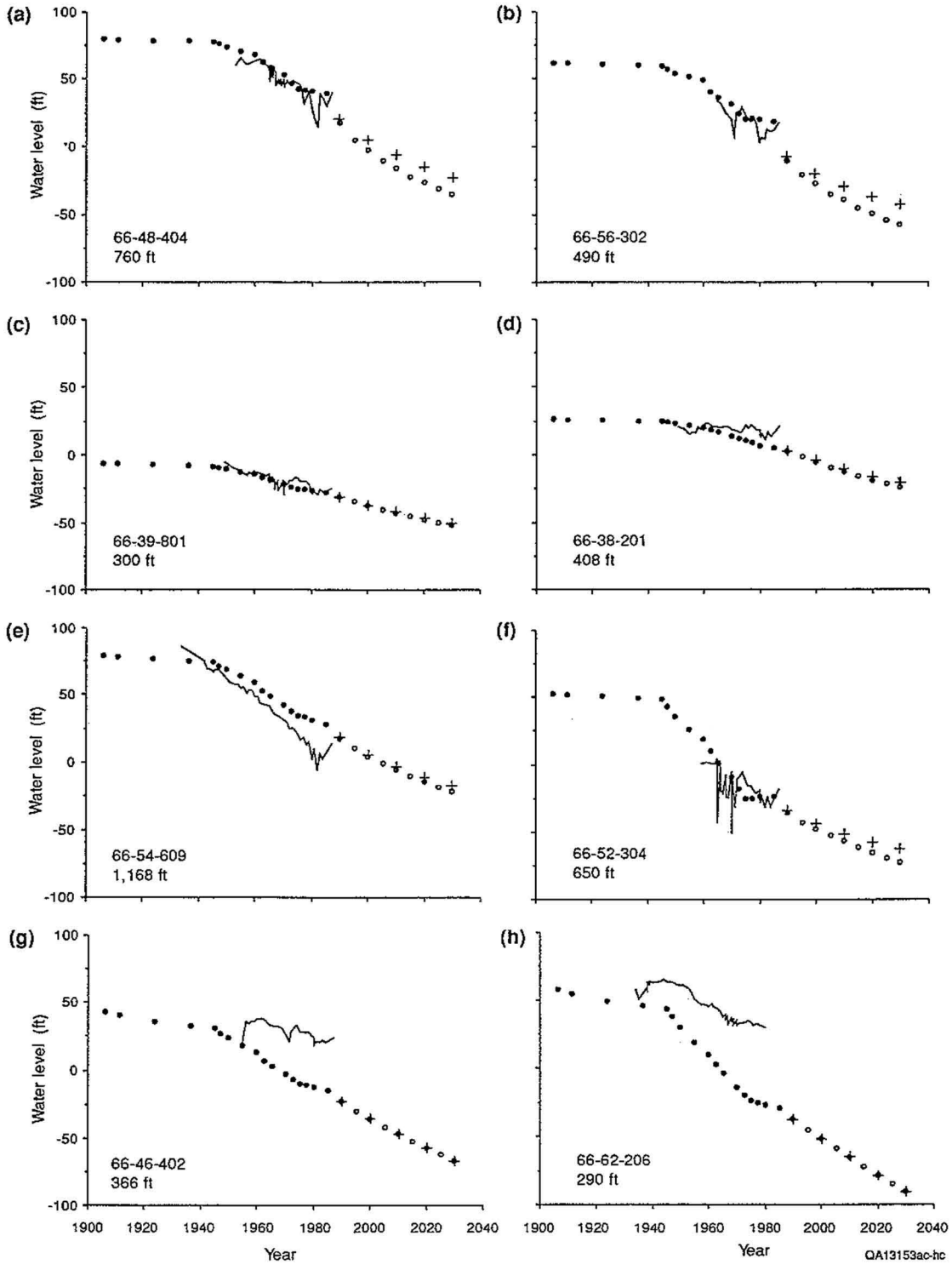

Figure 45. Comparison of observed (solid line) and simulated hydrographs for 1900 through 1985 and prediction of future water-level decline through 2030. Solid dots represent the historical period (1900–1985); open circles and pluses represent high and low estimates of future pumping periods (1986–2030). Figure parts (a–p) correspond to parts referenced in figure 44. Also given are the TWDB well identification number and well depth.

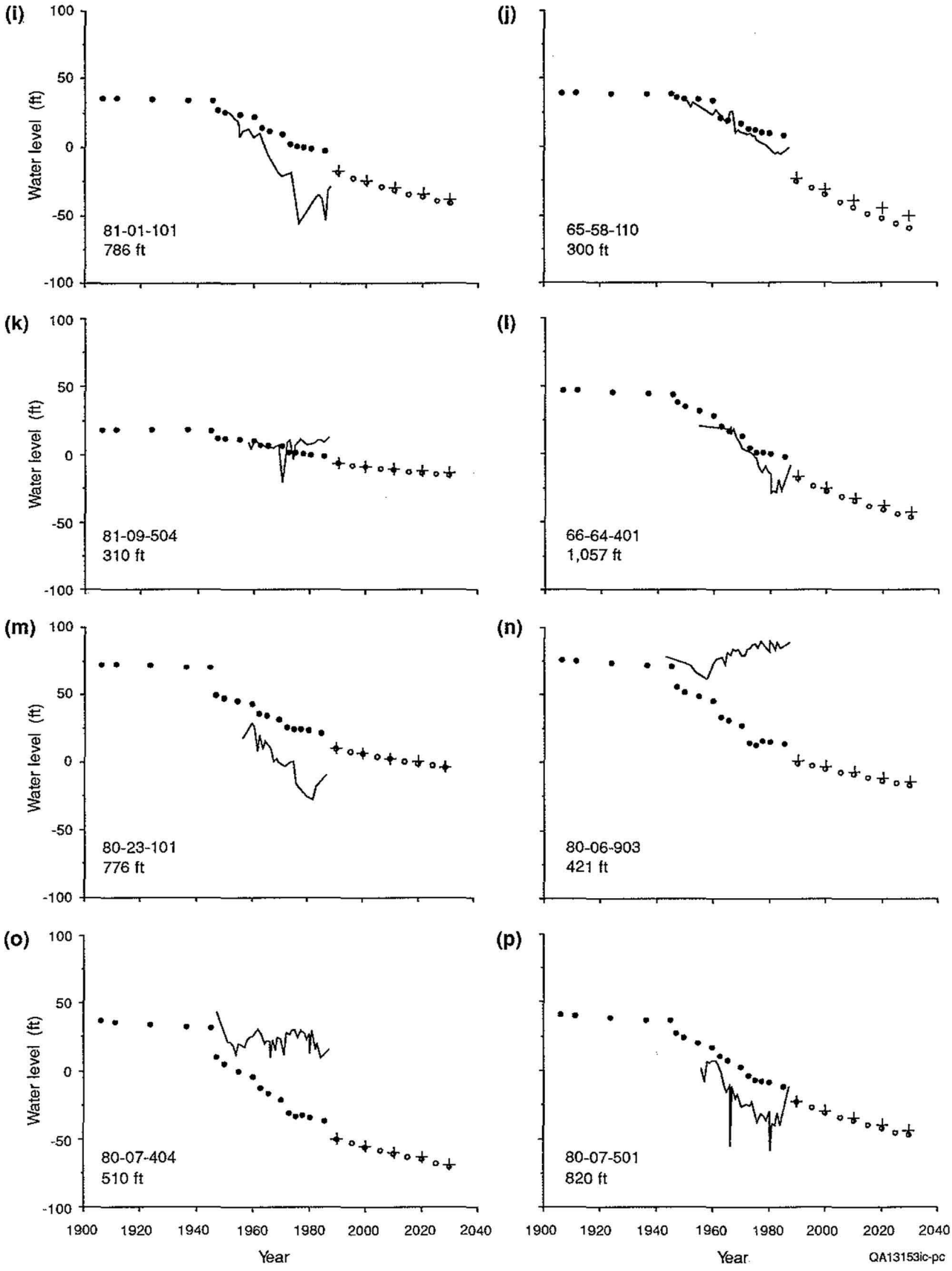

Figure 45 (cont.)

parts of the composite hydraulic head surface for 1965 shown in figure 19. The simulation overestimates drawdown in western Matagorda and eastern Jackson Counties. The 50- and 100-ft potentiometric contours of layer 2 and 3 also appear to have shifted too far inland in Wharton County in the simulation, compared with their position in figure 19. Simulated 1985 conditions are depicted in figures 48 through 50 for layers 1, 2, and 3, respectively. The match between simulated and observed 1985 hydraulic head patterns (fig. 20) overall is better than the match for 1965 patterns.

Note that significant drawdown was calculated in layer 1, representing the Beaumont Formation (fig. 51), although no ground-water production from layer 1 was included in the simulation. The decline in water level was due to drainage to the underlying model layer as the hydraulic head in layer 2 declined (fig. 52). As will be seen in results of simulations for 1986–2030, hydraulic-head decline in layer 1 is projected to continue with further decline in hydraulic head in layer 2. Figures 21 through 24 show that some decline has occurred that might be due either to ground-water production from the Beaumont or to leakage to the underlying Chicot aquifer unit. The amount of simulated drawdown in layer 1 probably is most sensitive to the conductance parameter assigned to the general-head (recharge) boundary; more recharge to the Beaumont would result in less head decline.

Hydraulic-head declines in layers 2 and 3 in the study area are as much as 75 and 175 ft, respectively (figs. 52 and 53). It is important to recall that the "no-flow" boundary along the northeastern side of the modeled area prevents recharge to, or discharge from, the model and isolates the study area from ground-water flow into the Houston area of ground-water production. Simulations of 1985 conditions show that areas of drawdown contact the "impermeable" no-flow model boundary. The impact of this error on simulation results probably is insignificant to predictions about Matagorda and Wharton Counties, but it probably is significant to counties adjacent to the southwestern and northeastern boundaries of the model.

Maximum rates of drawdown calculated at nodes in the model range from 0.7 ft/yr in layer 1 between 1900 and 1965 to 3.7 ft/yr in layer 3 between 1966 and 1985 (table 4a). At some model

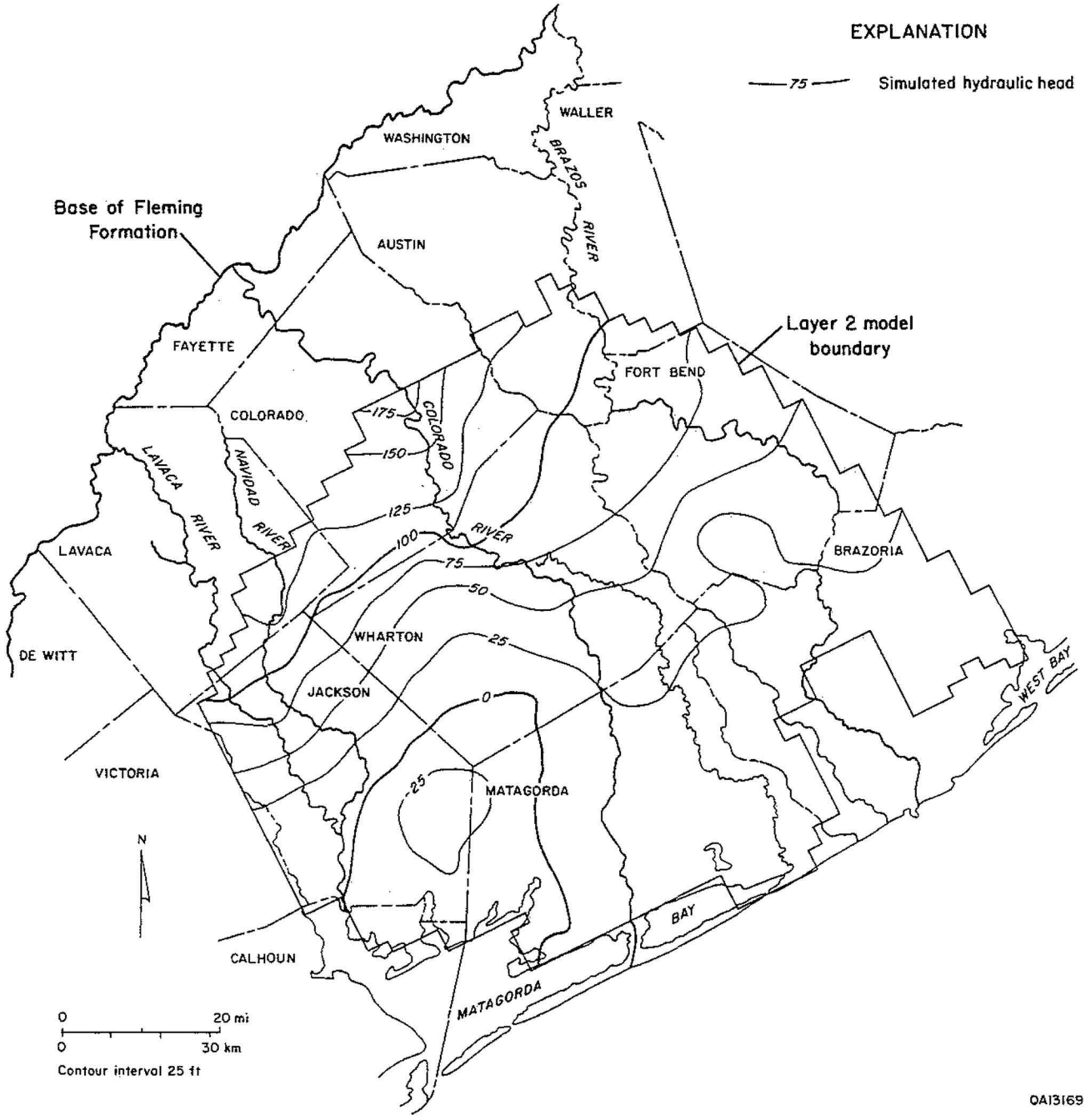

Figure 46. Simulated hydraulic-head surface for layer 2 representing 1965 conditions, comparable to that part of figure 19 representing the Chicot.

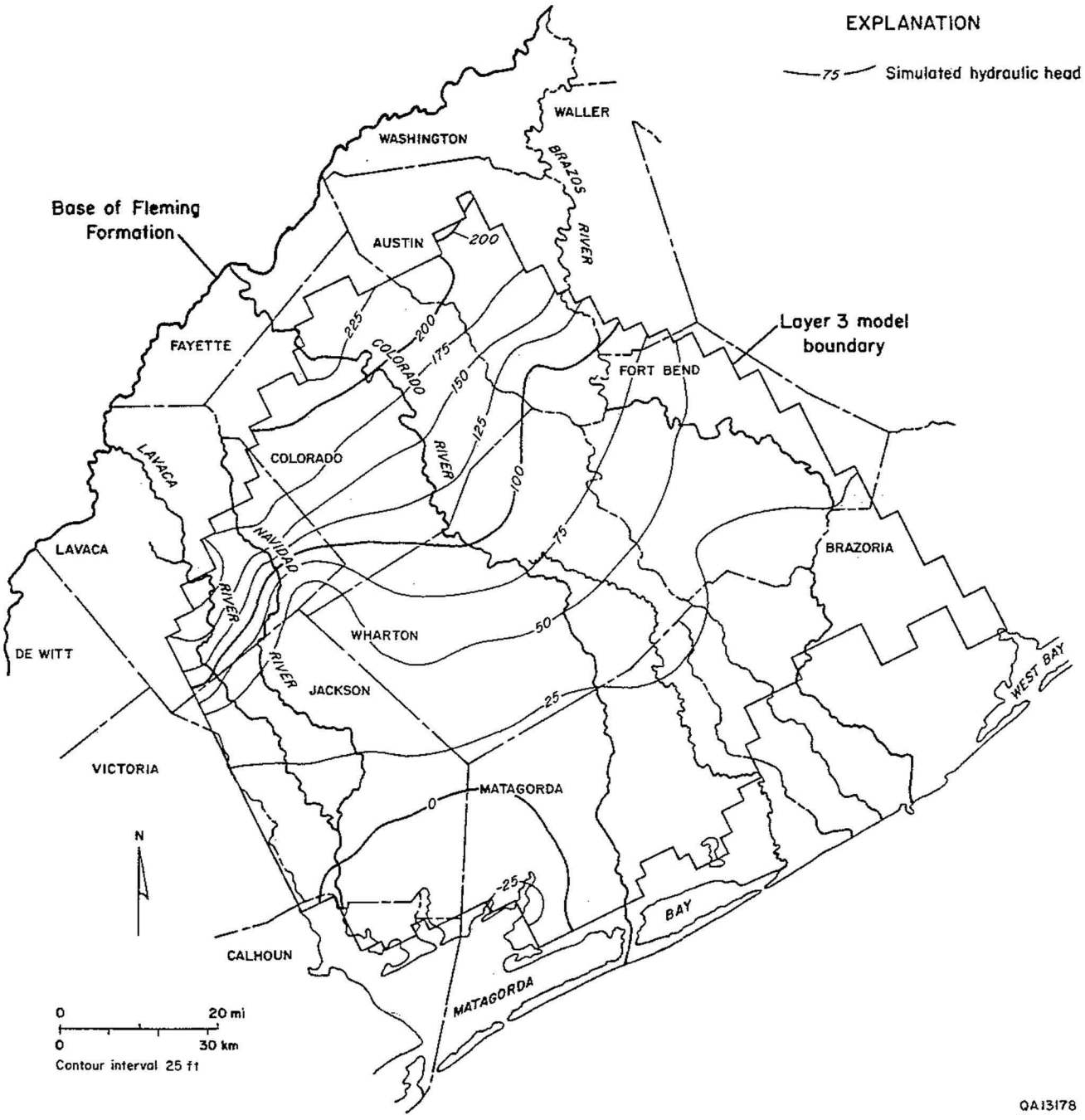

Figure 47. Simulated hydraulic-head surface for layer 3 representing 1965 conditions, comparable to that part of figure 19 representing the Evangeline.

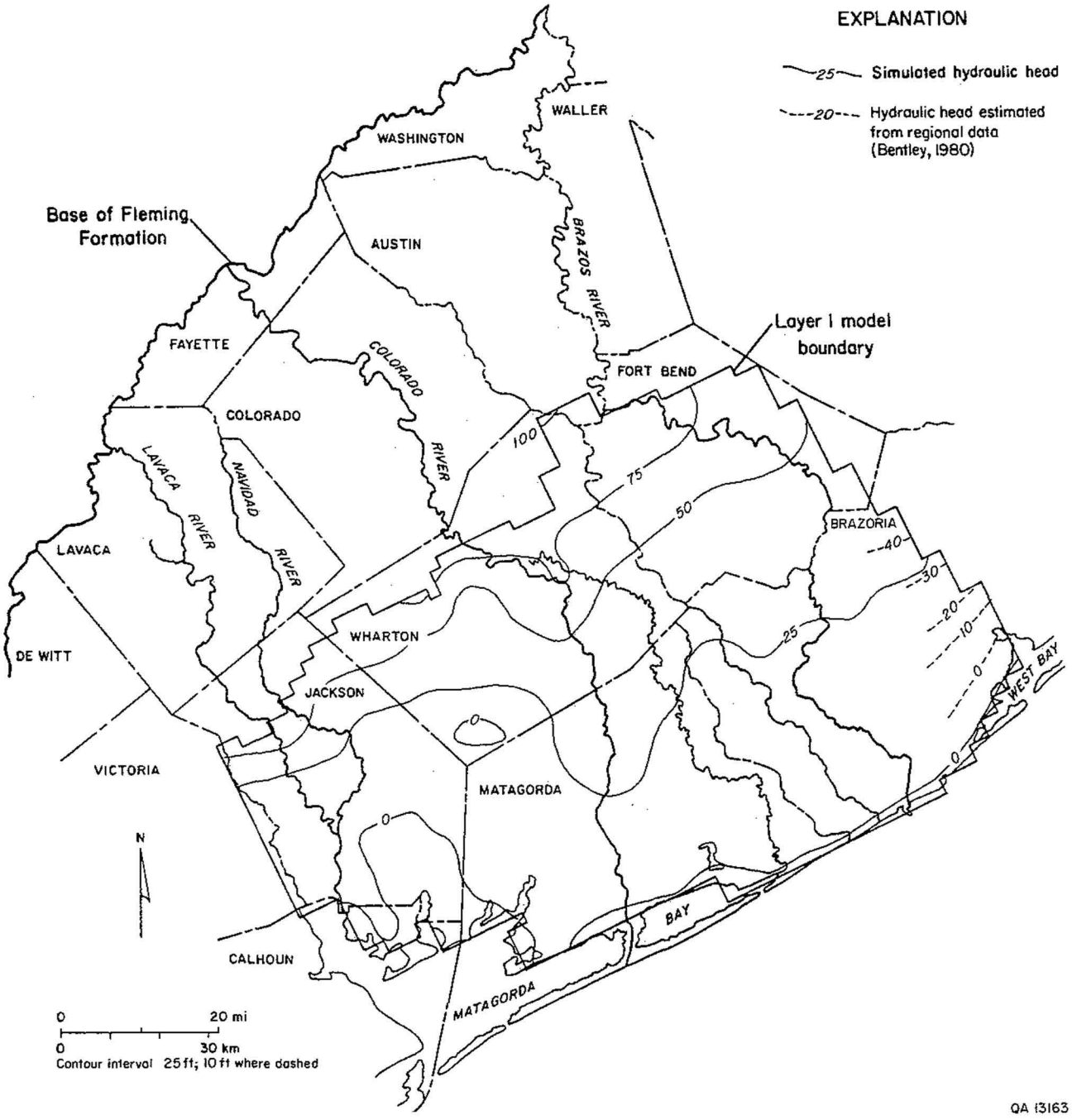

Figure 48. Simulated hydraulic-head surface for layer 1 representing 1985 conditions in the Beaumont Formation.

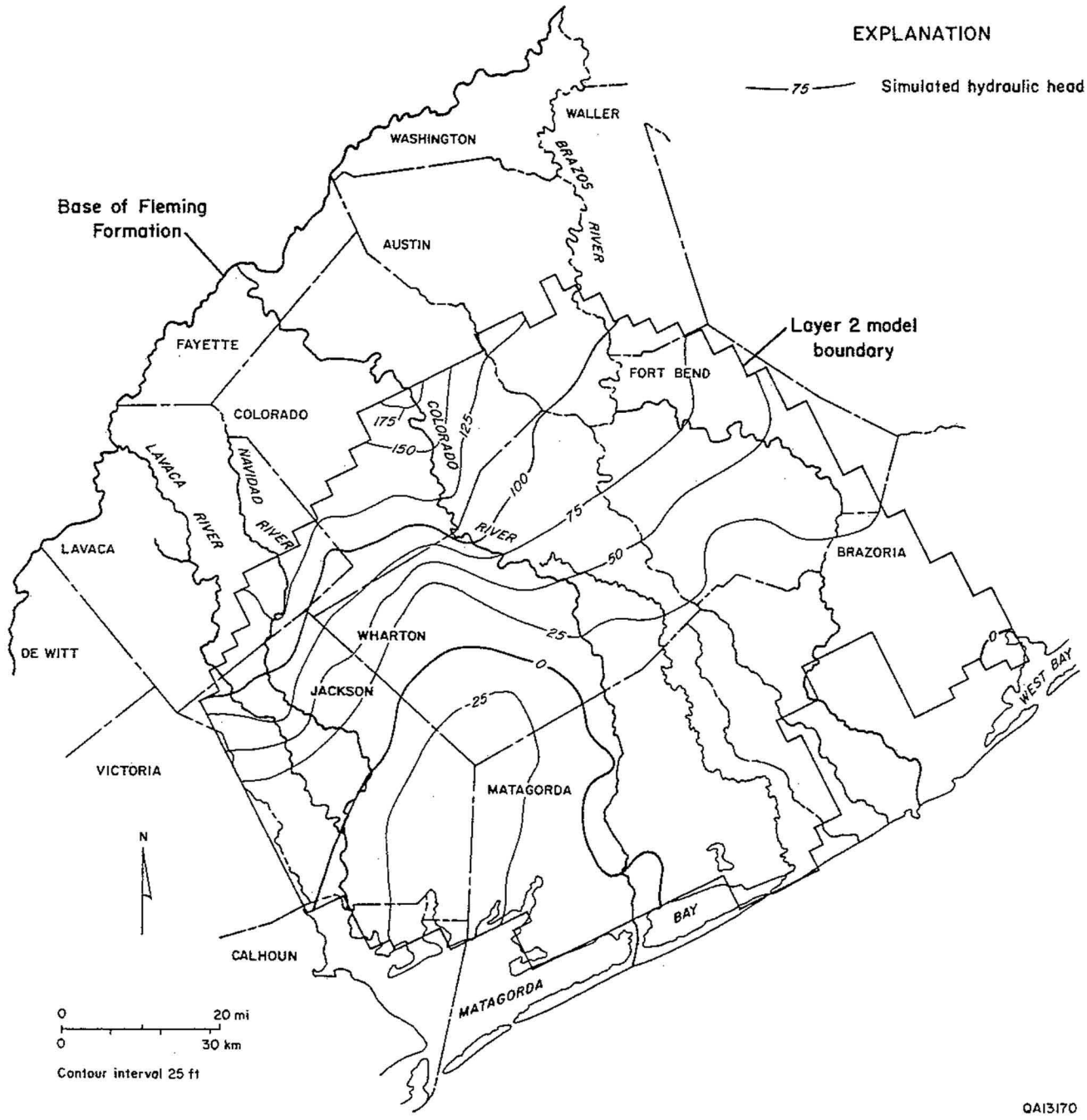

Figure 49. Simulated hydraulic-head surface for layer 2 representing 1985 conditions, comparable to that part of figure 20 representing the Chicot.

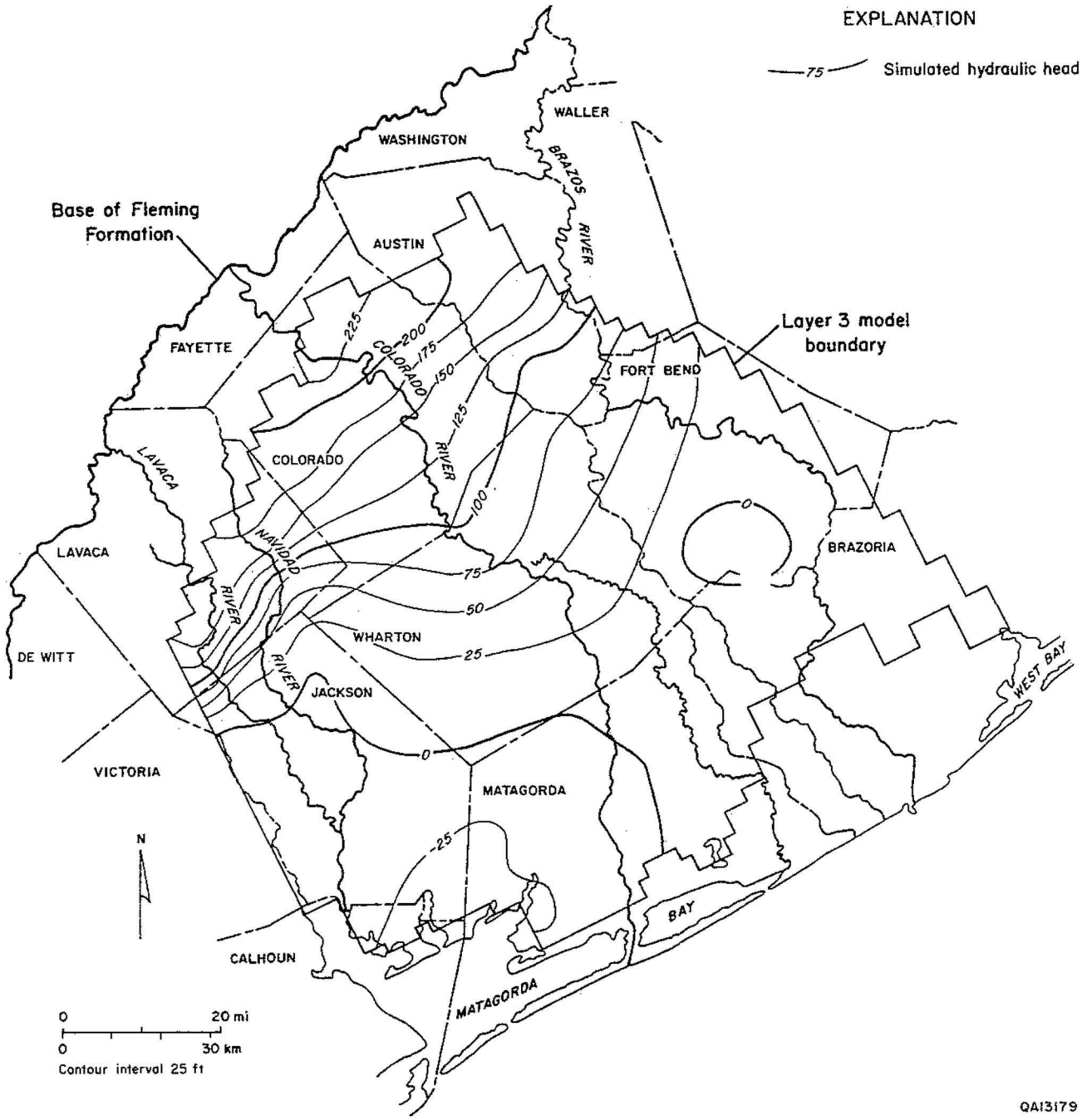

Figure 50. Simulated hydraulic-head surface for layer 3 representing 1985 conditions, comparable to that part of figure 20 representing the Evangeline.

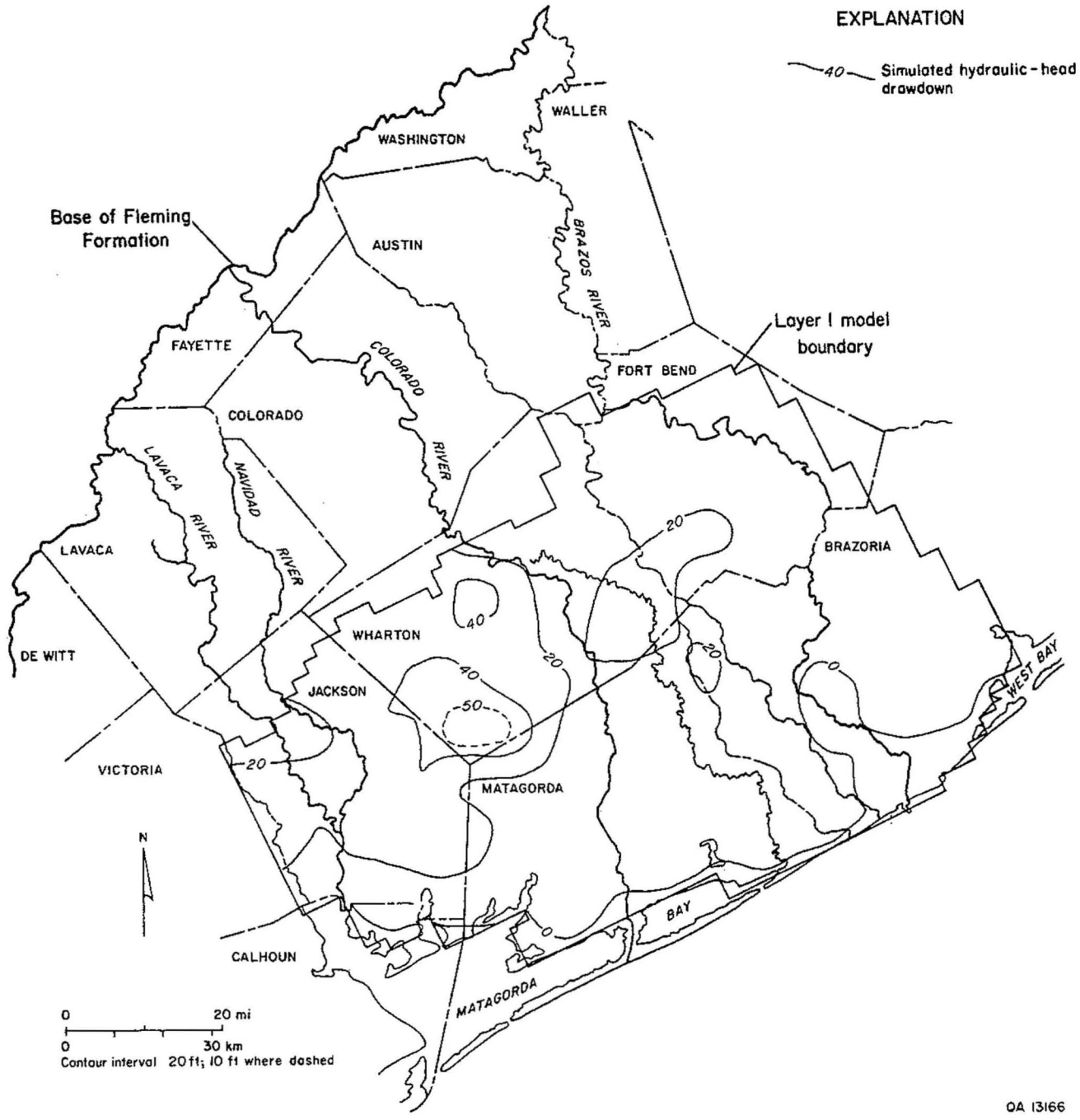

Figure 51. Drawdown in hydraulic head for layer 1 representing 1985 conditions in the Beaumont Formation.

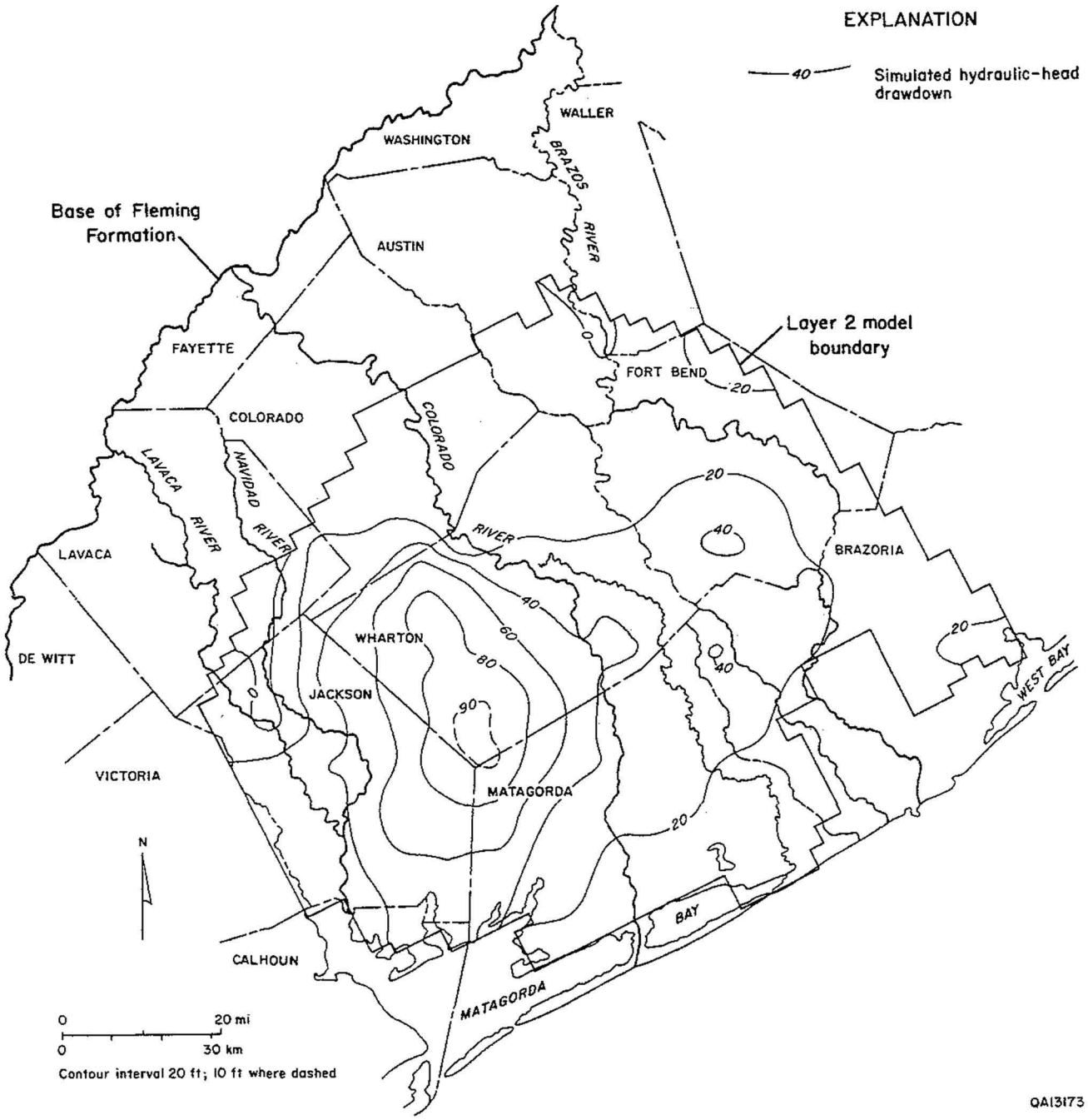

Figure 52. Drawdown in hydraulic head for layer 2 representing 1985 conditions in the Chicot.

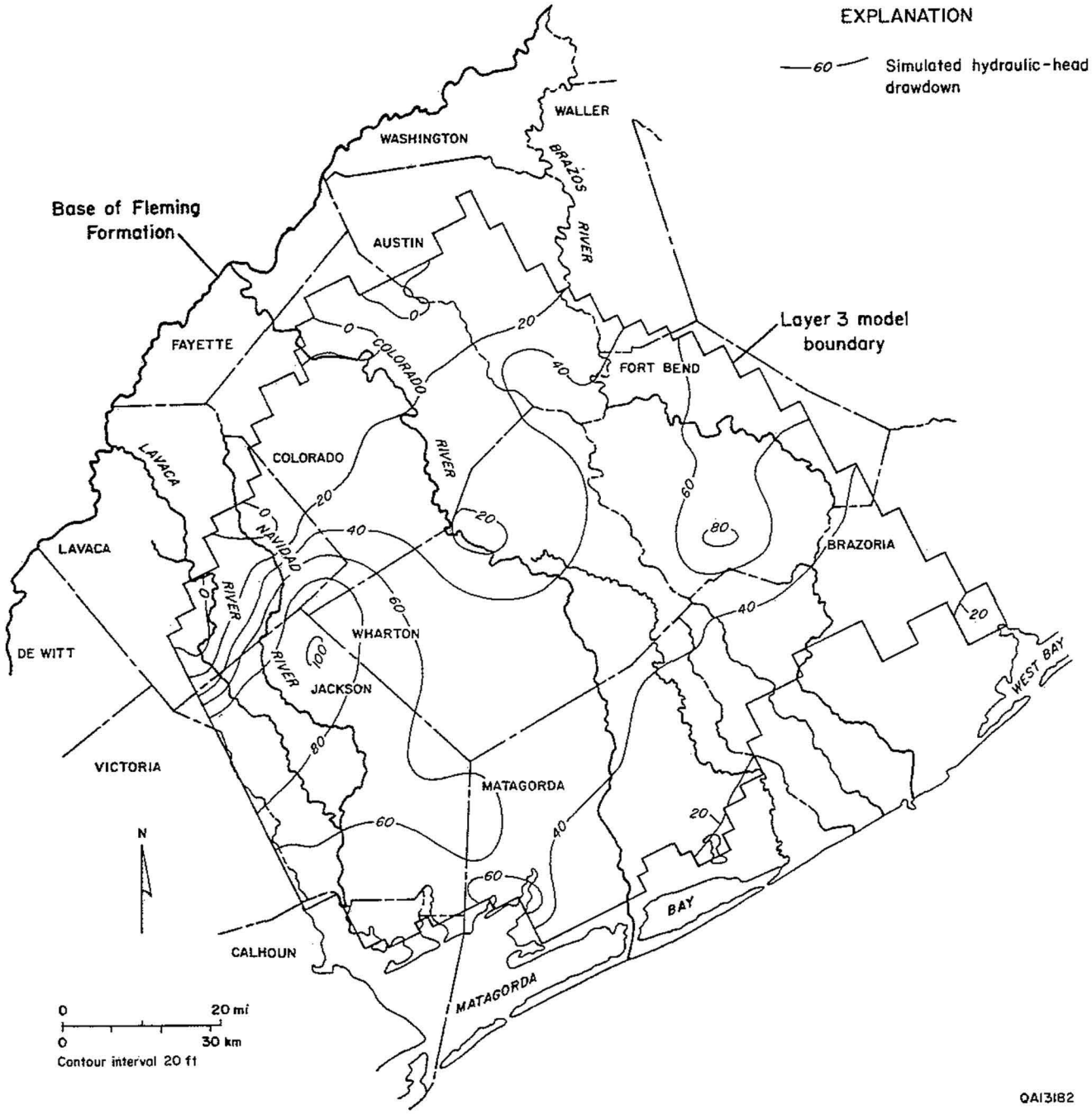

Figure 53. Drawdown in hydraulic head for layer 3 representing 1985 conditions in the Evangeline.

nodes, simulated water levels recovered when pumping rates were decreased between stress periods (table 4b; also compare figs. 47 and 50). Average historic drawdown rates in layer 2 were 0.3 to 0.5 ft/yr (table 4c). Average simulated drawdown rates in layer 1 were 0.1 to 0.4 ft/yr between 1900 and 1985.

Figure 54 shows the distribution of simulated recharge and discharge for 1985 across the study area, calculated using the general-head boundary option of MODFLOW (McDonald and Harbaugh, 1984). Discharge areas occur where the calculated heads in the uppermost aquifer unit are at higher elevations than the heads at the imaginary bounding node. Maximum calculated recharge is the same as simulated for the steady-state system (fig. 42). The predicted discharge area has shifted coastward, however, owing to the decline in hydraulic head in layer 1 relative to the constant heads at the imaginary bounding node.

Variation of river sediment conductances by a factor of 2 to 5 did not greatly change the volume of flow between the rivers and the aquifers. Vertical conductance values for the "recharge boundary," treated using the general-head boundary option in MODFLOW, are constrained within two orders of magnitude. Increasing conductance by a factor of 10 drives more water into the system than can be easily discharged, resulting in high estimates of head in the outcrop areas. In contrast, decreasing the conductance by a factor of 10 eliminates too much recharge, resulting in blocks dewatering in the outcrop areas.

Prediction of Future Ground-Water Levels

The open circles and pluses shown in figure 45 indicate the projected future decline in ground-water levels at selected points in the study area given projected high and low demands for ground water, respectively. The calibrated model predicts that average rates of future water-level decline will be approximately 1.2 to 2.1 ft/yr by 2000 and decrease to approximately 0.5 to 0.6 ft/yr by 2030 (table 4c). Maximum predicted rates of decline, given assumed high rates of pumping, range from 2.3 to 11.8 ft/yr (table 4a). Accuracy of these predictions is limited by the

Table 4. Rates of change in hydraulic head (ft/yr) in transient simulations. Positive values signify drawdown; negative values signify recovery.

a. Maximum rates of drawdown

	1900–1965	1966–1985	1985–2000	2001–2010	2011–2020	2021–2030
Layer 1	0.7	1.5	4.1	4.1	1.9	1.3
Layer 2	1.2	1.7	5.7	2.3	10.5	8.8
Layer 3	4.1	3.7	11.8	3.4	2.7	2.6

b. Maximum rates of recovery

Layer 1	0.0	0.0	0.0	0.0	0.0	0.0
Layer 2	0.0	–0.4	0.0	0.0	0.0	0.0
Layer 3	–0.3	–13.3	0.0	0.0	0.0	0.0

c. Rates of change averaged over active nodes

Layer 1	0.1	0.4	0.5	0.5	0.4	0.4
Layer 2	0.3	0.5	1.2	0.6	0.6	0.5
Layer 3	1.3	–2.2	2.1	0.9	0.8	0.6

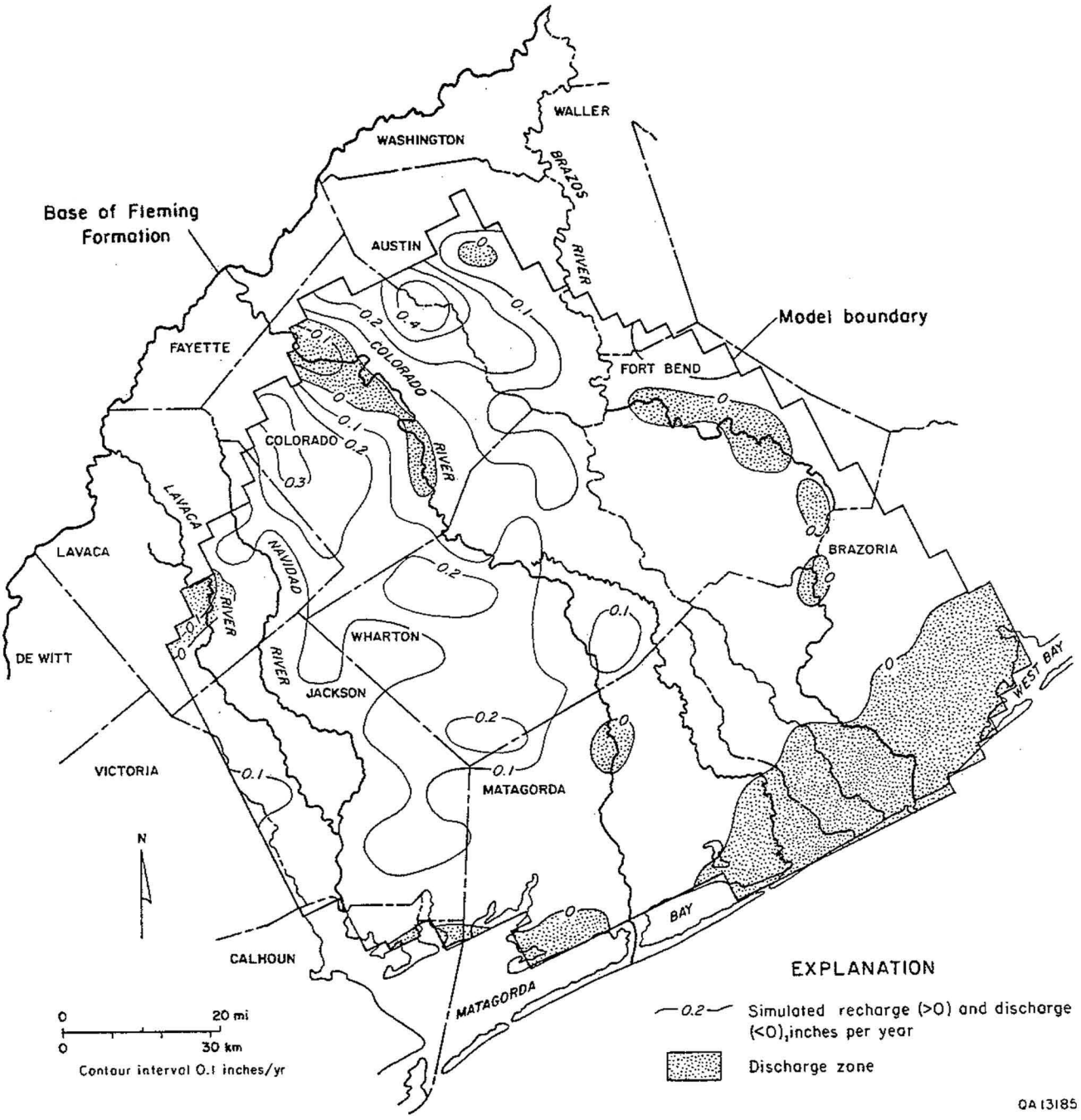

Figure 54. Distribution of recharge and discharge calculated for 1985 conditions.

degree of uncertainty in each component of the model. These results are sensitive to the imposition of a "no-flow" boundary between the study area and pumping areas in Harris and Brazoria Counties.

Figures 55 through 57 show predicted hydraulic-head surfaces in layers 1, 2, and 3, respectively, for the year 2020. Figures 58 through 60 show complementary maps of hydraulic-head drawdown relative to the original prepumping water levels. The 170-ft cone of depression in the hydraulic-head surface for layer 2 in western Wharton County (fig. 59) is calculated to reach an elevation of more than 75 ft below sea level (fig. 56). The 140-ft cone of depression for layer 2 in northwestern Brazoria County (fig. 59) is calculated to reach an elevation of more than 100 ft below sea level (fig. 56). The 340-ft cone of depression for layer 3 in southern Fort Bend County (fig. 60) is simulated to reach an elevation of more than 250 ft below sea level (fig. 57). The 140-ft cone of depression for layer 3 near the borders of Wharton, Jackson, Lavaca, and Colorado Counties (fig. 60) is simulated to reach an elevation of approximately 25 ft below sea level (fig. 57). Accuracy of the predicted drawdowns in Fort Bend and Brazoria Counties can be seriously questioned because of the proximity of the cones of depression to the model boundary. It is likely that simulated drawdown would be less extreme if the eastern and southern (coastal) boundaries of the model were constant-flux boundaries. The steep gradient in hydraulic head will, however, markedly increase the potential for seawater intrusion and deterioration of ground-water quality. The hydraulic-head gradient already had become directed inland from the coastline by 1965 because of extensive production of ground water. The influence of seawater intrusion on water quality is apparent in cross sections of salinity and hydrochemical facies shown in figures 32 through 35. In light of the potential for seawater intrusion, it is likely that the simulated pumping rates at nodes in this part of the model would not be actually conducted.

Figure 61 shows the distribution of simulated recharge and discharge for 2030 across the study area, calculated using the general-head boundary option of MODFLOW (McDonald and Harbaugh, 1984). Maximum calculated recharge remains the same as simulated for the steady-state system (fig. 42). The predicted discharge area has shifted farther coastward than shown in figure

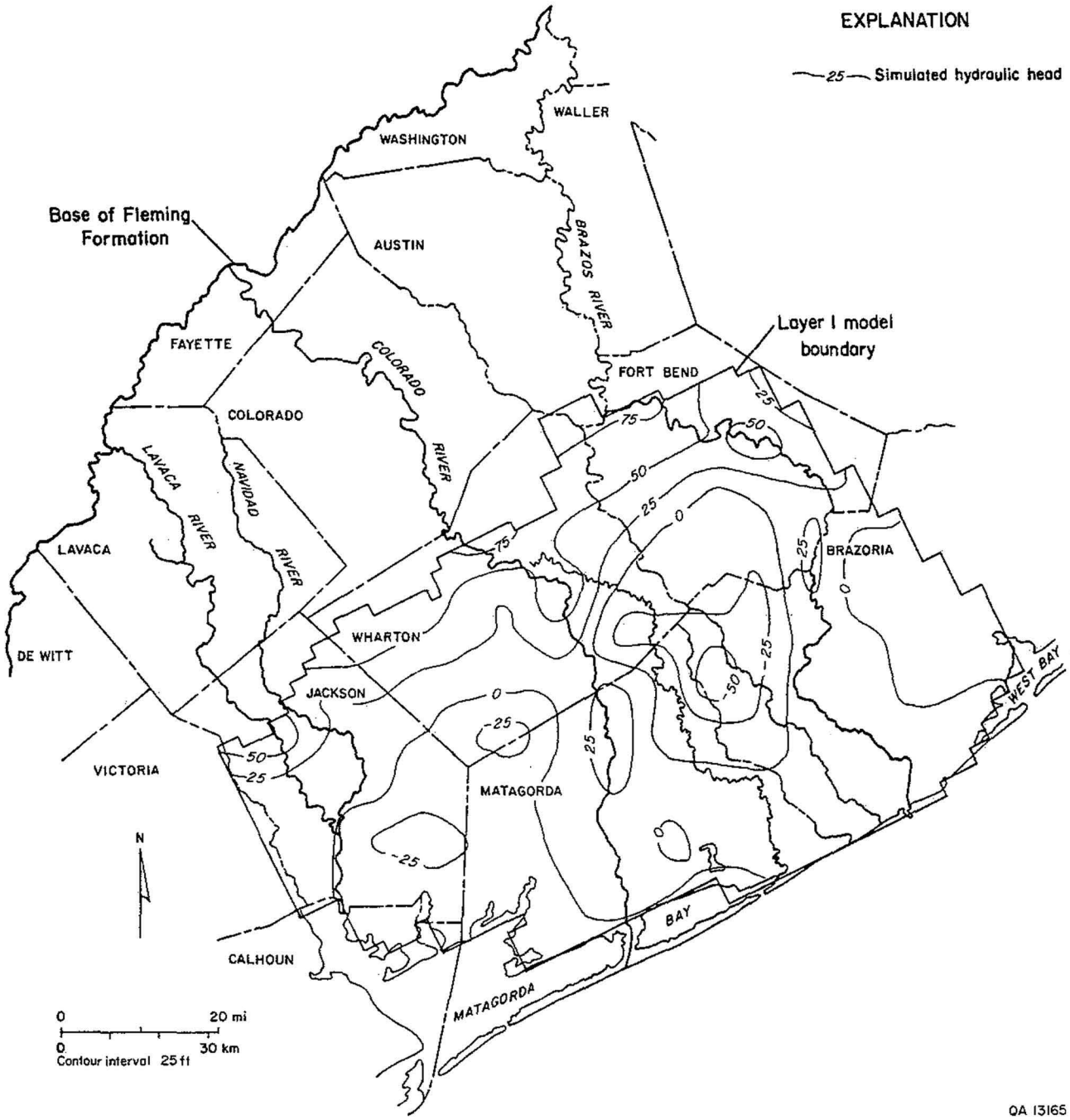

Figure 55. Simulated hydraulic-head surface for layer 1 representing 2030 conditions in the Beaumont Formation.

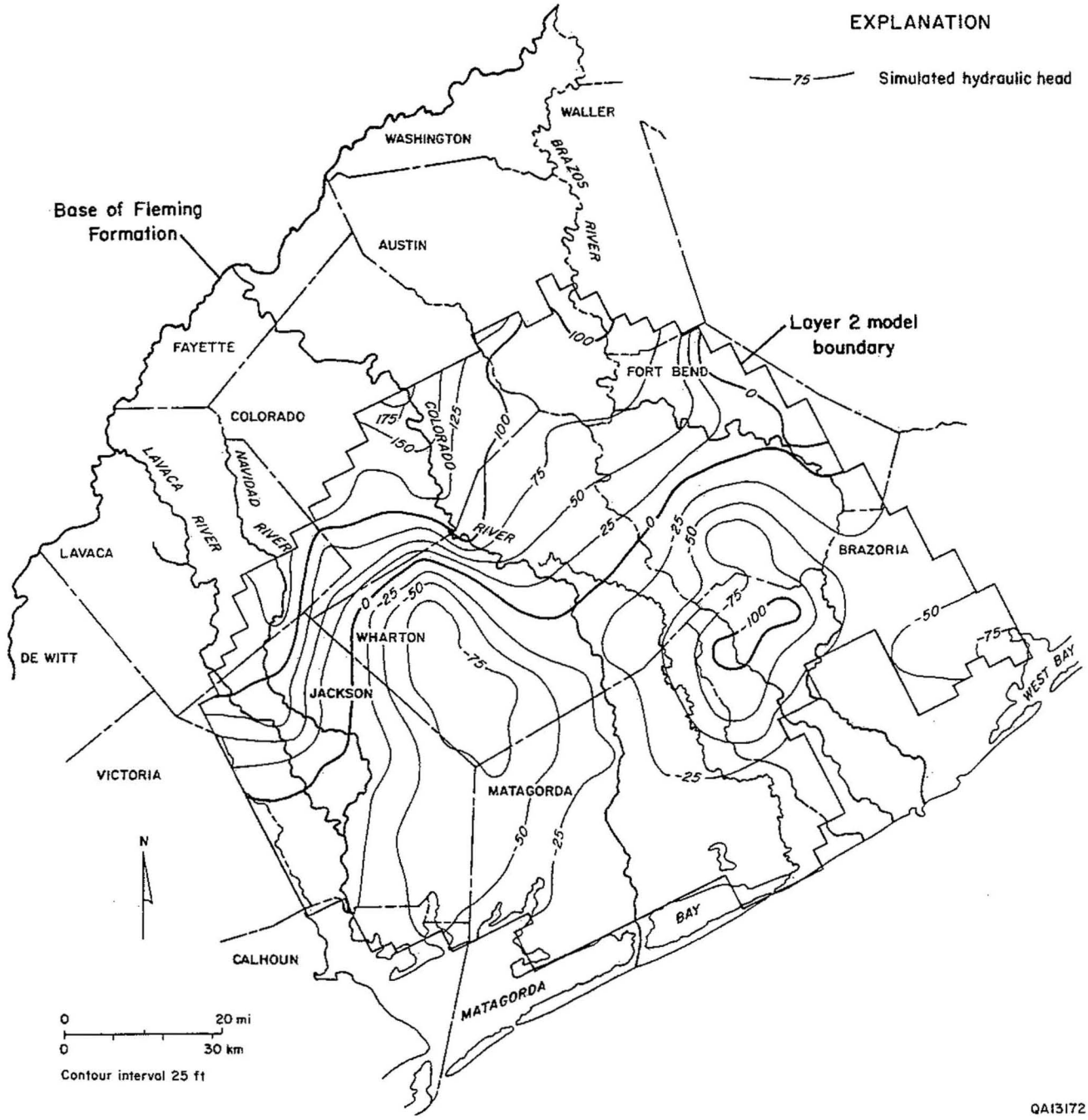

Figure 56. Simulated hydraulic-head surface for layer 2 representing 2030 conditions in the Chicot.

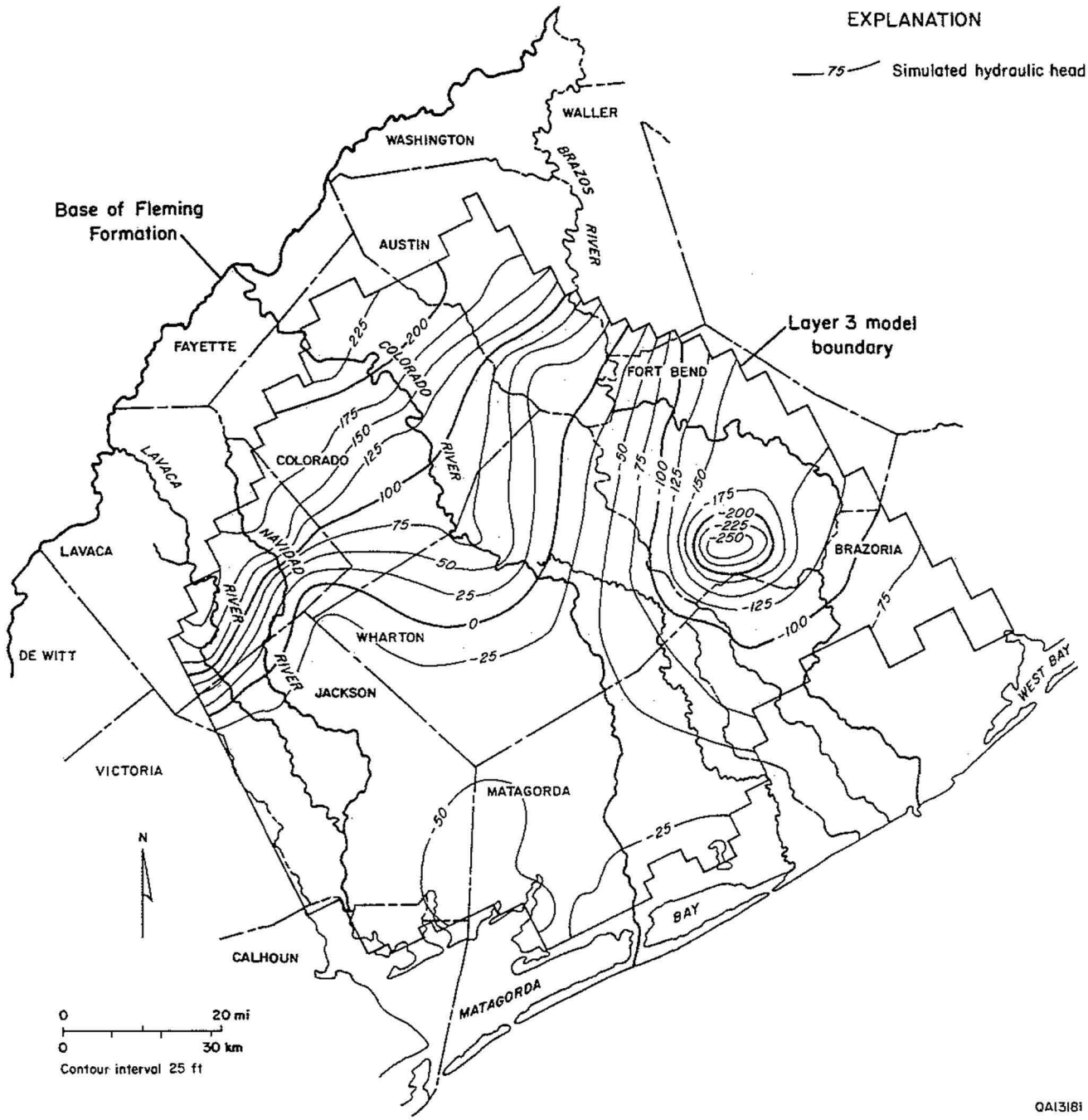

Figure 57. Simulated hydraulic-head surface for layer 3 representing 2030 conditions in the Evangeline.

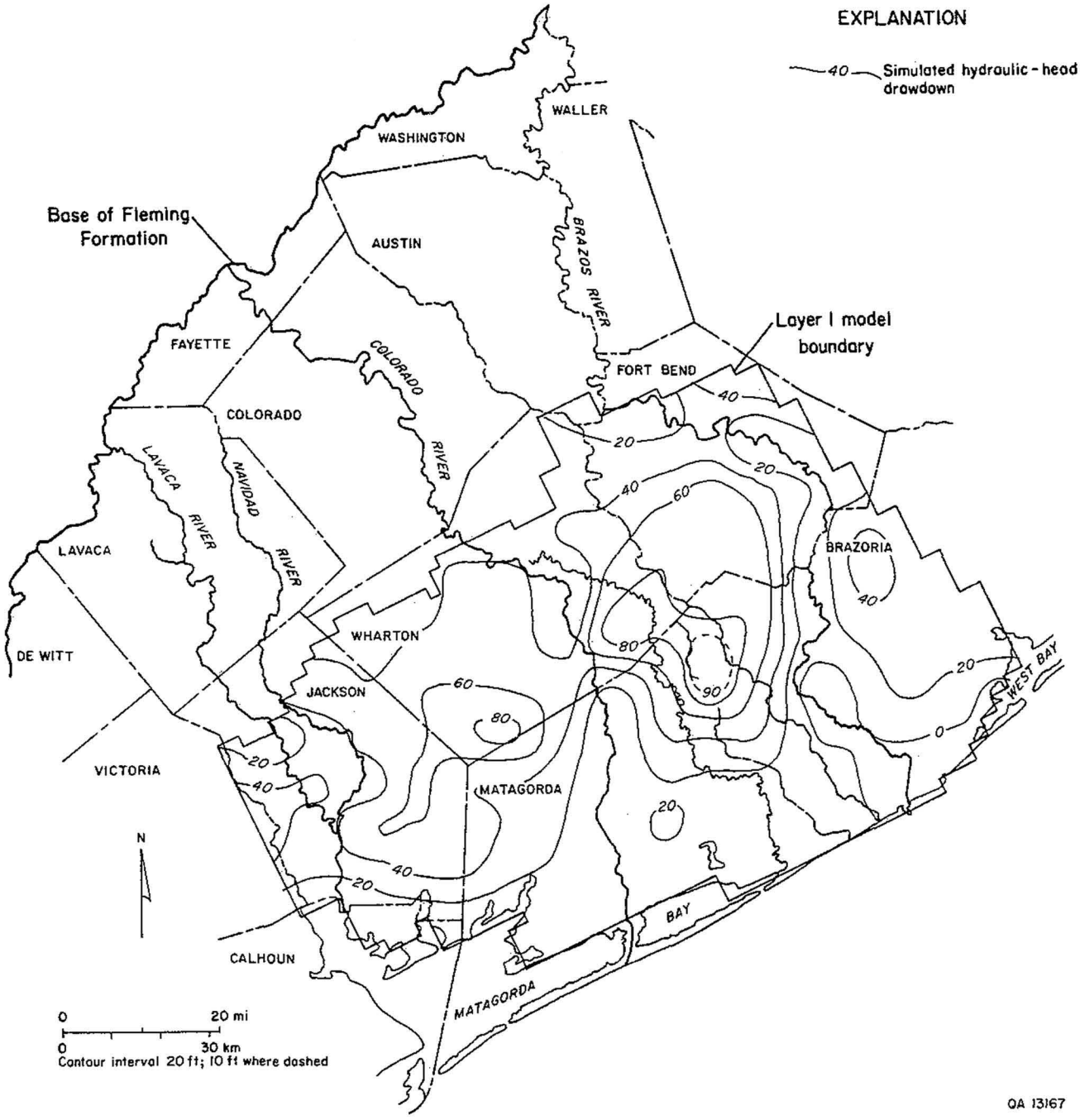

Figure 58. Drawdown in hydraulic head for layer 1 representing 2030 conditions in the Beaumont Formation.

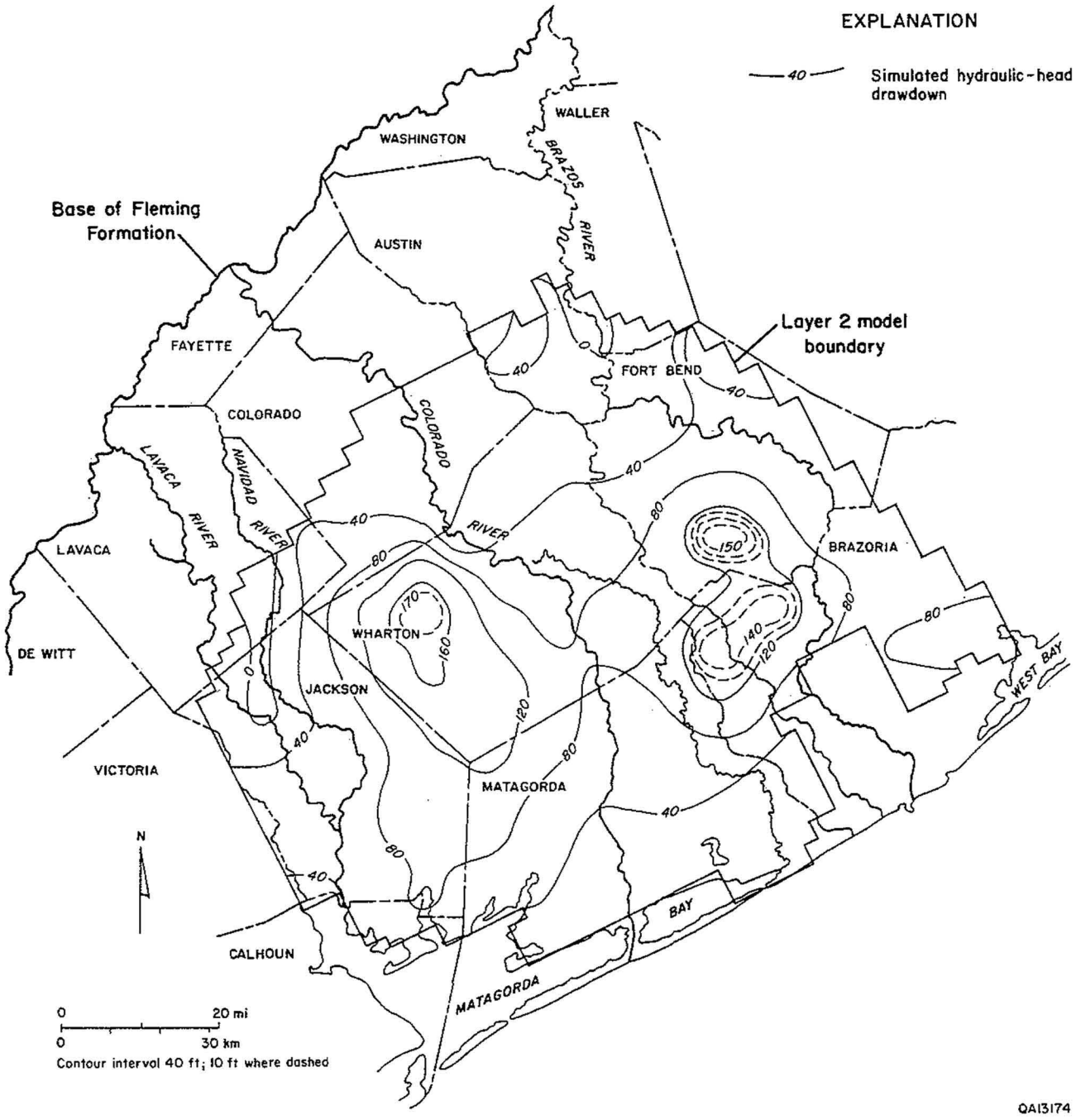

Figure 59. Drawdown in hydraulic head for layer 2 representing 2030 conditions in the Chicot.

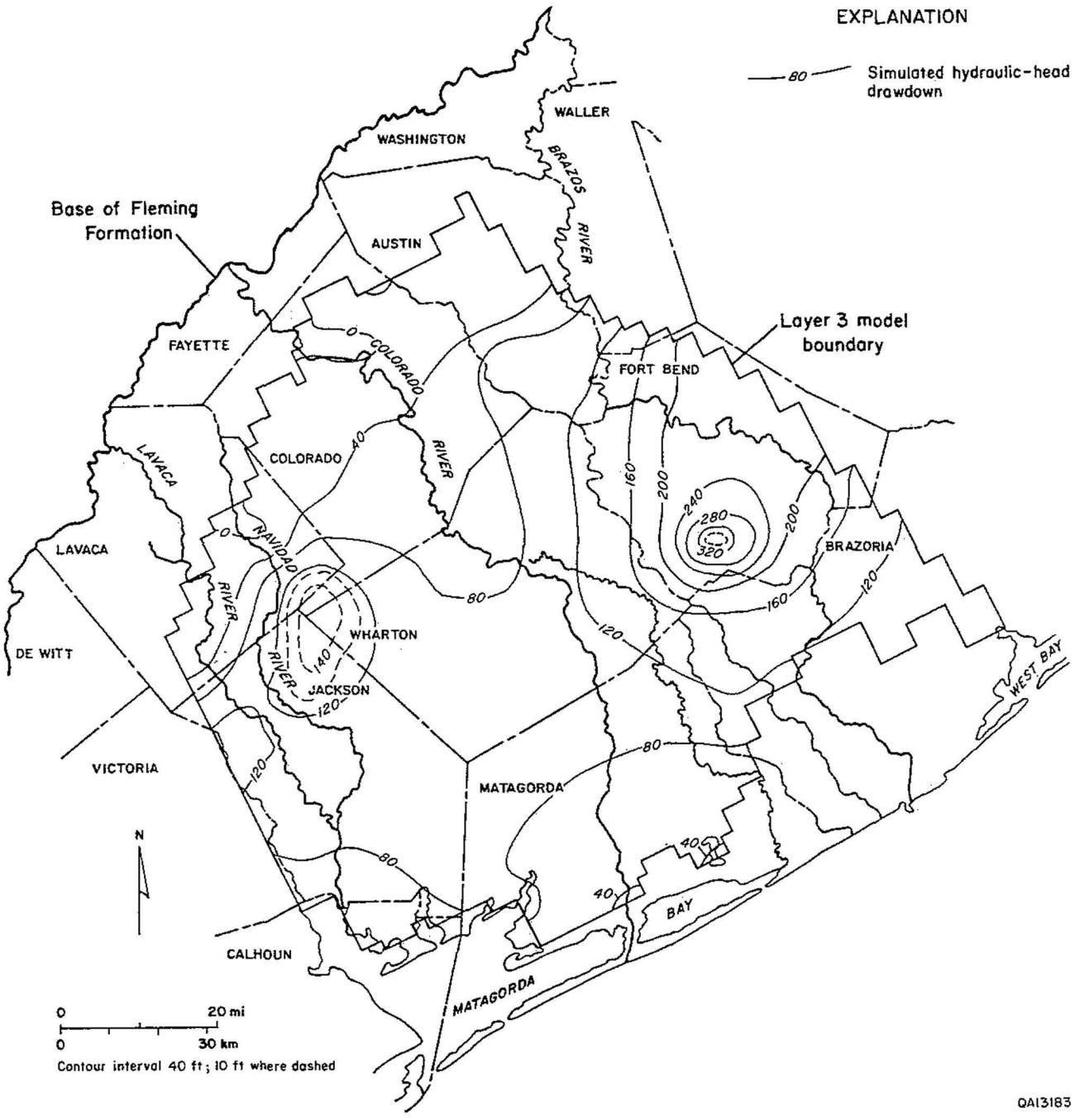

Figure 60. Drawdown in hydraulic head for layer 3 representing 2030 conditions in the Evangeline.

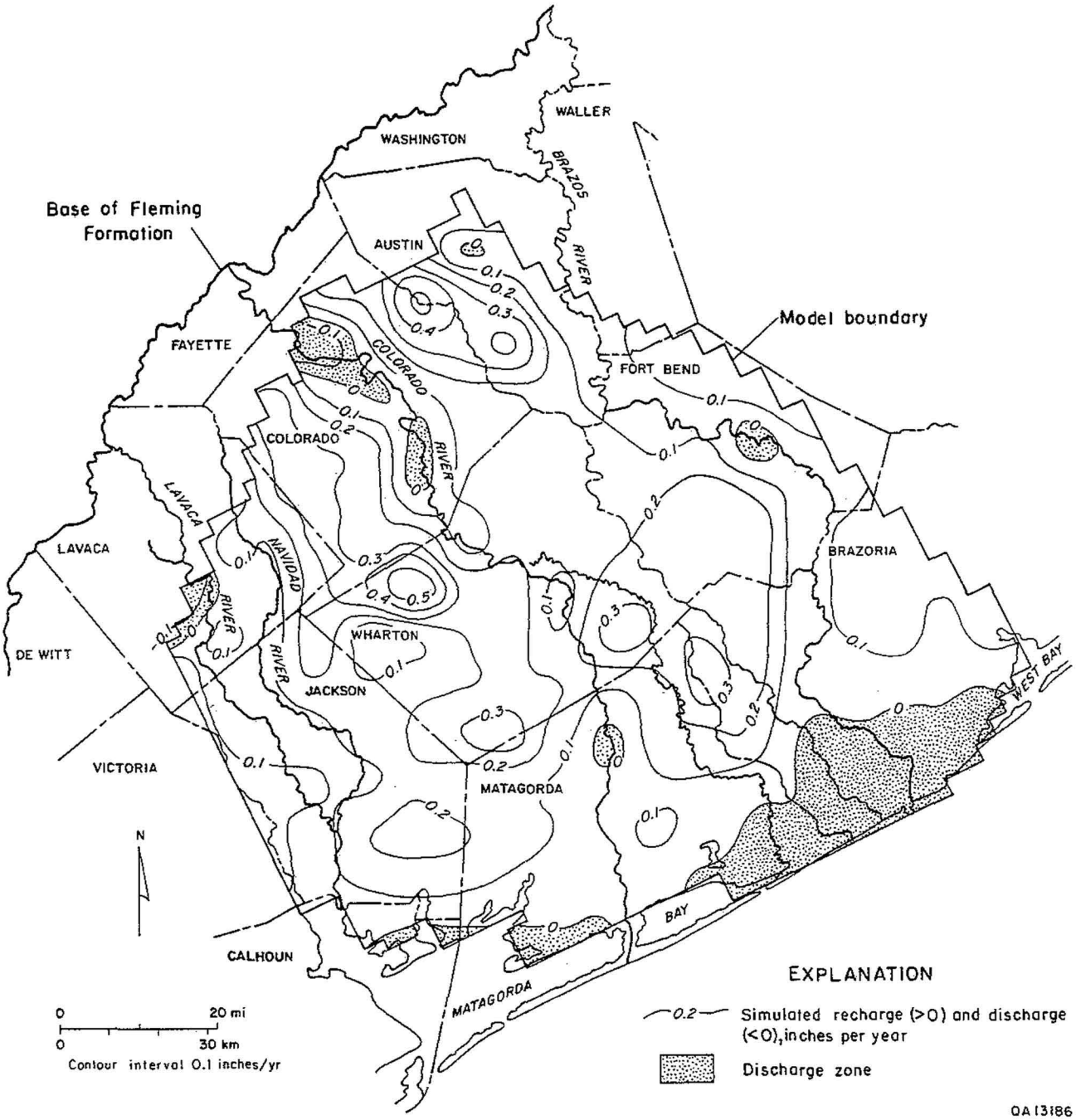

Figure 61. Distribution of recharge and discharge calculated for 2030 conditions.

54 for the 1985 flow system, owing to the continued simulated decline in hydraulic head in layer 1 relative to the constant heads at the imaginary bounding node.

Figure 62 summarizes the potential for drawdown in hydraulic head in the Gulf Coast aquifer system. The profiles show positions of the water table or potentiometric surface across the model layers representing aquifer units, assuming no variation in hydraulic head with depth. The predicted 20- to 40-ft drawdown in the water table in layer 1 that is estimated for 1985 only locally increases by 2030 (fig. 62a). Drawdown in the potentiometric surface of layer 2 expands the area of the Chicot aquifer unit that is under water table conditions (fig. 62b). The profile clearly shows that drawdown in layer 2 is more significant than that in layer 3. The numerical model assumed that ground water was produced from finite-difference blocks that represent the entire thickness of a model layer. The water level in wells actually completed in the upper part of the Chicot aquifer may drop below the base of the wells between 1985 and 2030.

Regional Water Budget

Table 5 shows a water budget calculated in the simulation of steady-state flow system. Note that the difference of 32 acre-ft between inflow and outflow is an insignificant error. For steady-state conditions, total inflow to aquifer blocks from influent (losing) river reaches nearly equals total outflow from aquifer blocks to effluent (gaining) reaches. Recharge simulated using the general-head boundary option in MODFLOW appears to be balanced partly by discharge from other blocks to the imaginary bounding node and partly by discharge of water from the continental flow system to the "constant-head" blocks along the coastal strip of of layer 1 (see fig. 33). This is a reasonable approximation of the natural system.

During simulation of transient conditions, the main added stresses were water-well pumping of approximately 330,000 acre-ft of water in 1985, for example, and of 640,000 acre-ft of water in 2030. For the 85-year historical period that ended in 1985, water losses from rivers quadrupled relative to steady-state fluxes owing to decline in hydraulic heads in the aquifers, and the size of

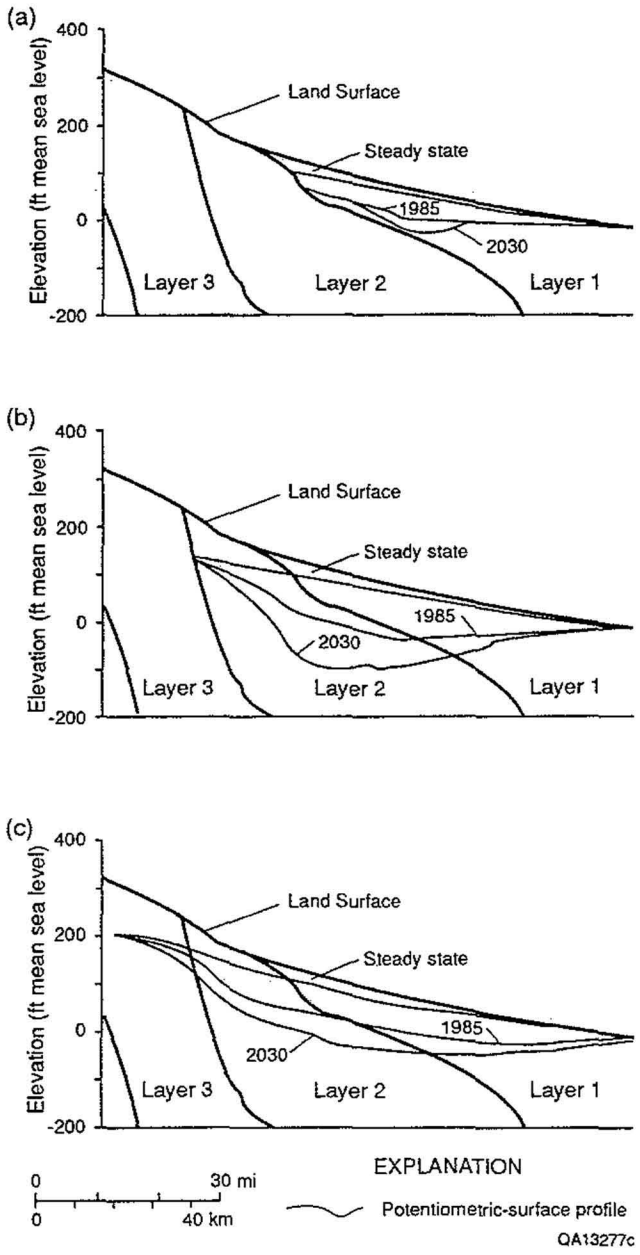

Figure 62. Profiles of potentiometric surfaces simulated for 1900 (steady state), 1985, and 2030 for layer 1 (a), layer 2 (b), and layer 3 (c).

Table 5. Simulated water budget of the Gulf Coast aquifer system in the model area. Average annual values are in acre-ft.

	Steady state	1985	2030	2030 with well field
Inflow				
Constant-head nodes	0	3,630	10,031	10,233
Rivers	22,513	85,501	167,684	176,146
Head-dependent boundaries	12,551	26,954	50,058	50,725
Wells	0	0	0	0
Subtotal	35,064	116,084	227,773	237,104
Outflow				
Constant-head nodes	9,467	2,341	645	580
Rivers	21,099	4,573	2,452	2,471
Head-dependent boundaries	4,466	1,826	1,202	1,194
Wells	0	330,529	639,635	661,536
Subtotal	35,032	339,268	643,934	665,781
Difference (Inflow-Outflow)	32	-223,184	-416,161	-428,678
Storage Decrease	0	223,692	416,095	428,781
Storage Increase	0	563	0	0
Storage Net Change	0	223,129	416,095	428,781
Percent Error	0.09	-0.02	-0.01	0.02

discharge areas decreased (compare figs. 42 and 54). There appears to be a greater potential for recharge with lower water-table elevations. The large ground-water withdrawals result in an average annual decrease in storage of more than 220,000 acre-ft in 1985 and of more than 416,000 acre-ft in 2030. The decrease in fluid pressure accompanying the storage decrease results in land-surface subsidence, discussed in the following section. Note that in addition to calculating increased losses from rivers, the water budget also shows significant increases in inflow to the constant head nodes in layer 1. This flux, required to keep the head equal to zero at those coastal nodes, is interpreted to represent the landward flux of seawater induced by the regionally lower hydraulic heads in layer 1. Because the model uses "no-flow" boundaries at the seaward edges of layers 2 and 3 (see fig. 30), that is, because the base of fresh water is fixed, a comparable estimate of the seawater intrusion rate is not made for those layers.

Subsidence Potential

Land subsidence owing to decline in hydraulic head or fluid pressure with ground-water production is a natural hazard of the Texas Coastal Zone (Brown and others, 1974). The potential for subsidence varies regionally and depends on amount of ground-water withdrawal (ΔV), amount of hydraulic-head or fluid-pressure decline (Δh or Δp, respectively), compressibility of clay beds (α), total thickness of clay beds (b'), and degree of compaction of clay. One equation for estimating potential for compaction of clay is

$$\alpha \, \Delta\sigma = -\Delta V/V = -\Delta b'/b', \tag{3}$$

where $\Delta\sigma$ is change in effective stress (de Marsily, 1986). Effective stress is equal to specific weight of water times its hydraulic head

$$\Delta\sigma = \Delta p = -\gamma \, \Delta h. \tag{4}$$

Compaction of clay beds, therefore, can be calculated by substituting equation 3 into equation 2 and rearranging to give

$$\Delta b'_i = b'_i \gamma_i \alpha_i \Delta h_i \quad (5)$$

where the subscript (i) refers to each layer of the ground-water flow model.

In the Gulf Coast aquifer clay beds are discontinuous and are complexly intercalated with sand deposits that compose the aquifer units (see figs. 5–13). To apply this one-dimensional model to estimate subsidence potential in the study area, total thickness of clay beds within aquifer units was determined by multiplying layer thickness by the complement of sand percentage. Values for hydraulic-head drawdown were previously discussed (figs. 52–54 for 1985 conditions and figs. 58–60 for 2030 conditions). Total compaction potential was determined by applying equation 4 to each layer (i) of the model and summing the calculated compaction ($\Delta b'_i$) for each vertical column of finite-difference blocks. Resulting spatial estimates of subsidence were compared to measured values reported by Ratzlaff (1982) and Loskot and others (1982). Compressibility estimates (α_i) then were repeatedly adjusted and results recompared to obtain a reasonable match between observed subsidence and subsidence predicted from 1985 drawdown estimates (fig. 63). Final adjusted values of aquifer compressibility were $10^{-5.36}$ psi^{-1} ($10^{-9.2}$ m^2/N) for layer 1, $10^{-3.86}$ psi^{-1} ($10^{-7.7}$ m^2/N) for layer 2, and $10^{-5.26}$ psi^{-1} ($10^{-9.1}$ m^2/N) for layer 3. In comparison, Freeze and Cherry (1979, p. 55) estimated values of α for sand to be $10^{-5.16}$ to $10^{-3.16}$ psi^{-1} (10^{-9} to 10^{-7} m^2/N) and for clay to be $10^{-4.16}$ to $10^{-2.16}$ psi^{-1} (10^{-8} to 10^{-6} m^2/N). The difference in calibrated values of compressibility between layers 2 and 3 is required to reproduce the observed subsidence pattern (fig. 63). Maximum observed subsidence more closely coincides with the areas of maximum drawdown in layer 2 (fig. 52) than in layer 3 (fig. 53). The higher compressibility values for layer 2 compared to layer 3 are consistent with the shallower Chicot clays being less compacted than the more deeply buried lower Chicot and Evangeline clays. Carr and others (1985) indicated that subsidence of as much as 0.25 ft has occurred throughout Matagorda and Wharton

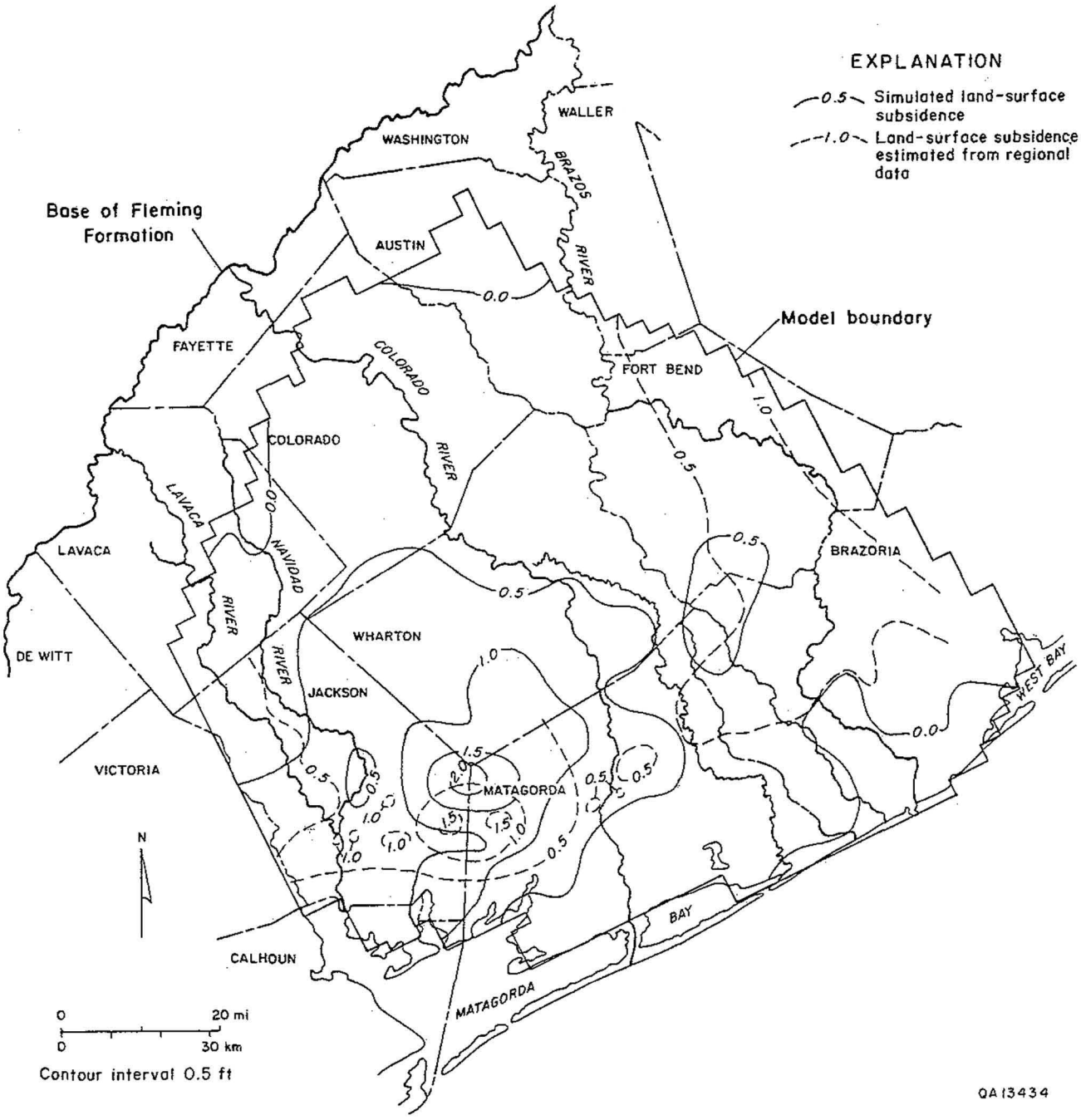

Figure 63. Distribution of estimated and simulated land surface subsidence for 1985. Regionally estimated subsidence from Ratzlaff (1982).

Counties, maximum subsidence being more than 1.5 ft near the junction of Matagorda, Wharton, and Jackson Counties.

Error in estimated compressibility values derives from errors in other numerical-model parameters. In addition, use of equation 4 assumes that clay-bed compaction and land-surface subsidence are simultaneous, whereas subsidence may lag significantly behind compaction (Brown and others, 1974), so that estimated compressibility may underestimate ultimate land-surface subsidence. Results are not sensitive to compressibility values for layer 1 because of the relatively small amount of drawdown in that layer and because layer 1 drawdown is correlated with layer 2 drawdown.

The adjusted estimates of aquifer compressibility were used to predict clay-bed compaction and land-surface subsidence in 2030 (fig. 64) based on simulated drawdown in hydraulic head (figs. 58–60). Simulated 2030 drawdown increases the potential for subsidence by 0.5 ft in northwestern Matagorda County and by approximately 1 ft in eastern Matagorda, northern Brazoria, and southern Fort Bend Counties, compared with 1985 subsidence. Accuracy of subsidence potential calculations depends largely on accuracy of hydraulic-head drawdown predictions. As previously mentioned, drawdowns estimated for southern Fort Bend and northern Brazoria Counties probably are overestimated owing to proximity to model boundaries. Subsidence potential in that area, therefore, is probably overestimated also.

The difference between original and subsided land-surface elevations calculated for each block in the model is 1.53 million acre-ft by 1985 and 3.24 million acre-ft by 2030. These volumes represent 12 to 18 percent, respectively, of the cumulative amount of water removed from storage due to ground-water withdrawal by 1985 and 2030.

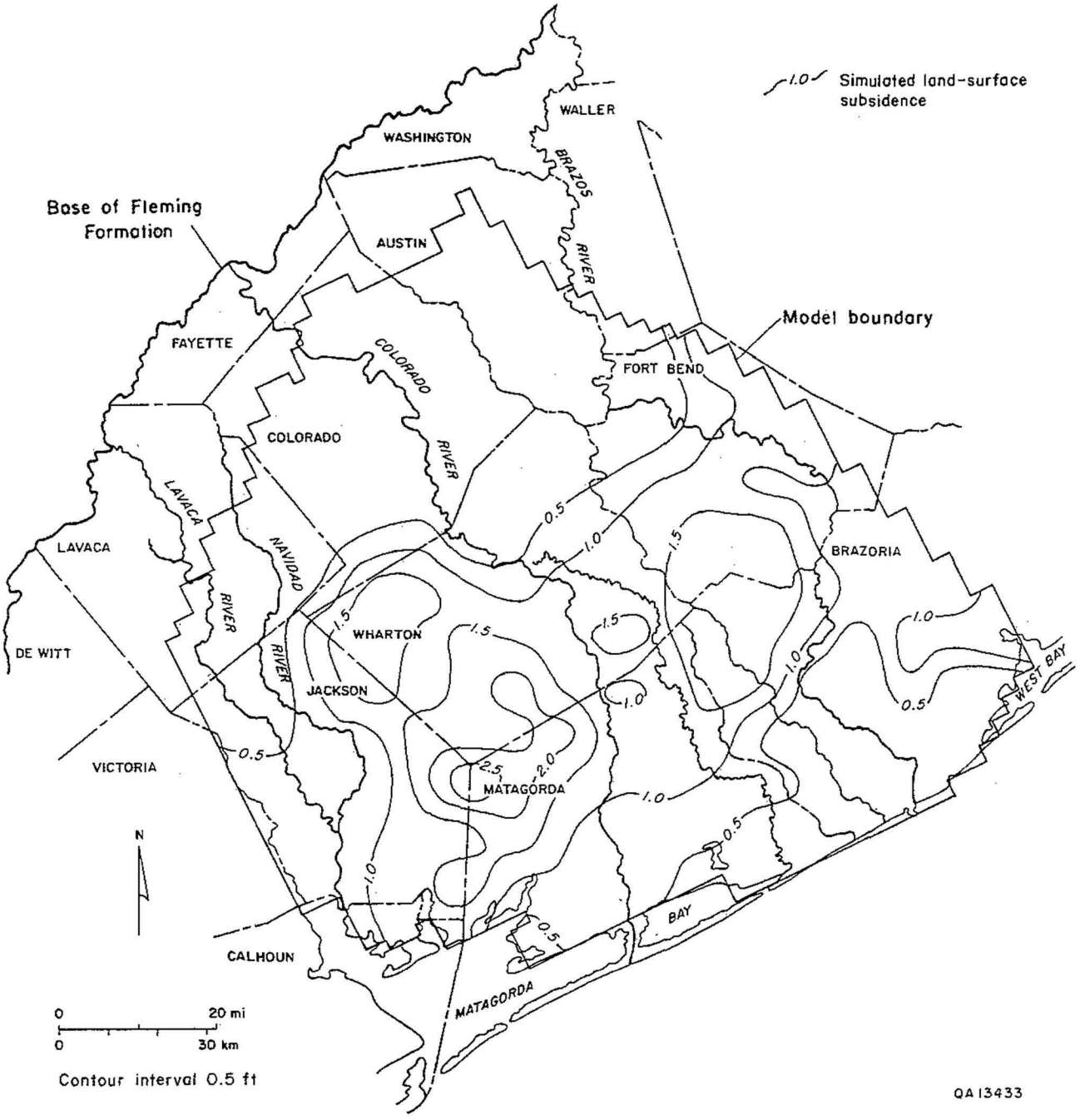

Figure 64. Distribution of predicted land-surface subsidence accrued by the year 2030 given the hydraulic-head declines depicted in figures 58 through 60.

DISCUSSION

Application to Evaluating Water-Resources Projects

Well-Field Project

To demonstrate the applicability of the numerical model for evaluating water-management strategies, a well field to supplement surface water supplies with ground water produced from the upper Chicot aquifer (layer 2 of the model) was simulated. Fifteen finite-difference blocks in columns 28 and 29 of the model were assigned to the well field, as shown in figure 65. Pumping rates from the blocks were increased by -2.1 ft^3/s. Pumping rates at these blocks without the simulated well-field project range from -0.008 to -0.825 ft^3/s; four blocks otherwise have no simulated pumping without the project. The 12-month project total of 22,820 acre-ft of water from the 15 blocks is equivalent to 30,427 acre-ft produced during a 9- month irrigation season. Initial distribution of hydraulic head for the well-field simulation was the simulated 1990 condition, taken as the twelfth time step of a 5-yr stress period following 1985 conditions previously discussed. Pumping at the well field was continued at -2.1 ft^3/s for 40 yr, in addition to the background projected pumping. Figure 65 shows the drawdown in hydraulic head in 2030 after 40 yr of pumping. These drawdown estimates would be superposed on the drawdown calculated with a projected high demand for ground water (see fig. 59). Node 1979 in the well field has the greatest amount of predicted drawdown, reaching 83 ft by 2030 (fig. 66). Figure 66 also shows that when the well-field operation is discontinued, for example, in 2010 after 20 yr of pumping, water levels recover relatively rapidly but after another 20 yr will not return to the background water level predicted to occur without the well-field project. The added drawdown owing to the well field would increase the potential for seawater intrusion and land-surface subsidence. The additional component of land-surface subsidence locally at the well field could be as great as 1.6 ft.

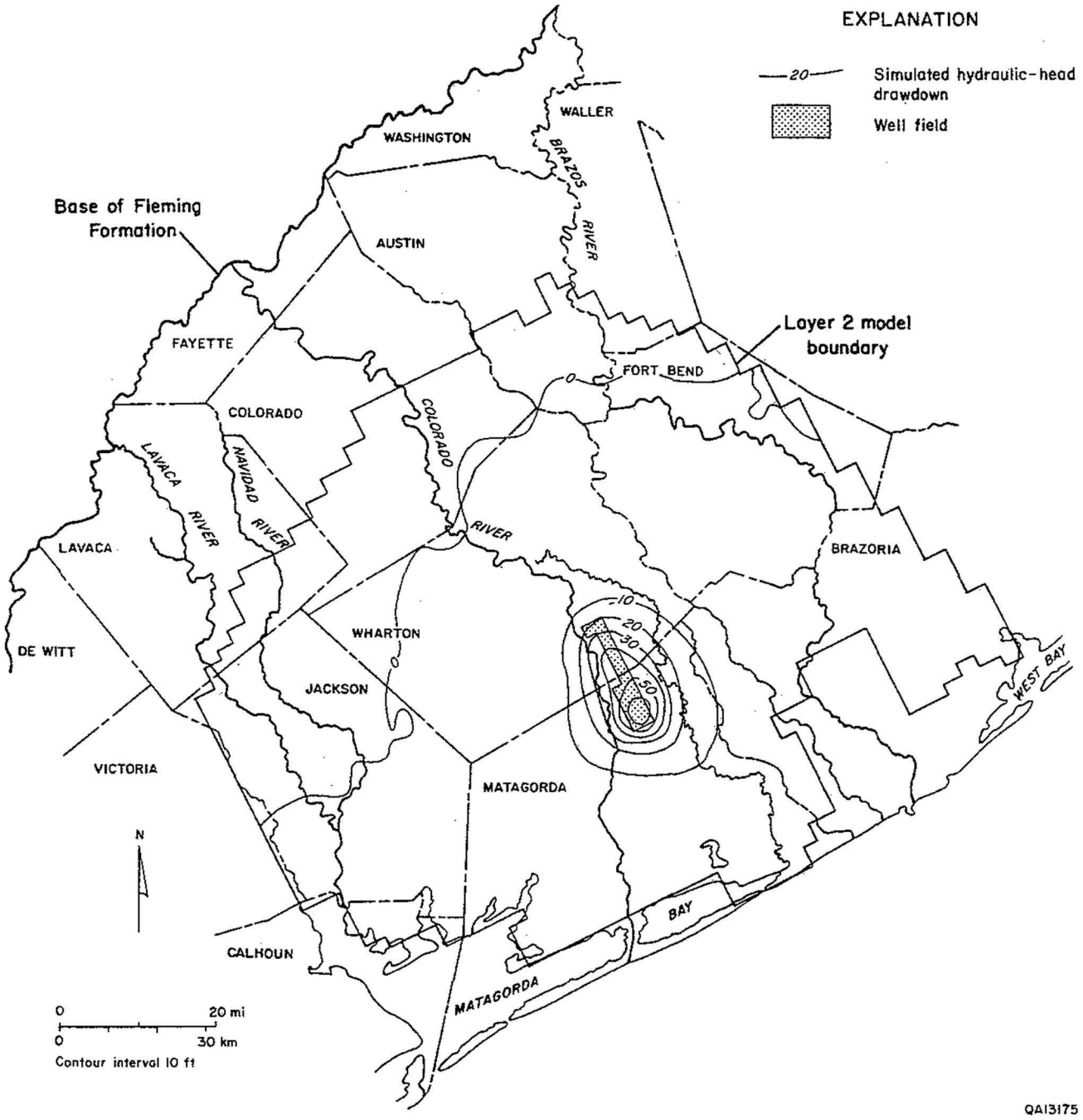

Figure 65. Drawdown of hydraulic head in a well field in layer 2 superposed on future predicted drawdown by the year 2030 after 40 yr of pumping. The 15 blocks that encompass the well field lie east of the Colorado River in model columns 28 and 29.

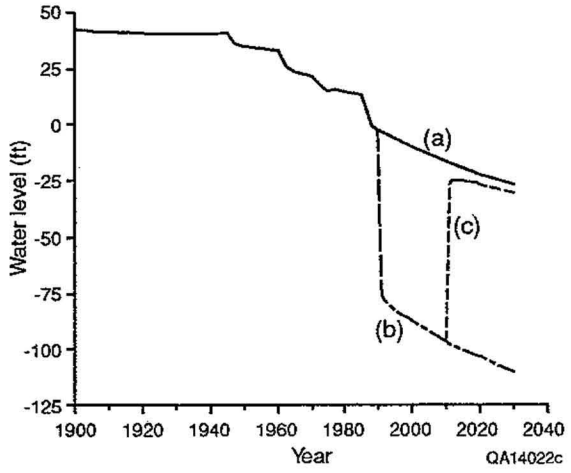

Figure 66. Simulated change in water level at node 1979 (row 40, column 29) in wellfield project, including historical and predicted future water level without wellfield project (a), drawdown induced by wellfield (b), and recovery of water level when wellfield pumping is discontinued after 2010 (c).

Artificial Recharge

Artificial recharge from ponds is conceptually identical to leakage from a river reach, except that the former is an isolated reach. Artificial recharge from ponds, therefore, can be treated in the model using the River Package option of MODFLOW. Artificial recharge through a specially constructed well can be included using the Well Package. The following discussion focuses on recharge through ponds and conjunctive use of surface and ground waters.

As described by McDonald and Harbaugh (1984) the river reach (or recharge pond) is defined as a rectangle with width "W," length "L," and a base layer of sediment of thickness "M." Water is simulated as moving from the recharge pond into the underlying aquifer as long as hydraulic head in the pond (H_r) is higher than that in the aquifer (H_{aq}). The rate of recharge (Q_r) is

$$Q_r = - \text{COND} \times (H_{aq} - H_r), \tag{6}$$

where conductance (COND) is

$$\text{COND} = K\,L\,W / M, \tag{7}$$

where K is hydraulic conductivity of the media lining the base of the recharge pond. The recharge flux, Q_r, is added to the right-hand side of the ground-water flow equation; it is subsumed by the term "W" in equation 2.

Recharge projects reported in various studies vary in size, from a 1-acre experimental recharge pond (Wood and Signor, 1975) to a 4-pond project covering 74 acres (Idelovitch and Michail, 1985). To demonstrate the applicability of using this model for evaluating artificial recharge, a pond of 2.5-acre extent was arbitrarily defined. Simulation runs were first made without a recovery well and then with a recovery well. The pond was assigned a stage height 5 ft above land surface and a 2-ft-thick base layer that ranges in vertical hydraulic conductivity from 13.6 to 136 ft/day. The hypothetical pond was located at grid node 1978 (row 40, column 28) near

the Colorado River and overlying the well-field project previously described. Artificial recharge operations were simulated as beginning in 1990 and continuing uninterrupted for 40 yr.

Simulation results without a recovery well indicate that infiltration rates would be 6 to 20 ft/day during the first 33 days of operation but would decrease to approximately 2 ft/day. Initially, recharge water is taken into storage in layer 1, which raises the water table under the recharge pond. As the water table rises, the gradient in hydraulic head and the infiltration rate beneath the pond decrease. Influence of the pond on the water table is local and limited to the grid blocks adjacent to the block containing the simulated recharge pond. The total volume of water recharged during the first year of operations would be approximately 2,500 to 8,200 acre-ft, depending on the conductance of the base material. Average annual recharge decreases to approximately 2,000 to 2,300 acre-ft. The recharge mound produced in layer 1 has a relatively small impact on movement of water downward to layer 2.

Adding a recovery well to the operation, of course, significantly increases the recharge potential of the pond. Recharge water is only temporarily taken into storage before being removed by the recovery well. The ground-water withdrawal at the recovery well causes a local drawdown in the water table to be superposed on the infiltration process, which effectively increases the hydraulic-head gradient beneath the pond. Careful balancing of recovery-well production rate and recharge infiltration rate can yield a stable management system for water storage.

Brown and others (1978) and Huisman and Olsthorn (1983) discussed conceptual designs for artificial recharge projects. Key controls on the success of recharge operations include (1) maintaining continuity of infiltration so that the subsurface remains saturated beneath the pond, (2) keeping the permeability of the base material high through removal of suspended sediment from surface water before it reaches the recharge pond and through periodic draining and tilling of the pond's base, (3) selecting an area underlain by highly permeable material, and (4) keeping the water level in the pond as high as possible.

As with all parts of the numerical model, accuracy of simulation results depends on the validity of model parameters. Important variables in simulating artificial recharge include pond

size, stage above the water table, and thickness and permeability of the base material. In practice, the permeability of the base material decreases with time owing to plugging of pores with fine-grained sediment, growth of algae and bacteria in pores, and development of vegetation across the base of the pond. Another variable that influences short-term performance is the duration of dry periods owing to cutoff of surface-water supplies or during pond maintenance when infiltration is not continuous. Wells can continue to recover ground water from storage while a recharge pond is shut down (Huisman and Olsthorn, 1983).

Simulating a recovery well in the same block as an existing river reach is conceptually the same as simulating a separate artificial recharge pond. Such well production systems are often used to remove suspended material and bacteria out of the surface water using the natural filtering capacity of the aquifer.

Recommendations for Further Study

Further study is warranted to document the sensitivity of model simulations to components of the conceptual model and to imposed boundary conditions. As stated in the introduction, refinement of the conceptual and numerical models is expected after future validation studies.

There are few data to constrain hydraulic conductivity values in the Beaumont; however, the Beaumont is generally perceived to be less transmissive than the deeper aquifers. Additional field tests to measure hydraulic head and hydraulic conductivity in the Beaumont Formation in Matagorda and Wharton Counties would provide useful data for refining this model. Ground-water production from layers 2 and 3 resulted in drawdown of hydraulic head in layer 1 in excess of what probably occurs, most likely because of the lack of adequate recharge allowed by the general-head-boundary conductance. Further study to test the sensitivity of model results to the conductance parameter is needed.

The "no-flow" boundary at the eastern side of the study area also affects simulation results, as previously mentioned. Historically, major ground-water withdrawals in the Houston area and in

eastern Brazoria County created significant cones of depression that by the 1970's and 1980's expanded to the edge of the study area (Carr and others, 1985). It is probable that some ground water leaves the study area and is drawn into the Harris–Brazoria County pumping area; this is not reproduced in the conceptual model with a "no-flow" boundary. A further error arises in simulating drawdowns from sustained high rates of ground-water production within the study area from 1985 through 2030. Regional cones of depression that form near the lateral no-flow boundaries expand during that period. Upon encountering the "no-flow" boundary, apparent rates of water-level-decline increase. To some extent, this possibly compensates in the simulations for the amount of water that would be withdrawn from the basin into the Houston–Brazoria pumping area. Replacing the "no-flow" boundary along the northeastern side of the model with a specified flux boundary is the appropriate course to test the significance of this modeling error. The specified flux distribution could be taken from results of other regional models or calculated from local hydraulic-head gradients.

The influence of clay deposits is deemphasized in this conceptual model. Clay deposits are distributed throughout the aquifer units, as suggested by figures 5 through 13. Storativity of clay deposits generally is much lower than that of sand deposits, and clays in the Gulf Coast section are unconsolidated. Significant ground-water withdrawals, therefore, can effect great declines in fluid pressure in clay-rich sections, which in turn can lead to compaction of the clay beds and land-surface subsidence. To evaluate this phenomenon, other models of the Gulf Coast aquifers have incorporated distinct clay layers between aquifer units to represent all of the clay beds lying between the centers of adjacent aquifer units.

SUMMARY

The Gulf Coast aquifer in Matagorda and Wharton Counties comprises complex and heterogeneous packages of sand and clay. On the basis of detailed mapping of sand-bed distribution, hydraulic head, and hydrochemical facies in horizontal and vertical planes, it appears

that the Beaumont hydrologic unit in the study area should be treated as distinct from the Chicot aquifer unit.

A conceptual hydrologic model of the Gulf Coast aquifer includes recharge and discharge in the outcrop of the aquifer units, downdip flow of ground water, cross-formational flow directed upward beneath river valleys and in the vicinity of the coastline, and interflow between rivers and near-surface aquifers. Chemical composition and salinity of ground water are controlled by both mineralogic reactions and mixing with seawater. Seawater enters the system both by downward leakage through the Beaumont, which it enters as sea spray and during hurricane-driven floods, and by intrusion beneath the coastline driven by differences in fluid density between fresh and salt water. Hydrologic properties of the aquifers are highly variable but can be correlated to patterns in the distribution of sand deposits. Lateral boundaries to the ground-water basins originally were imposed by the valleys of the Lavaca and Navidad Rivers to the southwest and of the Brazos River to the northeast, but enlargement of the cone of depression of the hydraulic-head surface of the Gulf Coast aquifer system in Harris and Brazoria Counties has essentially breached the northeastern ground-water basin divide, draining some ground water from the study area off to the northeast.

A numerical model based on this conceptual model and calibrated by matching simulated hydraulic heads against historic head values was used to estimate future water-level declines in the Chicot and Evangeline aquifer units. Assuming that pumping rates are controlled by high projected demands for water, maximum calculated rates of water-level decline in the Chicot aquifer unit (layer 2) are predicted to be 5.7 ft/yr and in the lower Chicot–Evangeline (layer 3) to be 11.8 ft/yr between 1985 and 2030. The cumulative increase in drawdown of hydraulic head will increase the amount of seawater intrusion and will also effect further slight land-surface subsidence throughout the region.

The model can be used to evaluate water-resources projects such as well-field development and artificial recharge operations within the regional hydrologic setting. A well field producing 22,820 acre-ft of water per year from a hypothetical location east of the Colorado River in Texas

22,820 acre-ft of water per year from a hypothetical location east of the Colorado River in Texas would result in long-term decreases in water levels locally by as much as 83 ft. An artificial recharge project using surface-water spreading basins could recharge a fairly small amount of water, approximately 1,000 acre-ft/yr per acre of spreading basin. The low recharge rate is partly limited by the proximity of the water table to the land surface. Recharge rates could be somewhat increased through the use of additional recovery wells.

ACKNOWLEDGMENTS

This work was funded partly by the Lower Colorado River Authority (LCRA) under interagency contract number IAC (88-89)0910. We benefited from helpful discussion with and information from numerous individuals, particularly Quentin W. Martin of the LCRA, Paul D. Ryder of the U.S. Geological Survey, and Richard Raymond of The University of Texas at Austin Department of Geological Sciences. John Garber and John Nicol assisted in data analysis. Rick Edson and Diane M. Spinney assisted with computer programming and use of computer-aided graphics and mapping. Tucker Hentz reviewed drafts of this report. Word processing was by Melissa Snell and editing was by Amanda R. Masterson. Illustrations were drafted by Lynn Griffin, Wade W. Kolb, Annie K. Kubert, Joel L. Lardon, Yves Oberlin, Patrice A. Porter, Kerza Prewitt, and Maria Saenz, under the supervision of Richard L. Dillon. Report assembly was by Margaret Evans and Jamie H. Coggin.

REFERENCES

Aronow, S., Fisher, W. L., McGowen, J. H., and Barnes, V. E., 1982, Houston sheet: The University of Texas at Austin, Bureau of Economic Geology Geologic Atlas of Texas, scale 1:250,000.

Back, W., 1966, Hydrochemical facies and ground-water flow patterns in the northern part of the Atlantic coastal plain: U.S. Geological Survey Professional Paper 498-A, 42 p.

Baker, E. T., Jr., 1965, Ground-water resources of Jackson County, Texas: Austin, Texas Water Development Board Report 1, 229 p.

Baker, E. T., Jr., 1979, Stratigraphic and hydrogeologic framework of part of the Coastal Plain of Texas: Austin, Texas Department of Water Resources Report 236, 47 p.

BBN Software Products Corporation, 1987, RS/1 Users' Guide, Book 3, Using and Writing procedures: Cambridge, Massachusetts, BBN Software Products Corporation, variously paginated.

Bentley, M. E., 1980, Hydrogeology of the Beaumont Formation (Pleistocene), Brazoria County, Texas: The University of Texas at Austin, Master's thesis, 105 p.

Brown, L. F., Jr., Morton, R. A., McGowen, J. H., Kreitler, C. W., and Fisher, W. L., 1974, Natural hazards of the Texas Coastal Zone: The University of Texas at Austin, Bureau of Economic Geology Special Publication, 13 p.

Brown, R. F., Signor, D. C., and Wood, W. W., 1978, Artificial ground-water recharge as a water-management technique on the Southern High Plains of Texas and New Mexico: Austin, Texas Department of Water Resources Report 220, 32 p.

Brown, T. E., Brewton, J. L., McGowen, J. H., Proctor, C. V., Aronow, S., and Barnes, V. E., 1987, Beeville–Bay City sheet: The University of Texas at Austin, Bureau of Economic Geology Geologic Atlas of Texas, scale 1:250,000.

Carr, J. E., Meyer, W. R., Sandeen, W. M., and McLane, I. R., 1985, Digital models for simulation of ground-water hydrology of the Chicot and Evangeline aquifers along the Gulf Coast of Texas: Austin, Texas Department of Water Resources Report 289, 101 p.

de Marsily, Ghislain, 1986, Quantitative hydrogeology–groundwater hydrology for engineers: New York, Academic Press, 440 p.

Fogg, G. E., Seni, S. J., and Kreitler, C. W., 1983, Three-dimensional ground-water modeling in depositional systems, Wilcox Group, Oakwood salt dome area: The University of Texas at Austin, Bureau of Economic Geology Report of Investigations No. 133, 55 p.

Foster, M. D., 1950, The origin of high sodium bicarbonate waters in the Atlantic and Gulf Coastal Plains: Geochimica et Cosmochimica Acta, v. 1, p. 33–48.

Freeze, R. A., and Cherry, J. A., 1979, Groundwater: Englewood Cliffs, Prentice-Hall, 604 p.

Groschen, G. E., 1985, Simulated effects of projected pumping on the availability of freshwater in the Evangeline aquifer in an area southwest of Corpus Christi, Texas: U.S. Geological Survey Water Resources Investigations Report 85-4182, 103 p.

Guevara-Sanchez, E. H., 1974, Pleistocene facies in the subsurface of the southeast Texas coastal plain: The University of Texas at Austin, Ph.D. dissertation, 133 p.

Hammond, W. W., Jr., 1969, Ground-water resources of Matagorda County, Texas: Austin, Texas Water Development Board Report 91, 180 p.

Huisman, L., and Olsthoorn, T. N., 1983, Artificial groundwater recharge: Boston, Pitman, 320 p.

Idelovitch, E., and Michail, M., 1985, Groundwater recharge for wastewater reuse in the Dan region project: summary of five-year experience, 1977–1981, *in* Asano, T., ed., Artificial recharge of groundwater: Boston, Butterworth, p. 481-507.

Jorgensen, D. G., 1975, Analog-model studies of ground-water hydrology in the Houston district, Texas: Austin, Texas Water Development Board Report 190, 84 p.

Jorgensen, D. G., 1981, Geohydrologic models of the Houston District, Texas: Ground Water, v. 19, no. 4, p. 418–428.

Kreitler, C. W., Guevara, Edgar, Granata, George and McKalips, Dawn, 1977, Hydrogeology of Gulf Coast aquifers, Houston–Galveston area, Texas: Gulf Coast Association of Geological Societies Transactions, v. 27, p. 72–89.

Larkin, T. J., and Bomar, G. W., 1983, Climatic atlas of Texas: Austin, Texas Department of Water Resources Report LP-192, 151 p.

Loskot, C. L., Sandeen, W. M., and Follett, C. R., 1982, Ground-water resources of Colorado, Lavaca, and Wharton Counties: Austin, Texas Department of Water Resources Report 270, 242 p.

McDonald, M. G., and Harbaugh, A. W., 1984, A modular three-dimensional finite-difference ground-water flow model: U.S. Geological Survey Open-File Report 83-875, 528 p.

McGowen, J. H., Brown, L. F., Jr., Evans, T. J., Fisher, W. L., and Groat, C. G., 1976, Environmental geologic atlas of the Texas Coastal Zone—Bay City–Freeport area: The University of Texas at Austin, Bureau of Economic Geology, 98 p.

Piper, A. M., 1944, A graphic procedure in the geochemical interpretation of water analyses: American Geophysical Union Transactions, v. 25, p. 914–923.

Proctor, C. V., Brown, T. E., Brewton, J. L., Waechter, N. B., Aronow, S., Pieper, M. K., and Barnes, V. E., 1974, Seguin sheet: The University of Texas at Austin, Bureau of Economic Geology Geologic Atlas of Texas, scale 1:250,000.

Radian Corporation, 1979, CPS-1 Users' Manual, v. 2, Verb Documentation: Austin, Texas, Radian Corporation, variously paginated.

Ratzlaff, K. W., 1982, Land-surface subsidence in the Texas coastal region: Austin, Texas Department of Water Resources Report 272, 26 p.

Ryder, P. D., 1988, Hydrogeology and predevelopment flow in the Texas Gulf Coast aquifer systems: U.S. Geological Survey Water-Resources Investigations Report 87-4248, 109 p.

Sandeen, W. M., and Wesselman, J. B., 1973, Ground-water resources of Brazoria County, Texas: Austin, Texas Water Development Board Report 163, 199 p.

Senger, R. K., 1989, Hydrodynamics of gravity-driven flow systems in sedimentary basins: example of the Palo Duro Basin, Texas: The University of Texas at Austin, Ph.D. dissertation, 191 p.

Solis, R. F., 1981, Upper Tertiary and Quaternary depositional systems, central coastal plain, Texas–regional geology of the coastal aquifer and potential liquid-waste repositories: The University of Texas at Austin, Bureau of Economic Geology Report of Investigations No. 108, 89 p.

Wesselman, J. B., 1972, Ground-water resources of Fort Bend County, Texas: Austin, Texas Water Development Board Report 155, 176 p.

Williams, T. A., and Williamson, A. K., 1989, Estimating water-table altitudes for regional ground-water flow modeling, U.S. Gulf Coast: Ground Water, v. 27, no. 3, p. 333–340.

Wilson, C. A., 1967, Ground-water resources of Austin and Waller Counties, Texas: Austin, Texas Water Development Board Report 68, 236 p.

Wood, W. W., and Signor, D. C., 1975, Geochemical factors affecting artificial groundwater recharge in the unsaturated zone: American Society of Agricultural Engineers Transactions, v. 18, no. 4, p. 677–683

Appendix - Transmissivity and hydraulic conductivity data.

County	TWDB Number	Longitude UTM	Latitude UTM	Elevation at top of screen (ft)	Net screen length (ft)	Number of Screened Intervals	Transmissivity (ft2/d)	Hydraulic Conductivity (ft/d)	Coefficient of Storage	Sand Percent Minimum bed=0 ft	Sand Percent Minimum bed=20 ft	Aquifer Unit	Source
Austin	66-22-301	475365.1	3288254.0	126	268	1	5,120	19	-	45	45	E	6
"	66-23-402	476915.8	3284711.8	1,185	447	1	8,356	19	-	45	45	E	3
Brazoria	65-50-101	516059.7	3231942.5	-263	501	1	12,300	25	-	55	50	UC	4
"	65-50-102	515973.2	3232328.3	-42	722	1	9,359	13	-	55	50	UC	4
"	65-51-902	534611.6	3222504.3	-488	58	1	936	17	-	55	45	UC	4
"	65-58-607	524253.4	3215472.8	-48	88	1	5,883	67	8.0E-4	57	48	UC	4
"	65-58-803	519913.3	3209657.5	-60	101	1	53,345	528	-	48	40	UC	2
"	65-59-410	524540.7	3215808.0	-99	15	1	4,813	321	5.0E-4	57	48	UC	4
"	65-59-411	525374.6	3215246.5	1,034	55	1	5,081	93	3.0E-4	57	48	UC	4
"	65-59-417	525349.8	3215284.0	-67	50	1	4,947	99	-	57	48	UC	4
"	65-60-201	544192.5	3220732.0	1,029	49	1	3,209	65	-	45	25	UC	4
"	65-61-507	554522.1	3213063.5	1,021	35	1	2,273	65	-	35	18	UC	3
"	81-05-301	559434.5	3207619.0	-1,017	102	1	35,430	347	6.0E-4	39	15	UC	4
"	81-05-304	560392.2	3206634.5	-191	20	2	5,081	254	3.0E-4	39	48	UC	4
"	81-05-305	559597.0	3207879.8	-193	20	2	8,824	441	1.0E-4	38	15	UC	4
"	81-05-306	558849.0	3207781.8	-182	40	1	5,749	143	3.0E-4	38	15	UC	4
"	81-05-315	559334.3	3207370.5	-970	150	1	36,767	245	-	39	15	UC	4
"	81-05-317	560042.3	3206113.0	-921	133	1	33,157	249	5.0E-4	40	10	UC	4
"	81-05-602	561030.6	3201658.5	-222	20	1	1,738	87	6.0E-5	40	10	UC	4
"	81-06-102	563814.5	3203966.5	-206	37	1	4,011	108	-	35	15	UC	4
"	81-06-209	567282.5	3205651.0	-252	16	1	267	17	-	30	10	UC	4
"	81-06-421	562211.6	3200064.3	-162	50	2	1,203	24	-	40	18	UC	4
"	81-06-503	567351.0	3202392.5	-971	157	2	4,546	29	4.0E-3	40	12	UC	4
"	81-06-505	567040.3	3202878.0	-207	20	2	2,406	120	1.0E-4	40	12	UC	4
"	81-06-506	565814.7	3200729.0	-196	20	4	2,540	127	1.0E-4	40	12	UC	4
"	81-06-514	566564.9	3201958.8	-984	136	1	13,102	96	7.0E-4	40	12	UC	4
"	81-06-517	566663.6	3201399.0	-1,003	119	1	12,701	107	-	40	12	UC	4
Colorado	66-20-903	447669.2	3277967.5	128	180	1	1,000	6	-	30	42	LC	3
"	66-21-601	462985.2	3284772.5	55	300	1	7,380	25	-	30	31	LC	6
"	66-28-901	448081.2	3265545.5	110	250	1	3,050	12	-	45	30	LC	3
"	66-30-101	467398.3	3273335.0	-189	110	5	3,984	36	-	38	55	LC	3
"	66-30-102	467505.4	3273171.3	-171	115	4	6,380	55	-	38	55	LC	3
"	66-30-203	469739.0	3275776.5	-170	220	1	9,860	45	-	37	65	LC	3
"	66-37-204	456057.3	3262450.5	-175	370	1	3,780	10	-	45	40	LC	3
"	66-20-505	445643.5	3285209.3	43	65	2	670	10	-	30	30	E	3
"	66-20-602	447989.3	3285815.0	6	79	2	780	10	-	30	30	E	3
"	66-21-301	459935.2	3287172.0	-150	400	1	3,400	9	-	30	30	E	3
"	66-28-303	450761.0	3273877.0	-61	291	1	3,130	11	-	35	35	E	3
"	66-35-304	439262.6	3259785.3	-435	90	3	1,400	16	-	52	52	E	3
Fort Bend	65-25-202	506792.0	3274376.0	-45	116	1	14,707	127	-	65	75	LC	5
"	65-25-203	507156.7	3274202.0	-36	110	1	10,428	95	-	65	75	LC	5
"	65-26-602	521252.0	3269471.3	-45	250	1	13,905	56	-	45	22	LC	5
"	65-26-603	523311.7	3272210.5	-292	130	1	11,297	87	-	65	22	LC	5

Appendix - Transmissivity and hydraulic conductivity data.

County	TWDB Number	Longitude UTM	Latitude UTM	Elevation at top of screen (ft)	Net screen length (ft)	Number of Screened Intervals	Transmissivity (ft2/d)	Hydraulic Conductivity (ft/d)	Coefficient of Storage	Sand Percent Minimum bed=0 ft	Sand Percent Minimum bed=20 ft	Aquifer Unit	Source
Fort Bend	65-33-802	507032.4	3249465.3	-232	36	2	1,765	49	1.0E-4	85	65	LC	5
"	65-33-803	507107.1	3249827.8	-228	38	1	1,872	49	-	85	65	LC	5
"	65-34-901	523801.8	3253793.0	-12	320	1	16,044	50	-	75	68	LC	5
"	65-35-303	535320.8	3261209.5	-385	72	1	14,707	204	1.0E-3	64	53	LC	5
"	65-35-304	535568.2	3261541.5	-383	193	2	15,242	79	-	64	53	LC	5
"	65-42-303	524180.0	3249047.3	-159	420	1	16,712	40	-	65	35	LC	5
"	65-43-201	531125.7	3248247.0	-226	555	1	20,857	38	-	60	35	LC	5
"	65-44-101	537243.4	3246719.5	-159	658	1	11,859	18	-	55	49	LC	5
"	65-26-812	517808.8	3267310.0	-700	185	1	8,784	47	-	30	30	E	5
Jackson	66-61-803	458456.8	3209826.3	-4	139	1	11,364	82	-	45	50	UC	1
"	80-05-301	462051.0	3206446.5	21	252	1	31,018	123	5.9E-4	55	40	UC	1
"	80-05-310	461913.5	3205871.5	-54	83	1	9,265	112	-	55	40	UC	1
"	80-06-101	464640.8	3207604.5	-20	260	1	25,270	97	-	55	42	UC	1
"	80-06-102	464493.1	3204668.3	-46	156	1	16,579	106	-	55	22	UC	1
"	80-06-104	464779.7	3204339.0	6	160	1	15,910	99	1.4E-3	55	22	UC	1
"	80-06-703	467378.5	3194206.8	-118	220	1	10,562	48	-	50	52	UC	1
"	80-06-704	463526.9	3195068.3	-110	171	1	14,012	82	-	50	52	UC	1
"	80-13-901	461785.0	3184606.8	-118	262	1	5,776	22	-	18	65	UC	1
"	80-14-103	464546.6	3189600.3	-169	239	1	9,814	41	-	50	50	UC	1
"	80-21-601	461896.3	3173758.3	-305	190	1	8,156	43	-	20	30	UC	1
"	80-22-501	468195.5	3175207.5	-272	57	1	2,754	48	-	20	24	UC	1
"	66-50-801	422671.4	3222348.5	-101	401	1	6,016	15	-	38	29	LC	1
"	66-51-305	438229.1	3231984.8	-105	404	5	3,235	8	-	32	70	LC	1
"	66-51-505	433299.4	3228476.0	-172	208	1	5,615	27	-	35	44	LC	1
"	66-51-509	432880.6	3228401.5	-148	312	1	8,744	28	-	35	44	LC	1
"	66-51-604	438603.6	3229247.0	-130	309	1	4,639	15	-	32	70	LC	1
"	66-51-904	437546.7	3223404.5	-5	242	1	7,754	32	-	30	62	LC	1
"	66-52-407	440294.3	3225942.8	-175	341	1	7,848	23	-	30	70	LC	1
"	66-52-704	441410.1	3221261.3	-118	400	1	8,009	20	-	30	75	LC	1
"	66-52-705	441684.4	3221165.5	-200	512	1	9,038	18	2.6E-3	30	75	LC	1
"	66-52-706	441662.3	3221391.8	-80	306	1	9,172	30	-	30	75	LC	1
"	66-52-907	447715.1	3222623.8	-70	258	1	6,190	24	-	80	80	LC	1
"	66-58-801	420613.0	3209643.0	-43	391	1	6,257	16	-	40	28	LC	1
"	66-58-903	423276.3	3209460.0	-114	392	1	6,284	16	-	40	42	LC	1
"	66-59-303	437219.5	3218403.8	30	349	1	18,850	54	-	30	60	LC	1
"	66-59-308	437298.6	3220498.5	-116	238	1	7,153	30	-	30	60	LC	1
"	66-59-501	432342.9	3214510.0	-43	285	1	4,840	17	-	35	50	LC	1
"	66-59-601	438321.3	3215640.3	-150	320	1	6,391	20	-	30	65	LC	1
"	66-59-901	435319.7	3209629.8	-106	327	1	7,848	24	-	35	70	LC	1
"	66-60-106	440287.9	3218649.3	-120	207	1	7,460	36	-	30	70	LC	1
"	66-60-201	446352.4	3220361.0	-89	339	1	10,856	32	-	79	80	LC	1
"	66-60-205	446807.5	3219720.0	-14	128	1	12,554	98	-	80	80	LC	1
"	66-60-603	451232.4	3214554.5	7	161	1	8,717	54	-	85	85	LC	1

Appendix - Transmissivity and hydraulic conductivity data.

County	TWDB Number	Longitude UTM	Latitude UTM	Elevation at top of screen (ft)	Net screen length (ft)	Number of Screened Intervals	Transmissivity (ft2/d)	Hydraulic Conductivity (ft/d)	Coefficient of Storage	Sand Percent Minimum bed=0 ft	Sand Percent Minimum bed=20 ft	Aquifer Unit	Source
Jackson	66-60-608	451171.9	3215601.8	-39	113	1	7,100	63	-	85	85	LC	1
"	66-60-609	451076.3	3215210.5	30	138	1	18,718	135	4.2E-3	85	85	LC	1
"	66-60-703	443081.8	3209393.8	-66	320	2	7,688	24	-	30	82	LC	1
"	66-61-702	452630.1	3208659.3	-66	151	1	17,822	118	-	45	61	LC	1
"	80-02-601	424807.8	3202284.5	-93	278	1	8,610	31	-	35	38	LC	1
"	80-03-202	431438.0	3205108.3	-123	475	1	18,050	38	-	45	55	LC	1
"	80-03-301	437096.4	3206056.5	-890	157	1	3,610	23	-	30	75	LC	1
"	80-04-403	441447.7	3202157.3	-162	267	1	5,081	19	-	30	90	LC	1
"	80-05-507	456211.1	3201655.5	-126	282	1	13,798	49	-	45	50	LC	1
"	80-05-701	452239.0	3197369.3	-70	140	1	5,870	42	-	35	60	LC	1
"	80-11-201	434512.6	3194304.0	-60	295	1	7,086	24	-	10	45	LC	1
"	80-12-502	446361.5	3187205.0	-54	146	1	9,225	63	-	10	45	LC	1
"	80-13-404	454328.2	3188961.5	-112	284	1	9,666	34	-	15	52	LC	1
"	80-21-201	456947.2	3178328.0	-392	42	1	2,554	61	-	15	38	LC	1
"	66-60-902	449675.7	3211749.8	-1,125	83	1	1,163	14	1.8E-5	45	45	E	1
Lavaca	66-35-902	437543.0	3250420.0	20	173	1	2,940	17	-	43	60	LC	3
"	66-50-401	418699.3	3227764.0	-44	280	1	4,970	18	-	40	20	LC	3
Matagorda	65-49-901	510854.4	3223608.5	-242	40	2	3,516	88	-	50	55	UC	2
"	65-57-702	500201.8	3209472.0	-277	50	2	3,423	68	-	45	38	UC	2
"	65-57-801	506258.0	3211736.0	-98	196	1	21,392	109	1.1E-3	10	19	UC	2
"	65-58-107	514969.3	3218045.5	-29	137	1	23,530	171	-	50	35	UC	2
"	65-58-108	514481.7	3217528.0	-103	124	1	11,578	93	-	50	35	UC	2
"	66-63-802	482056.7	3207939.3	-184	264	1	20,603	78	-	55	48	UC	2
"	66-63-902	485563.7	3208977.0	-165	110	1	11,070	101	9.1E-4	40	37	UC	2
"	66-64-401	488728.6	3213939.3	-246	416	9	21,660	52	-	50	49	UC	2
"	66-64-702	491796.9	3210540.0	-600	289	1	8,637	30	-	5	5	UC	2
"	80-07-501	480261.5	3202746.3	-170	297	2	16,045	54	-	26	15	UC	2
"	80-08-302	498693.9	3205250.8	-480	100	1	4,746	47	-	35	22	UC	2
"	80-08-701	489598.3	3195309.5	-263	94	1	2,634	28	-	10	6	UC	2
"	80-14-401	464595.6	3188923.8	-122	282	1	17,515	62	-	50	50	UC	2
"	80-15-102	478409.3	3193266.3	-466	100	3	6,123	61	-	28	4	UC	2
"	80-15-201	481016.7	3192388.3	-319	255	10	14,306	56	-	28	5	UC	2
"	80-15-301	486024.3	3191418.8	-529	165	1	9,050	55	-	15	5	UC	2
"	80-15-401	476177.8	3188129.0	-192	351	11	8,423	24	-	42	35	UC	2
"	80-15-502	483734.7	3187266.5	-218	299	1	4,185	14	-	20	12	UC	2
"	80-16-301	498343.4	3192277.5	-583	81	3	5,400	67	-	22	15	UC	2
"	80-23-101	477442.7	3179913.8	-169	240	2	11,030	46	-	42	35	UC	2
"	80-23-402	478870.1	3174696.5	-533	42	1	5,990	143	-	42	20	UC	2
"	80-23-403	479231.4	3174725.0	-531	36	1	5,682	158	4.6E-5	42	20	UC	2
"	81-01-101	502364.9	3205562.8	-514	141	5	9,158	65	-	50	41	UC	2
"	81-01-102	503626.6	3205699.3	-726	138	5	4,011	29	-	50	41	UC	2
"	81-01-601	508865.7	3202488.8	-182	112	3	5,722	51	-	12	10	UC	2
"	81-01-802	505296.4	3193987.5	-119	130	1	4,680	36	-	40	27	UC	2

Appendix - Transmissivity and hydraulic conductivity data.

County	TWDB Number	Longitude UTM	Latitude UTM	Elevation at top of screen (ft)	Net screen length (ft)	Number of Screened Intervals	Transmissivity (ft2/d)	Hydraulic Conductivity (ft/d)	Coefficient of Storage	Sand Percent Minimum bed=0 ft	Sand Percent Minimum bed=20 ft	Aquifer Unit	Source
Matagorda	81-09-401	501173.9	3185749.8	-331	180	1	5,923	33	-	34	27	UC	2
"	81-09-504	505236.1	3185790.0	-122	173	1	7,086	41	-	35	21	UC	2
"	81-09-904	509780.1	3181300.5	-344	60	3	5,749	96	1.3E-3	25	5	UC	2
Wharton	66-62-709	465781.7	3208885.5	-133	251	1	16,070	64	-	55	45	UC	3
"	66-62-713	467494.0	3211506.5	-132	211	1	19,080	90	-	70	50	UC	3
"	66-62-904	475450.5	3209993.0	-95	278	4	13,400	48	-	60	60	UC	3
"	66-31-901	486049.2	3267721.0	30	65	1	13,800	212	-	58	48	LC	3
"	66-31-902	485378.3	3267423.5	95	12	2	46,400	2,125	-	57	48	LC	3
"	66-31-903	485470.8	3267099.5	95	300	2	9,040	30	-	55	48	LC	3
"	66-38-303	472669.7	3262542.3	-63	225	1	45,630	203	-	40	48	LC	3
"	66-45-201	457563.2	3246658.0	152	235	1	27,000	115	-	40	38	LC	3
"	66-45-804	455690.3	3237963.0	13	278	1	16,440	59	-	65	40	LC	3
"	66-46-402	499665.2	3235934.0	35	250	1	32,100	128	-	80	60	LC	3
"	66-48-904	473088.2	3230718.8	-5	204	1	17,900	88	-	25	60	LC	3
"	66-54-601	473851.2	3229340.5	-587	171	6	4,800	28	-	37	37	LC	3
"	66-55-103	478028.9	3234010.5	-154	180	1	10,600	59	-	57	62	LC	3
"	66-61-302	460328.9	3219800.0	-421	75	2	8,640	52	1.8E-3	55	40	LC	3
"	66-61-305	460690.2	3219347.0	-52	230	1	15,100	66	-	55	40	LC	3
"	66-61-309	460661.5	3219793.8	-13	120	5	7,420	62	-	55	40	LC	3
"	66-63-201	482646.5	3221252.0	-36	361	1	19,100	55	-	85	85	LC	3
"	66-31-906	486226.4	3266651.3	-729	100	3	1,130	12	-	67	67	E	3
"	66-54-603	473876.0	3229352.5	-687	297	1	2,860	14	-	37	37	E	3

Aquifer unit: LC - lower Chicot; UC - upper Chicot; E - Evangeline

Source: 1 - Baker (1965); 2 - Hammond (1969); 3 - Loskot and others (1982);
4 - Sandeen and Wesselman (1973); 5 - Wesselman (1972); 6 - Wilson (1967)